Monthly Scientific-Technical and Production Journal

The Paton WELDING JOURNAL

June 2001 # 6

English translation of the monthly «Avtomaticheskaya Svarka» journal published in Russian since 1948

The National Academy of Sciences of Ukraine
The E.O. Paton Electric Welding Institute of the NAS of Ukraine
International Association «Welding»

«The Paton Welding Journal»
is published monthly by the
International Association «Welding»

Promotion group:
V.N.Lipodaev, V.I.Lokteva
A.T.Zelnichenko (Exec. director)
Translators:
S.A.Fomina, I.N.Kutianova,
T.K.Vasilenko

Editorial and advertising offices
are located at PWI,
International Association «Welding»,
11, Bozhenko str., 03680,
Kyiv, Ukraine
Tel.: (38044) 227 67 57
Fax: (38044) 268 04 86
E-mail: tomik@mac.relc.com
E-mail: office@paton.kiev.ua

State Registration Certificate
KV 4790 of 09.01.2001

Subscriptions:
$460, 12 issues, postage included

«The Paton Welding Journal» Website:
http://www.nas.gov.ua/pwj

CONTENTS

EFFECT OF FLUXES ON TEMPERATURE AND CURRENT DENSITY IN THE ARC COLUMN IN TIG WELDING OF TITANIUM

L.E. EROSHENKO, V.P. PRILUTSKY, V.Yu. BELOUS and **V.N. ZAMKOV**
The E.O. Paton Electric Welding Institute, NASU, Kyiv, Ukraine

ABSTRACT

The effect of barium, calcium, magnesium, sodium and aluminium fluorides, which are the main components of welding fluxes used for TIG welding of titanium, on temperature of the arc column and its distribution in the anode region has been studied. It has been found that in TIG welding over the flux layer (TIG-F) the temperature and electrical conductivity of the arc column plasma increase and shape of the temperature field in the anode region of the arc is close to the cylindrical one. Deep penetration characteristic of this welding method is caused by higher temperature and current density in the arc near the anode.

Key words: *argon-arc welding, titanium, flux, spectral line, arc column temperature, electrical conductivity*

The main distinctive feature of tungsten-electrode argon-arc welding over the flux layer (TIG-F) is a high current density in the anode spot [1 – 3]. It is this fact that determines technological benefits of this welding method, such as deep penetration, narrow welds and relatively low heat input [4 – 6]. Physical-chemical processes occurring in the arc zone, which cause contraction of the arc and, hence, an increase in the current density at the anode are considered in detail in [7, 8]. It was established that the degree of arc contraction and the growth of the current density in the anode spot depend upon the chemical composition of a flux and activity of its interaction with metal welded [7, 9]. However, no experimental data are available in the literature on the effect of fluxes on temperature parameters of the arc column. The only exception is reference [10], where it is suggested, on the basis of the derived relationship between the degree of blackening of spectral lines of vapours of the base metal, its penetration depth and composition of a flux, that fluxes do have an effect on temperature of the arc near the anode. At the same time, it is the temperature and current density in the anode region that are those basic parameters which are responsible for the character and mechanism of metal penetration.

This study gives results of investigation into the effect of barium, calcium, magnesium, sodium and aluminium fluorides, which are the main components of welding fluxes for titanium, on the temperature of the arc column and its distribution in the anode region. 4 mm thick plates of commercial titanium of the VT1-0 grade were used as the anode. Welding of samples was performed using tungsten electrode of the SVI-1 grade with a diameter of 3 mm and a pointing angle of 30°. The welding current in this case was 100 A, the welding speed was 8 m/h and the set arc length was 5 mm. The method used for determination of the arc temperature and schematic of the experimental setup are described in [11]. Photography of transverse spectra of the arc was done starting at a distance of 0.1 mm from the anode surface and then along the arc column at an interval of 0.25 mm in a direction to the cathode (Figure 1).

Like in study [11], radial distributions of temperature at different cross sections of the arc column were determined from the absolute intensity of glow of continuum of the argon plasma and atomic spectral lines ArI. Transition from the radial distributions of

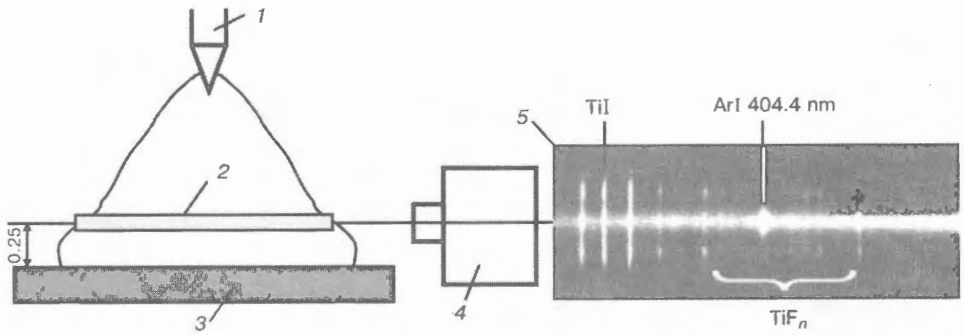

Figure 1. Schematic of photography of transverse spectra of the arc column: *1* — electrode; *2* — section of the arc column being investigated; *3* — titanium anode; *4* — spectrograph STE-1; *5* — spectrogram of the arc column region being investigated

temperature T to the radial distributions of electrical conductivity, σ, was done on the basis of theoretical curve $\sigma(T)$ given in [12]. Value r at which $\sigma \approx 0$ was taken as the arc column radius. As transverse sizes of the argon arc column are determined only from the glow of the continuous spectrum of braking and recombination radiation of electrons, the value of the current-conducting diameter may be under-estimated. This is caused by the fact that in photography of the arc spectra the continuum radiation is registered only at temperatures above 8500 – 10500 K [13], while electrical conductivity of the pure argon plasma is decreased to zero values only at $T \approx 6000$ K [12]. Therefore, the diagram of the radial distribution of temperature, $T(r)$, across the arc column was plotted in two stages.

First the radial distribution of temperature was determined from the intensity of the glow of continuum in a high-temperature region of the arc. Then the distribution of temperature in a low-temperature region of the arc, starting from a zone where the continuum glow was ended, was found from the intensity of the glow of argon spectral lines ArI. After that both curves were combined by aligning the points along the arc column radius, at which the values of temperatures obtained from the glow of continuum and lines ArI coincided.

However, it should be emphasized that in order to determine the axial distribution of temperature in the arc column, it is sufficient to know only the radial distributions of the intensity of the glow of continuum [11]. The axial distributions of temperatures thus determined (Figure 2) are indicative of the fact that in welding over the flux layer the temperature in a region adjoining the anode is higher than in welding using no flux. The degree of an increase in temperature, as well as in penetration depth [9], grows in the following order: $BaF_2 \rightarrow CaF_2 \rightarrow MgF_2 \rightarrow NaF \rightarrow AlF_3$, and in a direction to the anode. The length of the zone with a higher temperature along the arc column increases in the same sequence. Results of these investigations are an experimental proof that the use of fluxes in TIG welding causes an increase in temperature of the plasma in the anode region of the arc.

It should be noted that in the spectra taken directly at the anode, in the case of using sodium fluoride as the flux, the number of spectral lines was so large that it gave no way to correctly determine the temperature of the arc at a distance less than 0.5 mm from the anode surface. At the same time, in welding without flux no TiI spectral lines were fixed in the arc spectrum (in contrast to the spectra observed in welding over the flux layer). This is indicative of their insignificant concentration at the arc column periphery. Analysis of the theoretical dependence of the intensity of radiation of argon atomic line ArI upon the temperature, $I(T)$, at the presence of impurities of the anode vapours in the argon plasma [14, 15] showed that at a concentration of the anode, e.g. iron, vapours of up to 10 wt.% the temperature at the

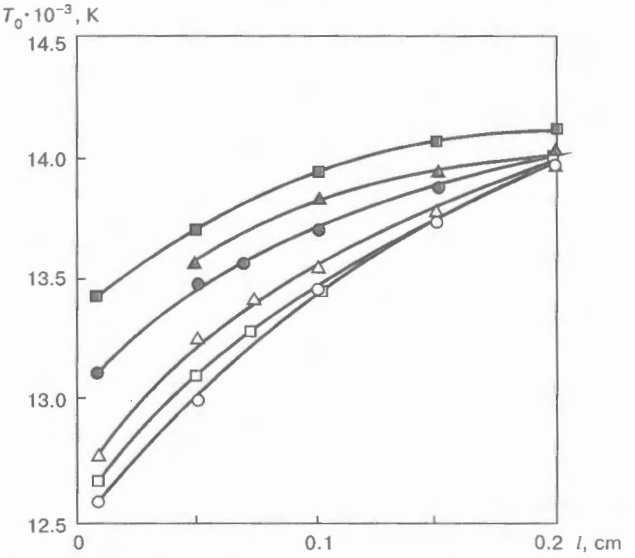

Figure 2. Distribution of temperature along the arc column axis: ○ – Ti; ❐ – BaF_2; Δ – CaF_2; ● – MgF_2; ▲ – NaF; ■ – AlF_3

arc column periphery could be measured using an impurity-free argon plasma. As potentials of iron and titanium have close values (7.87 and 6.82 eV, respectively), this possibility is likely to persist also for the plasma composed of Ar + Ti. The presence of fluxes in the welding zone makes determination of radial distributions of temperature, $T(r)$, and electrical conductivity, $\sigma(r)$, at the arc column periphery much more complicated. So, in welding over the flux layer an intensive glow of the TiI lines and molecular bands TiF_n (see Figure 1) was observed in the arc regions with a temperature of $\approx$ 8500 – 9000 K. Maxima of their glow spatially coincide and are at a distance of about 4 mm from the arc axis. Therefore, in this case, starting from a temperature of about 8500 – 9000 K the plasma is no longer the pure argon one, which does not allow the impurity-free argon plasma to be used for a correct determination of temperature and electrical conductivity in the peripheral arc regions. Given that titanium fluorides are prone to formation of negative molecular ions [14, 15], it can be suggested that electrical conductivity of electrons in these regions of the plasma would dramatically decrease. Therefore, Figure 3 shows temperature fields only for the central part of the arc in welding over a layer of CaF_2, MgF_2 and AlF_3.

As it can be seen from Figure 3, *a*, the temperature field of the arc column in welding without flux is similar in shape to the glow of a free-burning arc in argon [16]. It has the shape of a cone expanding in a direction from the cathode to the anode. Near the surface of the latter there is a spatial narrowing of the arc column, caused by peculiarities of heat transfer from the plasma to the metal anode. In welding over the flux layer this spatial narrowing and conicity of the temperature field in the anode region decrease (Figure 3, *b* – *d*). The temperature field in this case has a nearly cylindrical shape. The degree of the effect of fluxes both on this shape and on an increase in temperature in the arc column (see Figure 2), as well

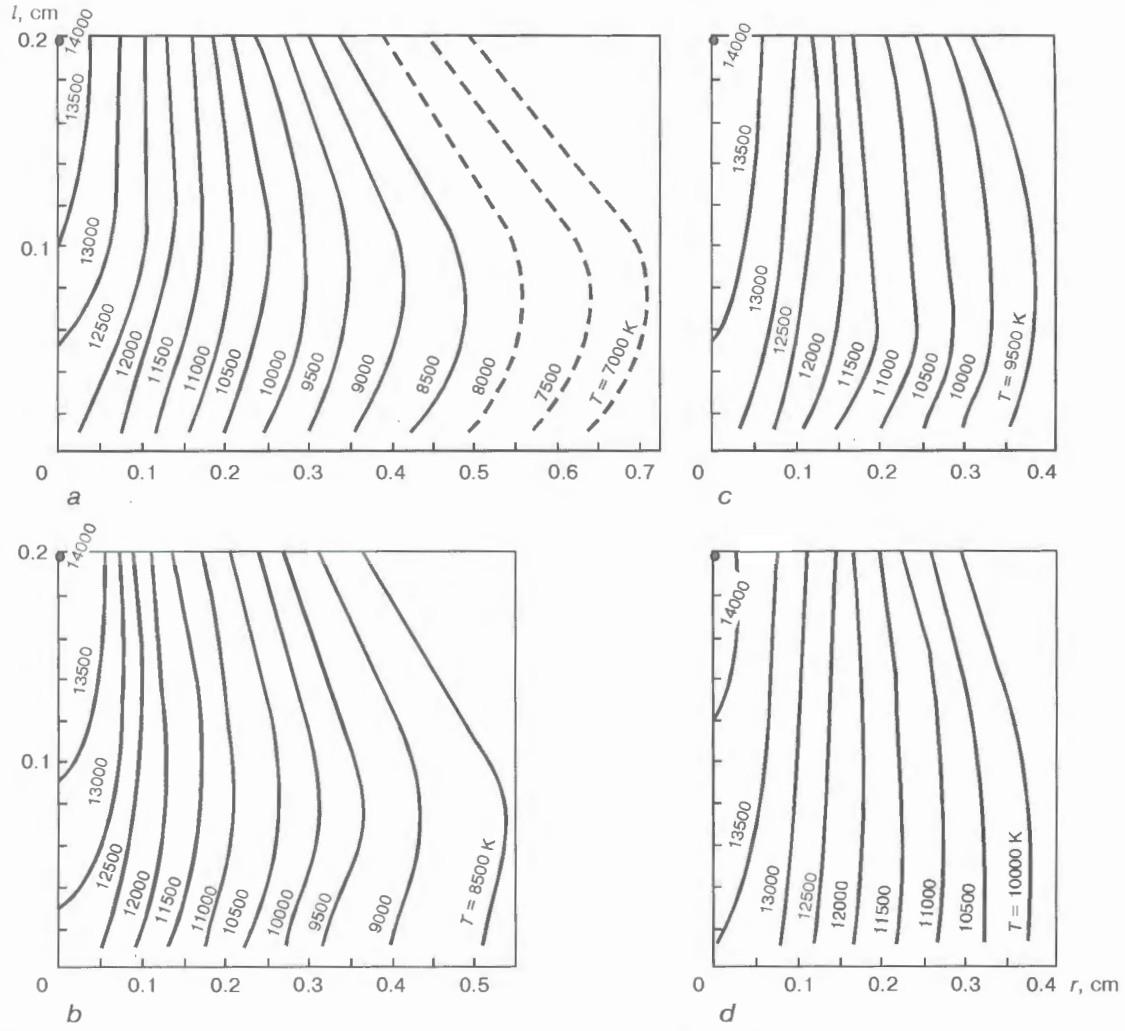

Figure 3. Temperature fields in the arc column in welding using an anode: *a* — Ti; *b* — Ti + CaF_2; *c* — Ti + MgF_2; *d* — Ti + AlF_3

as an increase in the penetration depth, depends upon the chemical composition of a flux and grows in an order from CaF_2 to AlF_3. At the same time, the radius of the zone with a higher temperature also increases in the arc column. For example, at a distance of 3.5 mm from the arc axis in a section located at a distance of 0.2 mm from the anode surface the temperature of the plasma in welding over a layer of AlF_3 increased by more than 1000 K, as compared with the temperature in the same region in welding without flux.

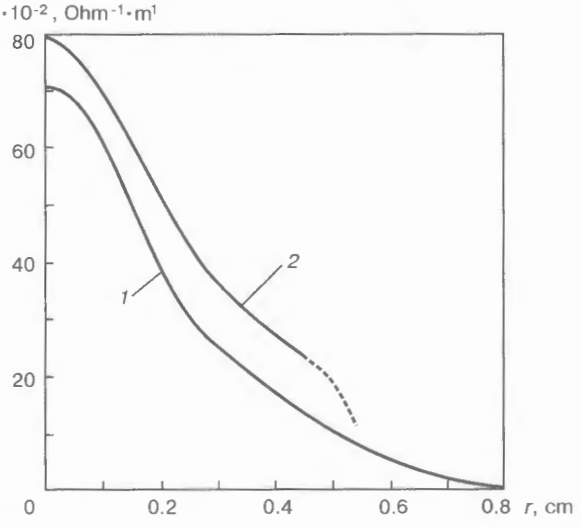

Figure 4. Radial distribution of electrical conductivity in the arc column at a distance of 0.5 mm from the anode: *1* — Ti; *2* — Ti + AlF_3

Growth of temperature in central regions of the arc column in welding over the flux layer causes a corresponding increase in electrical conductivity of these regions of the plasma (Figure 4). It should be noted here that in welding without flux the electrically conducting zone ends at a distance of ≈ 8 mm from the arc axis, whereas in welding over a layer of such fluxes as MgF_2, NaF and AlF_3 the character of the curve which describes the distribution of electrical conductivity, $\sigma(r)$, would undergo a drastic change already at a distance of about 4 mm from the arc axis (at the arc length of 5 mm). It is here, as noted above, that maximum intensities of the glow of the molecular lines of titanium fluorides and, hence, a drastic drop in electrical conductivity of the plasma because of capture of electrons by titanium fluorides and formation of the negative molecular ions of the TiF_n^- type [7, 9] are observed. At the same time, the experimental conditions required that the total electrical conductivity of the arc column be unchanged in all cases. This is associated with the fact that in all the experi-

ments the welding current remained unchanged (100 A), as well as the intensity of the field in the arc column did, as it did not depend upon the presence of flux in the welding zone [17].

Therefore, the fact that in welding over the flux layer the electrical conductivity of the plasma of a central part of the arc column increases (see Figure 4) and its total electrical conductivity remains unchanged allows us to state that the conducting channel of the arc column in welding over the flux layer is contracted. Its radius becomes smaller than in welding without flux. However, as noted above, it seems impossible to correctly determine the radial distributions of temperature, $T(r)$, and electrical conductivity, $\sigma(r)$, in the peripheral region of the arc column in welding over the flux layer by the experimental methods. In turn, this makes it impossible to experimentally determine the radius of the conducting zone of the arc column. The character of distribution of electrical conductivity in the peripheral zone of the arc column is conditionally shown in Figure 4 by a dotted line.

The only fact that can be stated on the basis of approximate estimations made by the data of Figure 4 is that in welding over a layer of the AlF_3 flux the electrical conductivity of the central zone of the arc column, confined by a radius of 0.4 cm, at a distance of 0.5 mm from the anode is about 75 % of the total electrical conductivity of the arc and no more than 47 % of that in welding without flux.

CONCLUSIONS

1. It has been experimentally proved that in TIG-F welding the temperature and electrical conductivity of the arc column plasma are increased and the shape of the temperature field in the anode region of the arc becomes close to the cylindrical one.

2. Deep penetration, which is characteristic of this welding method, is caused by the higher temperature and current density in the arc near the anode.

REFERENCES

1. Zamkov, V.N., Prilutsky, V.P. (1987) Distribution of current density in the anode spot in arc welding of titanium. *Avtomaticheskaya Svarka*, **3**, 19 – 22.
2. Ostrovsky, O.E., Kryukovsky, V.N., Buk, B.B. *et al.* (1977) Effect of activating fluxes on the penetrating power of the arc and concentration of energy in the anode spot. *Svarochnoye Proizvodstvo*, **3**, 13 – 15.
3. Savitsky, M.M., Gvozdetsky, V.S., Skrypnik, V.I. *et al.* (1979) Current density in the anode spot in welding of conventional and refined steels. *Avtomaticheskaya Svarka*, **7**, 17 – 20.
4. Gurevich, S.M., Zamkov, V.N., Blashchuk, V.E. *et al.* (1986) *Metallurgy and technology of welding titanium and its alloys*. Kyiv: Naukova Dumka.
5. Savitsky, M.M., Kushnirenko, B.N., Olejnik, O.I. (1999) Peculiarities of welding steels using tungsten electrode and activating fluxes (A-TIG process). *Avtomaticheskaya Svarka*, **12**, 20 – 28.
6. Paton, B.E., Zamkov, V.N., Priloutsky, V.P. (1998) Le soudage A-TIG du titane et de ses alliages. *Soudage et Techn. Connexes*, **11/12**, 23 – 26.
7. Paton, B.E., Zamkov, V.N., Prilutsky, V.P. *et al.* (2000) Contraction of the welding arc caused by the flux in tungsten-electrode argon-arc welding. *The Paton Welding J.*, **1**, 5 – 11.
8. Savitsky, M.M., Leskov, G.I. (1980) Mechanism of the effect of electrically negative elements on the penetrating power of the arc with a tungsten cathode. *Avtomaticheskaya Svarka*, **9**, 17 – 22.
9. Zamkov, V.N., Prilutsky, V.P., Gurevich, S.M. (1977) Effect of composition of a flux on the process of non-consumable electrode welding of titanium. *Ibid.*, **4**, 22 – 26.
10. Eroshenko, L.E., Zamkov, V.N., Mechev, V.S. *et al.* (1979) Investigation of glow of the anode vapours for evaluation of technological characteristics of the arc in argon. *Ibid.*, **9**, 33 – 35.
11. Eroshenko, L.E., Prilutsky, V.P., Belous, V.S. *et al.* (2001) Axial distribution of temperature in arc in GTA welding of titanium. *The Paton Welding J.*, **3**, 10 – 12.
12. Mechev, V.S., Eroshenko, L.E. (1974) Electrical conductivity of the electric arc in argon. *Avtomaticheskaya Svarka*, **7**, 13 – 16.
13. Mechev, V.S., Eroshenko, L.E. (1975) Radial distribution of temperature of the electric arc in argon. *Ibid.*, **3**, 6 – 9.
14. Messey, G. (1979) *Negative ions*. Moscow: Mir.
15. McDaniel, I. (1967) *Collision processes in ionized gases*. Moscow: Mir.
16. Olsen, H.N. (1963) The electric arc as a light source for quantitative spectroscopy. *J. Quant. Spectrosc. and Radiat. Transfer*, **3**, 305 – 333.
17. Gurevich, S.M., Zamkov, V.N. (1966) Some peculiarities of welding of titanium using non-consumable electrode and fluxes. *Avtomaticheskaya Svarka*, **12**, 13 – 16.

ARGON-ARC TREATMENT OF WELDED JOINTS ON 30KhGSA STEEL

V.M. KULIK, M.M. SAVITSKY, D.P. NOVIKOVA, V.G. VASILIEV and G.N. GORDAN
The E.O. Paton Electric Welding Institute, NASU, Kyiv, Ukraine

ABSTRACT

Effect of parameters of conditions and thermal cycle of a local argon-arc treatment without melting on changing the metal structure and mechanical properties of the high-strength steel welded joint was studied. It is shown that the arc heating within the wide ranges of treatment speed up to the temperatures of austenization of the welded joint metal, being hardened during welding, causes the repeated hardening, while at the temperatures below the austenization temperatures a short-time tempering is occurred. After the local argon-arc treatment the ductility and impact strength of the welded joint metal are increased, the mode of fracture is improved, the sensitivity to stress raisers is decreased.

Key words: *welded joint, arc treatment, high-strength steel, heating, cooling, hardening, tempering, structure, bainite, martensite, residual austenite, dilation curve, hardness, mechanical properties, fractogram*

Achievement of high values of ductility, impact toughness, strength and crack resistance of the welded joint in welding of high-strength hardening steels is a complicated task. It can be solved by lowering the rate of the joint cooling after welding by applying preliminary, concurrent and postweld heating, as well as multilayer welding [1 – 3], performance of furnace tempering after welding with minimal interval or without it, local treatment of the welded joint by the mains and high frequency currents, using fuel elements, different kinds of radiators, gas flame, solid fuel, etc. [4]. All these measures, however, make the process more complicated, increase the labour and energy consumption, lower the productivity, increase the cost of work performance, require the use of special heat sources, differing from the welding sources, thus limiting the ability to apply preheating, especially in fabrication of large-sized structures.

Known are the cases of application of the electron beam as the heat source for welding and subsequent local treatment of welded joint [5]. In arc welding plasma is also used for such treatment, but this requires special equipment. Argon-arc treatment allows improvement of the structure and properties, and increasing the fatigue life of welded joints at shock and cyclic loads [6]. In this case, treatment with partial melting of the metal is mostly used. The same process, but without partial melting, is so far applied on a limited scale, although it allows conducting surface hardening of gun barrels [7], and at a low speed of treatment also refining the joint metal structure and improvement of weld metal impact toughness [8]. The values of heating temperature, as well as the nature of change of the structure and properties of tempered base metal [9] essentially depend on the mode of arc treatment without partial melting. However, the use of these data for a welded joint is rather difficult, as the quenched and tempered, cast and rolled metals have their features of transformations in heating and cooling [10]. The associated difficulties increase in square-edge narrow-gap ATIG welding with deep penetration.

The aim of this study was to determine the possibilities and features of changing the structure of welded joint metal, hardened during welding, improvement of its mechanical properties, in particular toughness, by argon-arc treatment in different modes without melting. In this case, it is rational to refine the structure of the welded joint metal to achieve a favourable proportion of its components, as well as improve the stressed state of the metal at the expense of development of tempering and self-tempering processes.

30KhGSA (C – 0.28 – 0.34; Si – 0.9 – 1.2; Mn – 0.8 – 1.1 wt.%) steel joints 3 mm thick produced by tungsten electrode argon-arc welding without filler metal were studied. After welding the welded joint metal has a bainite-martensite hardening structure [8]. As the weld metal composition is close to that of the base metal, it allows analysing the transformations, proceeding in it in arc treatment, using the known diagrams [11, 12], derived for 30KhGSA steel, that is produced and rather widely applied in fabrication of welded structures in Ukraine and abroad.

Single-pass welding and the first pass in two-pass welding were performed by full penetration ATIG process. In the second pass, made with transverse oscillations of the electrode with 5 – 6 mm amplitude and 2 – 3 Hz frequency without the activating flux, the metal of the weld and the adjacent base metal areas were partially melted to the depth of 1.0 – 1.5 mm. Welding was performed in the following modes: I_1 = 130 – 180 A (in the first pass); I_2 = 110 – 160 A (in the second pass); v_w = 12 – 17 m/h. The welded joints were subjected 1 – 5 times to argon-arc treatment across their entire width without partial melting, by a tungsten electrode at the current I_{tr} =

Parameters of argon-arc treatment of welded joint

v_{tr}, m/h	I_{tr}, A	Sample side	T_h, °C	Cooling time, τ, s				w_{6-5}, °C/s
				up to 850 °C	up to 550 °C	up to 370 °C	up to 150 °C	
4.5	55 – 60	F	1200 – 1330	15 – 25	30 – 50	90 – 120	210 – 280	4 – 6
		R	1100 – 1200	14 – 17	20 – 30	60 – 80	140 – 180	10 – 12
12.5	80	F	950 – 1100	2 – 6	10 – 20	40 – 60	160 – 220	8 – 10
		R	730 – 910	≤ 1 – 3	8 – 12	20 – 40	110 – 150	20 – 22
37.0	100 – 105	F	930 – 1070	≤ 1 – 2	3 – 6	10 – 25	150 – 200	20 – 24
		R	500 – 650	–	–	–	90 – 140	–
80.0	145	F	730 – 900*	–	< 3*	3 – 10*	130 – 170	3 – 10*
		R	400 – 500*	–	–	–	70 – 120	–

Note: 1. F, R are the face and reverse side of the sample, respectively. 2. Values, marked by an asterisk, are extrapolated. 3. w_{6-5} is the rate of cooling in the temperature range of 600 – 500 °C.

= 55 – 145 A with the treatment speed v_{tr} = 4.5 – 80.0 m/h at the arc length of 8 – 9 mm. The electrode was imparted transverse oscillations with 7 – 9 mm amplitude (larger than in welding) and 2 – 3 and 3 – 4 Hz frequency at v_{tr} = 4.5 – 42.0 and 80 m/h, respectively. The absence of partial melting was determined by the absence of the metal pool, unchanged appearance of the joint surface, as well as measurement of the temperatures of thermal cycles of additional treatment of the metal in different modes (Table), that is partially described in [9].

The macro- and microstructure of the welded joint metal was studied in Neophot-32 microscope at 25-, 200-, 400- and 1000-fold magnifications after etching the sections in water solutions of ammonium persulphate, nital and picric acid. Hardness was determined by *HRC* scale at the load of 1500 N with averaging over five results, the microhardness — by a LECO hardness meter, at loads of 500 mN (for identifying the structural constituents) and 2000 mN (for determination of its zonal distribution). It should be noted that at greater load the readings are averaged and the scatter of their values becomes smaller. Phase composition was evaluated by volumetric changes, using a vacuum differential Shevenar dilatometer in heating 3 × 3 × 30 mm samples, cut out of the weld metal without machining its face surface, and of as-delivered base metal (after high tempering). Heating was conducted up to the temperature of 550 °C at the rate of 150 °C/h, which was followed by soaking for 1 h and cooling in air. Mechanical testing of welded joints was performed to GOST 699–66, using flat tensile samples, machined flush from the other side, with and without side recesses along the weld, as well as impact samples with a round notch. Fractures were studied in JEOL scanning microscope JSM-T200, when applying 25 kV accelerating voltage and at passage of probe current equal to 4 nA.

Argon-arc treatment was characterised by a short (several minutes) thermal cycle, given in the Table. It can be seen from the Table that the temperature of heating T_h the welded joint during this treatment in the given modes is essentially lower, than the melting temperature of 1460 – 1520 °C, which is also indicative of the absence of partial melting. The face side of the welded joint at v_{tr} = 4.5 – 37.0 m/h is deliberately heated above A_{c_3} temperature, this being accompanied by complete austenization of the metal. When v_{tr} = 80.0 m/h, the heating temperature may not reach A_{c_1} (735 °C), may exceed A_{c_3} (850 °C) or be in the range of $A_{c_1} - A_{c_3}$, thus resulting in the absence of austenization, incomplete or complete austenization, especially in the periphery of the treatment zones, along which alternating areas are located, that were formed at different specific powers of the arc and duration of its impact. Current increase is used to achieve a deliberately complete austenization that can be avoided by lowering the current. From the reverse side of welded joint, the heating temperature and the possibility of metal austenization are determined by the treatment speed: at v_{tr} = 4.5 m/h metal austenization invariably takes place; at v_{tr} = = 12.5 m/h it may or may not occur (heating temperature is close to A_{c_1} and A_{c_3}); in the case of $v_{tr} \geq$ ≥ 37.0 m/h it is absent. Metal austenization process is essentially shortened with the increase of the treatment speed.

Depending on heating temperature and composition (within the grade composition range) of 30KhGSA steel, according to diagrams from [11, 12], the values of temperatures of minimal resistance of austenite to diffusion and intermediate transformations are close to 650 and 550 – 400 °C, the time of cooling to the above temperatures being not less that 3 – 10 and 2 – 10 s, respectively, whereas the temperature of the beginning of martensite transformation M_b = 320 – 370 °C is reached in 2 – 15 s. Martensite transformation is practically absent at w_{6-5} = = 1.5 – 2.0 °C/s and less, but prevails at $w_{6-5} \geq$ ≥ 40.0 °C/s.

Cooling at argon-arc treatment occurs 3 – 40 times faster (depending on the treatment speed), than in welding, after making the second pass at w_{6-5} = 1.5 – 2.5 and 3.0 – 5.0 °C/s from the face and the reverse side of the sample, respectively, and the hardening

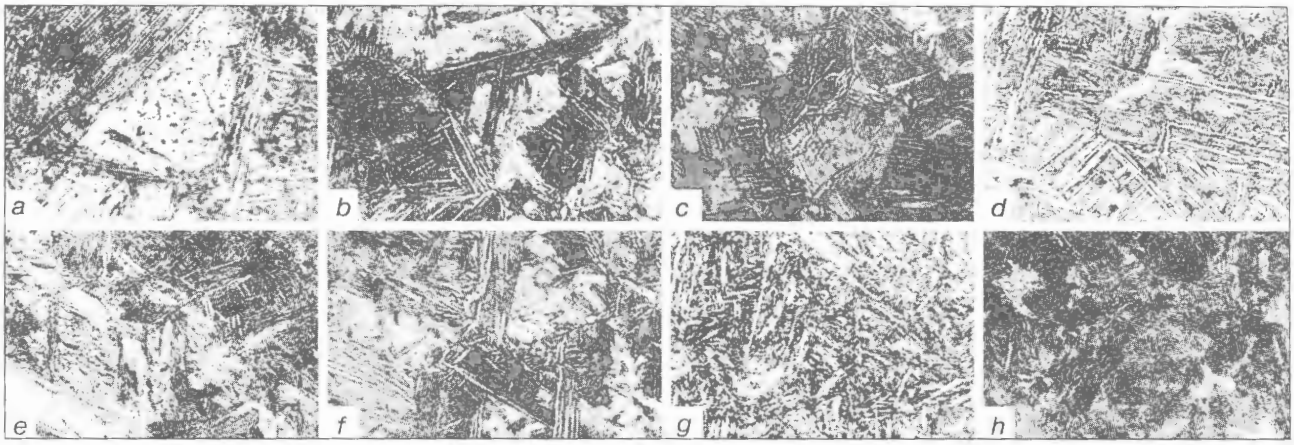

Figure 1. Microstructure of weld metal from the face (*a* – *d*) and reverse (*e* – *h*) sides prior to (*a*, *e*) and after argon-arc treatment at the speed of 4.5 (*b*, *f*), 12.5 (*c*, *g*) and 37.0 (*d*, *h*) m/h (×500)

structure is formed. The time and rate of cooling in treatment are such (see Table), that diffusion transformation of austenite is absent, but the following transformations are possible: bainite at v_{tr} = 4.5 – 12.5 m/h, bainite or martensite at v_{tr} = 37.0 m/h, predominantly martensite at v_{tr} = 80.0 m/h.

Therefore, in argon-arc treatment with heating above A_{c_3} temperature the metal of the welded joint face side is subjected to repeated hardening. From the reverse side at $v_{tr} \leq 12.0$ m/h, it can be complete or incomplete, and at $v_{tr} \geq 17.0$ m/h, it is absent. The metal heated below A_{c_1}, undergoes tempering, with its maximal temperature increasing with decrease of treatment speed.

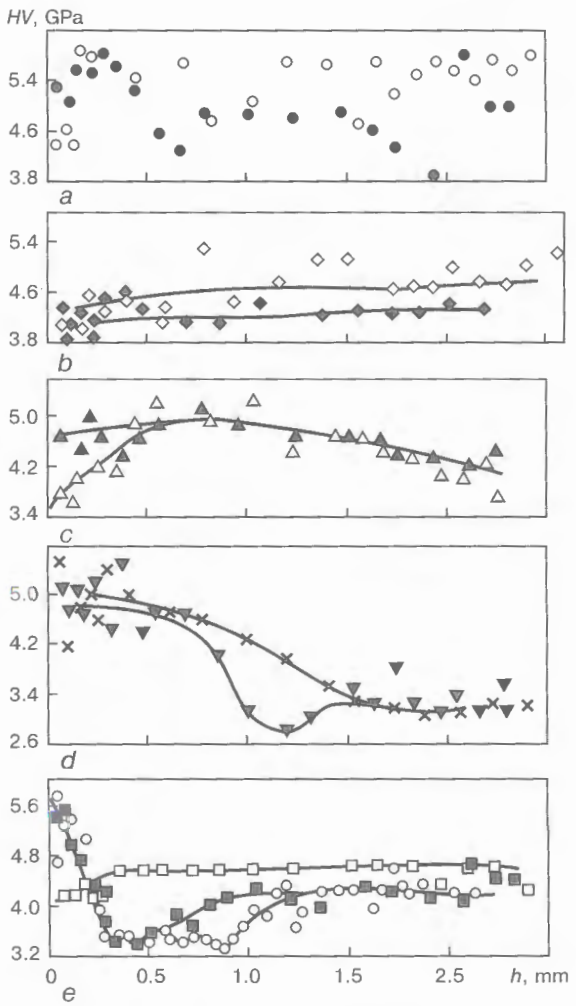

Figure 2. *HV* microhardness distribution by height *h* of the weld (●, ◆, ▲, ▼, ■) and HAZ overheated zone (○, □, △, ×, ✧) of the joint as-welded (*a*) and after argon-arc treatment at the speed of 4.5 (*b*), 12.5 (*c*), 37.0 (*d*) and 80.0 (*e*) m h

The time of cooling the face and reverse side of the welded joint sample to the temperature of 150 °C, taken to be the lower boundary of essential structural changes in the metal, is equal to 130 – 280 and 70 – 180 s, respectively. It becomes shorter with the increase of treatment speed. The time of cooling to the temperature of 320 °C, when self-tempering of the repeatedly quenched metal occurs, is 100 – 180 and 50 – 100 s, respectively, and natural cooling to room temperature takes several minutes. The above data can lead to the conclusion that a more complete running of the processes of tempering and self-tempering of the metal being treated can be anticipated in the case of decreasing the treatment speed.

Weld metal microstructure and microhardness distributions in the welded joint after welding and argon-arc treatment are given in Figures 1 and 2.

In as-welded condition the microstructure of the weld metal and the overheated zone of the HAZ is a coarse-crystalline bainite-martensite mixture, i.e. is a hardening structure (Figure 1, *a*, *e*). Needles of upper and lower bainite in the light-coloured matrix of martensite are visible in the metal microstructure across the entire weld thickness. Microhardness *HV* 3.8 – 5.8 GPa of the weld metal and HAZ overheated zone changes only slightly along its height and has a great (2 GPa) scatter of values. A certain lowering of microhardness of the HAZ overheated zone is observed from the face side of the sample to 0.15 mm depth (Figure 2, *a*). Weld metal hardness from the face and the reverse side is *HRC* 51.0 and 51.9, respectively, and the austenite grain size in the HAZ overheated zone is 5 – 6 points.

After treatment at the speed of 4.5 m/h, accompanied by heating of the entire joint above A_{c_3} temperature, the microstructure of the weld metal and the HAZ overheated zone becomes refined and is a mixture of slightly etching zones of martensite with

upper bainite needles. Microhardness of the weld metal along the entire height is equal to *HV* 3.8 – 4.6 GPa, HAZ overheated zone has *HV* 4.0 – 4.6 GPa from the weld face and *HV* 4.6 – 5.3 GPa from the reverse side (see Figure 2, *b*), and the weld hardness from the face and reverse side is equal to *HRC* 39.8 and 42.7, respectively, this being, on the whole lower than in as-welded condition. The lower hardness from the face side of the sample is due to a lower cooling rate at intermediate transformation of austenite (see Table). The size of the austenite grain of the metal in the HAZ overheated zone has the tendency to increase up to 5 points.

After treatment at v_{tr} = 12.5 m/h, the microstructure of the weld metal and HAZ overheated zone has the form of a mixture of martensite, upper and lower bainite (see Figure 1, *c*, *g*) that remains in the upper part of the welded joint. The amount of upper bainite is somewhat reduced, columnar crystallites are refined, and dendritic structure of the metal is transformed into a disoriented structure of equiaxed grains as a result of heating. The weld lower part preserves the structure of coarse needles, and decomposition is found in the deeply-etching somewhat blurred needles that can be seen by development of roughness caused by the presence of fine cementite particles. The boundaries of austenite grain of the HAZ overheated zone are more difficult to etch out, and its size is 5 – 6 points.

Hardness of weld metal, treated at v_{tr} = 12.5 m/h is *HRC* 48.2 (from the face) and 39.4 (from the reverse side), i.e. it is lowered compared to the initial one (especially, from the reverse side of the sample). Microhardness of the welded joint metal is, in general, also reduced (see Figure 2, *c*): in the weld metal it is equal to *HV* 4.3 – 5.1 GPa, and in the HAZ overheated zone to *HV* 3.5 – 5.3 GPa. The largest values of it are found at the depth of 0.5 – 1.0 mm with a gradual decrease towards the face and reverse surfaces of welded joint.

Change of the microstructure with preservation of a quite high hardness of the weld metal from the side of its face, is the result of heating deliberately higher than A_{c_3} up to the temperatures of elimination of the structural heredity [13] with further hardening in cooling at the rate of 8 – 10 °C/s. In the metal of the weld reverse side, heated up to temperatures close to A_{c_1} and A_{c_3}, a change of its microstructure and lowering of its hardness, are caused by a pronounced intensification of tempering processes at temperatures close to A_{c_1}, incomplete hardening from the intercrystalline interval, increase of M_b temperature and of the time of the martensite component self-tempering, as a result of the higher temperature of the start of intermediate transformation of less stabilised austenite and intensification of diffusion redistribution of carbon in it.

Subsequent increase of treatment speed up to 37.0 m/h leads to refinement and violation of the acicular nature of the welded joint metal microstructure only from its face side (see Figure 1, *d*, *h*), where a reduction of the austenite grain size in the HAZ overheated zone to 7 points is found. The microstructure is identified as a mixture of martensite with lower bainite, and a small amount of upper bainite. Gray granular needles of upper bainite and tempered martensite are visible in the metal microstructure from the reverse side of the weld.

After treatment the weld metal has the hardness of *HRC* 49.9 from the face side, close to the initial value in as-welded condition, and from the reverse side it is equal to *HRC* 40.6. Characteristic zones form along the weld height (see Figure 2, *d*). The first zone of higher microhardness *HV* 4.2 – 5.4 GPa extends from the weld face to the depth of 0.5 – 0.8 mm. The second zone, where the microhardness is lowered to *HV* 3.3 – 3.5 GPa, is located at the depth of 0.8 – 1.5 mm; a microhardness dip to *HV* 2.8 GPa is found within it at the depth of 1.0 – 1.3 mm. In the third zone at the depth of more than 1.5 mm the microhardness varies but slightly, in the range of *HV* 3.1 – 3.5 GPa. Therefore, the welded joint metal is subjected to repeated hardening only from the face side, and is tempered from the reverse side. Increased cooling rate (20 – 24 °C/s) of the repeatedly hardened metal (see Table) is responsible for a relative increase of its microhardness (compared to treatment at v_{tr} = 4.5 and 12.5 m/h).

Subsequent increase of the welded joint treatment speed to v_{tr} = 80.0 m/h at a 1.5 times increase of current, causes a reduction (to 0.2 – 0.3 mm) of the thickness of the repeatedly hardened metal layer of the welded joint in the sites of direct impact of the arc and increase of its microhardness to *HV* 5.3 – 5.7 GPa. An increase of the thickness of the welded joint metal layer, tempered from the reverse side and microhardness dips to *HV* 3.3 – 3.6 GPa, both in the metal of the weld and of the HAZ overheated zone are observed. In our opinion, these dips are a manifestation of zonal decarburization of the metal heated up to the temperatures, close to A_{c_1} at interphase redistribution of carbon. In the places of indirect impact of the arc on the HAZ overheated zone, where the metal is heated below the austenization temperatures, the areas of repeated hardening and microhardness dip, are absent, and just a lowering of the metal microhardness at the welded joint surface is observed, this being the result of tempering. Hardness lowering over the entire face of the welded joint can be achieved by lowering the current and increasing the treatment speed (the latter is less rational because of an abrupt increase of the nonuniformity of heating the welded joint metal, heating depth, and shortening of the time of its staying in the heated condition). In terms of surface strengthening, a small increase of current and lowering of the speed of treatment for heating deliberately above A_{c_3}, are admissible.

Performed dilatometric studies confirm the fact of the weld metal hardening after welding and subsequent argon-arc treatment at v_{tr} = 4.5 and

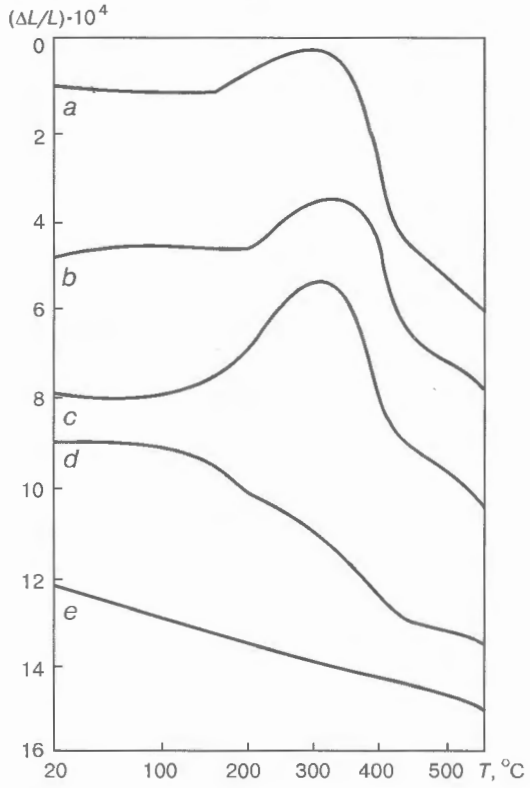

Figure 3. Dilation curve of the weld metal ($a - d$) and tempered base metal (e): $a - d$ — see designations in Figure 1; $\Delta L / L$ — relative change of sample length

12.5 m/h, this being manifested in violation of a monotonic change of sample length in heating (see Figure 3, $a - c$). The dilation curves demonstrate temperature regions of residual austenite transformation into martensite with the increase of the metal volume. Regions of carbide transformation at the temperature of 300 – 400 °C and regions of carbide coagulation at the temperature of 430 – 550 °C are superimposed on them. The dilatometric effects of residual austenite transformation confirm the presence of bainite in the structure.

Argon-arc treatment at v_{tr} = 4.5 and 12.5 m/h increases the amount of residual austenite in the weld metal by 3.0 – 3.5 and 7.5 %, accordingly, and also changes the temperature of the start of its transformation into martensite from 170 to 200 and 100 °C, respectively. It should be noted that in treatment at v_{tr} = 12.5 m/h the weld metal from the reverse side

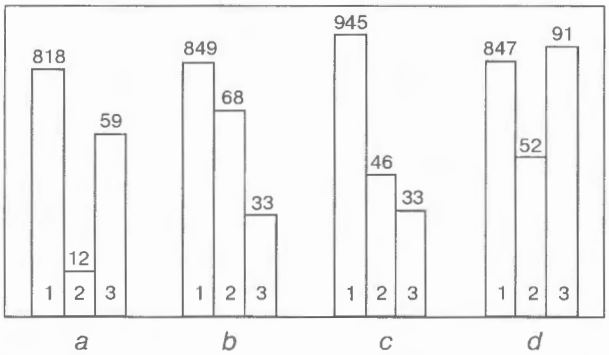

Figure 4. Mechanical properties of welded joint prior to and after treatment at v_{tr} 12.5 m/h: *1* — σ_t^w (MPa); *2* — a_n^w (J/cm^2); *3* — a_n^{HAZ} (J/cm^2); $a - d$ — see designations in Figure 1

is subjected to short-term tempering with residual austenite decomposition, and its amount in the repeatedly hardened metal is actually greater, than 8 %. Increase of the content of residual austenite in the metal with the bainite-martensite structure is indicative of the increase of the fraction of the bainite component at the expense of reduction of martensite fraction [13, 14]. This is confirmed by weaker dilatometric effect of carbide transformation.

As we envision it, the residual austenite content after such treatment increases due to lowering of the austenite stability compared to austenite, formed during solidification of the weld metal, and increase of the temperature of the start of intermediate transformation. The process of residual austenite formation becomes more intensive with the increase of the treatment speed from 4.5 to 12.5 m/h, because of lowering of the heating temperature by 230 – 250 °C and of austenization duration by 4 to 7 times (see Table). A slight increase of the residual austenite fraction can be accompanied both by further increase of its carbon content, and an increase of its stability. At the increase of residual austenite fraction by 2.5 to 2.7 times, its carbon content decreases, which results in lowering of the temperature of the start of austenite decomposition. Increase of the fraction of ductile structural constituents (bainite, residual austenite) in the hardened metal, should have a positive influence on the increase of ductility and impact toughness of a high-strength steel welded joint.

The dilation curve of a weld metal sample treated at v_{tr} = 37.0 m/h, differs essentially from the earlier described ones and is greatly similar to the dilation curves of tempered base metal (see Figure 3, *d*, *e*). However, a short horizontal section of the curve in the temperature region up to 100 °C and a step in the temperature interval of 200 – 250 °C are evidence of the presence of a small (about 0.5 %) amount of residual austenite in the sample. In the repeatedly hardened metal proper, with its layer thickness equal to 1/4 – 1/3 of the joint thickness, the residual austenite content is 1.5 – 2.0 %. Increase of the weld metal cooling rate by an order of magnitude, compared to the welding conditions (see Table), causes a lowering of the intermediate transformation temperature, 1.5 – 2.0 times lowering of the content of residual austenite and visually observed upper bainite (see Figure 1), and promotes an essential increase of the martensite component fraction in the structure of martensite-bainite mixture [13]. Weakening of the process of bainite transformation is a prerequisite to less carbonization of the non-transformed part of austenite, relative increase of M_b point and self-tempering temperature of the formed martensite.

The results of metallographic and dylatometric studies of welded joints of 30KhGSA steel indicate that in argon-arc treatment in different modes, the metal of the weld and HAZ overheated zone undergoes such transformations which may result in an improvement of the metal ductility and impact toughness.

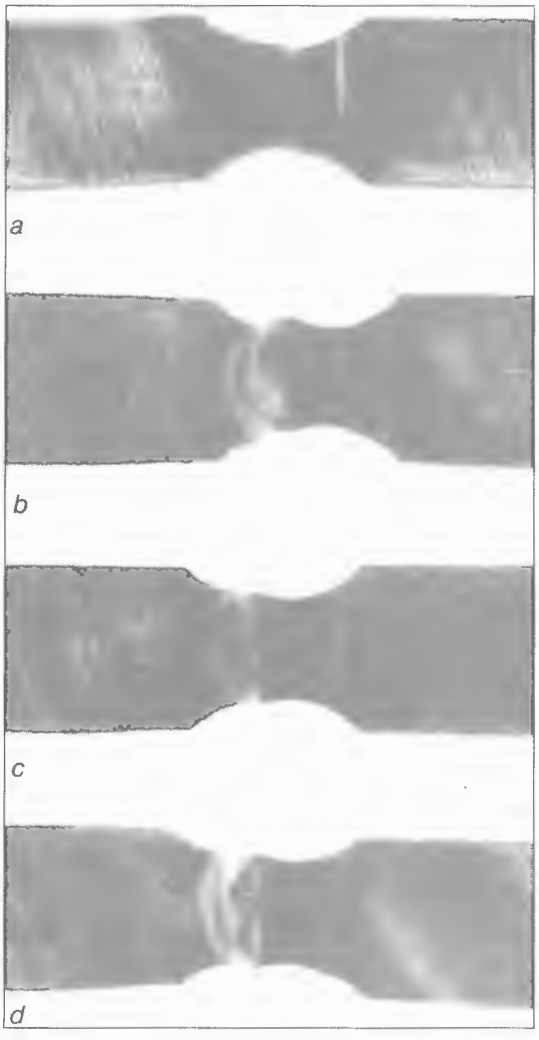

Figure 5. Welded samples after tensile testing (see designations in Figure 1)

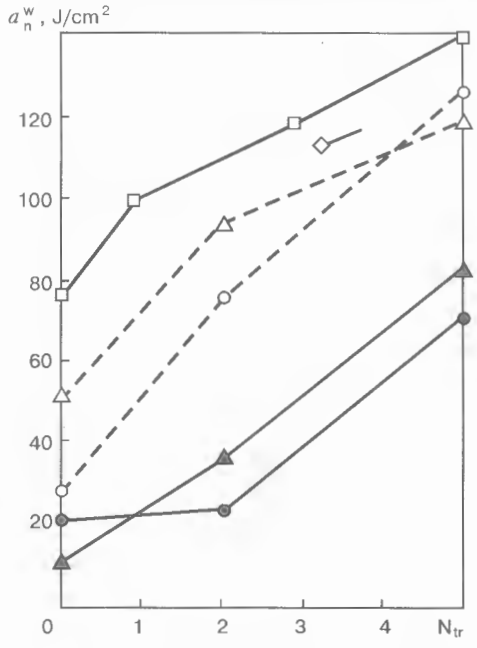

Figure 6. Influence of the number of operations, N_{tr}, of argon-arc treatment with different speeds on impact toughness a_n^w of the metal of single- (▲, ●) and two-pass (❐, ✧, Δ, ○) welds: ❐ 42.0; ✧ – 80.0; Δ, ▲ – 6.0; ○, ● – 17.0 m/h

The results of mechanical testing of welded joints in as-welded condition and after 1 – 5 times argon-arc treatment at v_{tr} = 4.5 – 80.0 m/h are given in Figures 4 and 5. The high strength of welded joint metal hardened during welding, predetermines constant cross-section samples failing beyond the weld in the less strong base metal. Samples with side recesses, not subjected to argon-arc treatment, fail in the smallest section of the weld with formation of tears in the HAZ metal in many cases (see Figure 4, *a*) with σ_t^w = 760 – 818 MPa (depending on the welding mode). After argon-arc treatment in different modes fracture runs beyond the welds (see Figure 4, *b* – *d*). This is indicative of a higher strength (σ_t^w > 703 945 MPa), than that of the base metal with a certain increase of ductility, as well as lowering of the weld metal sensitivity to stress raisers.

Impact toughness of the metal of a welded joint on hardening steel has low values in as-welded condition, especially in the weld center (Figures 5, *a* and 6). It is definitely improved after argon-arc treatment within a wide range of speeds (4.5 – 80.0 m/h) and increases with the number of treatment operations. It is notable that in treatment accompanied by metal

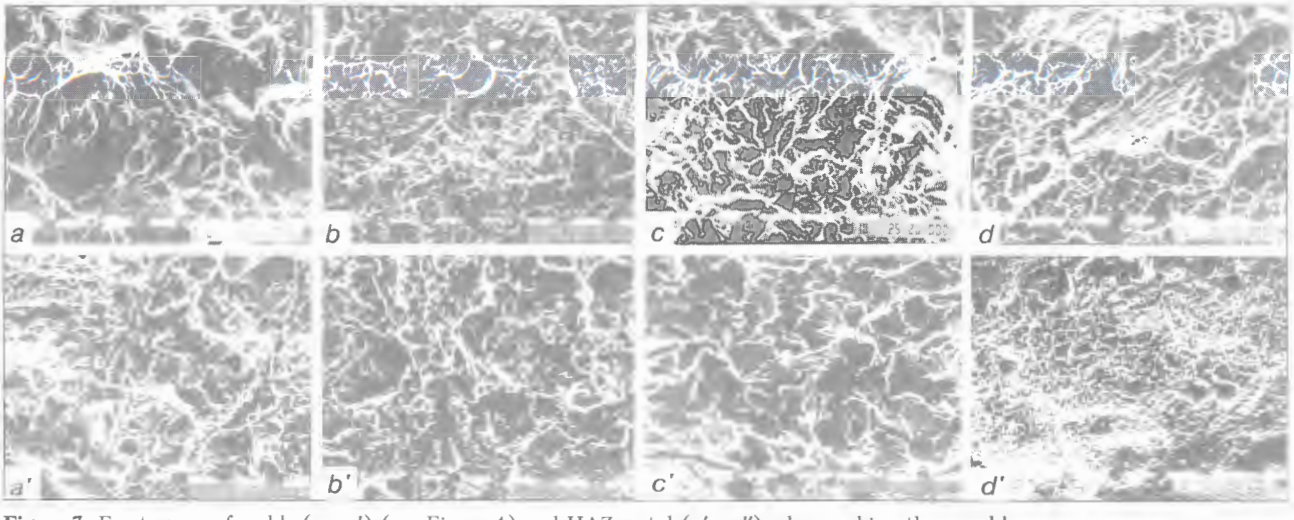

Figure 7. Fractogram of welds (*a* – *d*) (see Figure 1) and HAZ metal (*a'* – *d'*) when making these welds

tempering (v_{tr} = 37.0 – 80.0 m/h), the weld metal has high impact toughness values. Tempering of the metal of HAZ overheated zone predominantly at v_{tr} = = 80.0 m/h can be the reason for the greatest increase of the values of its impact toughness.

Positive influence of argon-arc treatment on impact toughness correlates well with the results of fractographic studies of the fracture sites (Figure 7). If in as-welded condition the fracture surface of a weld is coarse-crystalline with a few isolated zones of tough fracture, after argon-arc treatment the crystallite dimensions are reduced, and the number of plastic deformation areas is greatly increased. After argon-arc treatment at v_{tr} = 12.5 and 37.0 m/h the fracture surface has many facets, revealing a tough mode of fracture.

Increase of impact toughness and ductility of the metal of welded joint on quenched steel provides indirect evidence of structural stresses lowering and the possibility of improvement of the cold cracking resistance. Simultaneous preservation of a high strength ensures improved load-carrying capacity of the welded joint and its performance at cyclic loading.

CONCLUSIONS

In argon-arc treatment without partial melting, the metal of the welded joint hardened during welding, undergoes repeated hardening in the areas of heating up to the austenization temperatures and tempering in less heated regions. The nature and completeness of the transformations, formation and dimensions of the zones of repeated hardening and tempering are controlled by current and treatment speed. It allows refinement and transformation of the metal structure from the cast into the granular structure, change of its phase composition, controlling the hardness of different zones of the welded joint of hardened steel. Argon-arc treatment allows improvement of ductility and impact toughness, of the fracture mode, lowering the sensitivity to stress raisers with preservation of a rather high strength of welded joints. In order to enhance the positive effect of argon-arc treatment, it is rational to increase the number of treatment cycles. It can be anticipated that local treatment by the arc, especially in the mode of predominant tempering, will allow simplification, as well as partial or complete elimination of intermediate or subsequent furnace tempering operations.

REFERENCES

1. Kozlov, R.A. (1979) On weldability of heat-resistant steels. *Svarochnoye Proizvodstvo*, **2**, 12 – 15.
2. Makarov, E.A. (1981) *Cold cracks in welding of alloyed steels*. Moscow: Mashinostroyeniye.
3. Bursky, G.V., Savitsky, M.M., Novikova, D.P. (1998) Resistance of the HAZ of welded joints of hardening high-strength steels to delayed fracture in twin-arc welding. *Avtomaticheskaya Svarka*, **2**, 12 – 15.
4. Vinokurov, V.A. (1968) *Tempering of welded structures to lower stresses*. Moscow: Mashinostroyeniye.
5. Pavlov, A.S., Zakharov, V.I., Skorobogatov, I.V. *et al.* *Process of electron beam welding*. USSR author's certificate **1792035**, Int. Cl. B 23 K 15/00. Publ. 1996.
6. Asnis, A.E., Ivashchenko, G.A., Frenkel, I.Kh. *et al.* (1980) Argon-arc treatment – a potential for lowering the metal content of welded structures. *Avtomaticheskaya Svarka*, **6**, 69 – 70.
7. Bondarenko, L.I., Puzrin, L.G. (2000) Argon-arc surface quenching – method for hardening artillery barrels. *The Paton Welding J.*, **2**, 33 – 34.
8. Kulik, V.M., Savitsky, M.M., Novikova, D.P. *et al.* (1999) Investigation of arc treatment of high-strength steel welded joints. *Avtomaticheskaya Svarka*, **5**, 19 – 24.
9. Kulik, V.M., Bursky, G.V., Savitsky, M.M. (2000) Features of arc treatment of hardening steels without melting. *Ibid.*, **5**, 31 – 35
10. Grabin, V.F., Denisenko, A.V. (1978) *Metallurgy of welding low- and medium-alloyed steels*. Kyiv: Naukova Dumka.
11. Popov, A.A., Popova, L.E. (1965) *Isothermal and thermokinetic diagrams of decomposition of overcooled austenite*. Refer. Book. Moscow: Metallurgia.
12. Shorshorov, M.Kh., Belov, V.V. (1972) *Phase transformations and changes of the properties of steel in welding*. Atlas. Moscow: Nauka.
13. (1983) *Metals science and heat treatment of steel*. Refer. Book. Ed. by M.L. Bernshtein, A.G. Rakhshtadt. Moscow: Metallurgia.
14. Popov, A.A. (1963) *Phase transformations in metal alloys*. Moscow: Metallurgizdat.

ANALYSIS AND CLASSIFICATION OF PLATE WAVEGUIDES FOR ULTRASONIC WELDING OF POLYMERS AND POLYMER-BASED COMPOSITES

N.P. NESTERENKO[1] and **I.K. SENCHENKOV**[2]
[1]The E.O. Paton Electric Welding Institute, NASU, Kyiv, Ukraine
[2]S.P. Timoshenko Institute of Mechanics, NASU, Kyiv, Ukraine

ABSTRACT

A classification and systematized approach to selection of plate waveguides used as tools for ultrasonic welding of polymers and polymer-based composites have been proposed. The known types of long-contour tools have been considered and new types have been suggested.

Key words: *ultrasonic welding, polymers and polymer-based composites, plate waveguides-tools, oscillation modes, classification*

Ultrasonic oscillations, widely applied in engineering, medicine and other areas, are characterised by a low frequency and high power [1, 2]. The schematic of excitation of mechanical oscillations in typical process units for ultrasonic welding (USW) is given in Figure 1. Generator *1* converts standard frequency electric oscillations into high-frequency oscillations (20 – 40 kHz). Converter *2*, incorporating piezoactive components, transforms these electric oscillations into mechanical oscillations. Booster *3* and waveguide-tool (sonotrode) *4* are passive resonance elements of the system and serve for transferring the wave energy from the converter to the object being processed, namely parts being welded *5*. They simultaneously fulfil the functions of amplifying the oscillation amplitude and co-ordinating the generator — converter subsystem with the load [1].

In USW units [3] boosters are sufficiently versatile components. They have the shape of half-wave step concentrators. Batch-produced units for press USW usually come complete with a set of boosters with different coefficients of displacement transformations.

Sonotrode configurations determined by the shape of the welds in specific parts, are highly diverse due to a wide range of items being welded. Each new item, as a rule, requires development of a new sonotrode. Two main requirements are made of these elements: presence of a resonance at a certain frequency; resonance mode of motion, depending on the method of applying oscillations to the item, should be characterized by a uniform distribution of the normal or tangential components of displacements on the working surface. Additional requirements include the following: specified coefficient of displacement amplification, cyclic strength, tuning out parasitic frequencies, low level of vibration heating, etc.

The design problem consists in determination of the sonotrode configuration by the specified weld shape, that will meet the above requirements. Solution of this problem is essentially simplified if a sufficiently representative and systematised base of reference configurations, having the specified frequency-modal characteristics, is available.

Analysis of published sources [1, 3, 4] shows that the diverse passive resonance elements of the acoustic systems for process applications can be grouped into several classes. The elements are classified into a particular class based on the ability of interpreting the motions realized in them by certain sections of the curves of the resonance spectrum for a certain body of finite dimensions [5]. It turns out that a rather complete set of motions can be formed on the basis of the spectra of symmetrical modes of oscillation of a rectangle.

A positive effect of sonotrode classification is determined by two circumstances. First, well-studied and systematized types of motion in a rectangle or a cylinder facilitate the understanding of the nature of motion in the elements and outlining the methods of their frequency-modal control. Secondly, the information contained in the spectra, allows making practical use of some oscillation modes, having useful

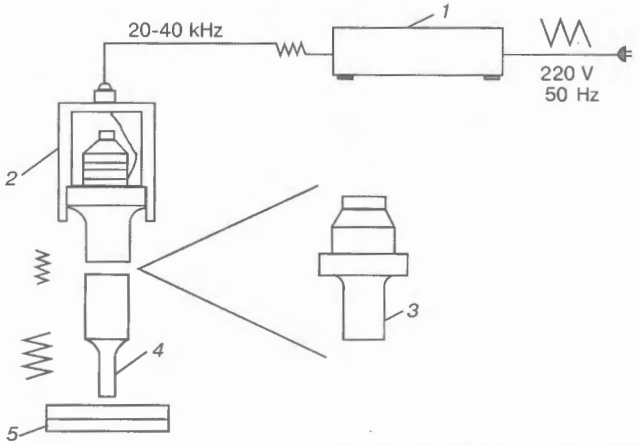

Figure 1. Schematic of an acoustic system for USW of polymers and polymer-based composites (for designations see the text)

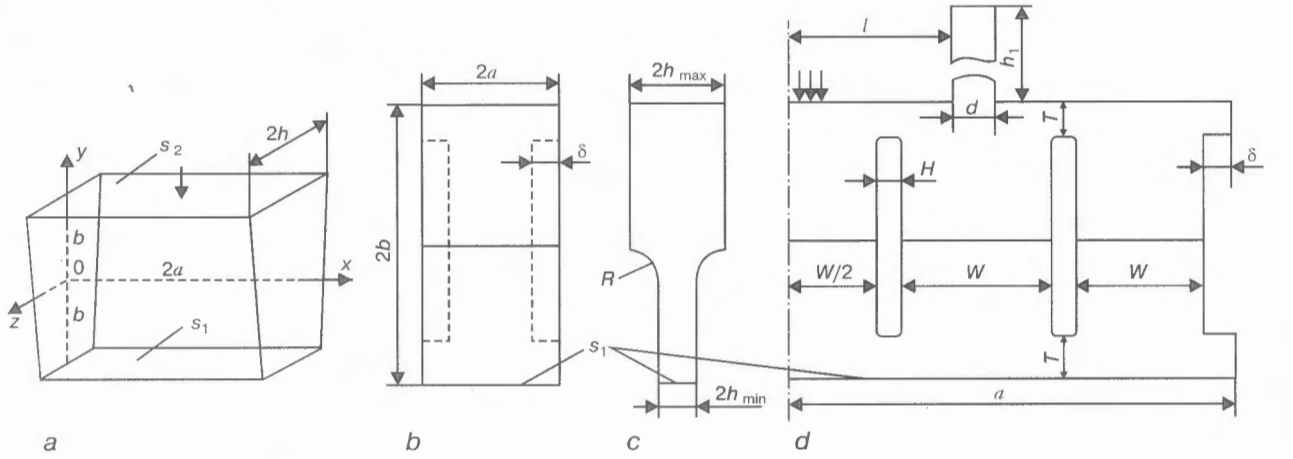

Figure 2. Shapes of solid (a – c) and sloted (d) plate sonotrodes

properties. This study is devoted exactly to formation of a system of basic configurations of plate sonotrodes, as well as their classification.

For plate sonotrodes (Figure 2) it is assumed that the characteristic size by thickness (in the direction of $0z$ axis) is essentially smaller, than the dimensions in plan and simultaneously smaller, than the characteristic wave length λ. Since at early stages of ultrasonics development the acoustic systems were synthesised of rod elements, λ is usually taken to be the length of the longitudinal wave in a thin rod for a certain frequency f: $\lambda = (E/\rho)^{1/2}/f$, where E is the Young's modulus and ρ is the material density.

The problem of sonotrode design is defined more specifically as follows: to determine the remaining geometrical parameters by the specified values of the emitting edge length (weld length), resonance frequency f_r, coefficient of amplification k_i of normal displacements from a certain point A on S_2 to point B on S_1 and coefficient of homogeneity k_h (for S_1), equal to

$$k_i = |u_{yB}/u_{yA}|, \quad k_h = u_{y\,\min}/u_{y\,\max}. \qquad (1)$$

Let us consider the main types of plate sonotrodes and methods of their modal control. The elements in the form of single-tie plates of a variable cross-section (Figure 2, b, c) at $2a \le \lambda/3$ and at $2a \cong \lambda/3$ ensure quasi-reciprocating motion of working edge S_1 with uniformity $k_h \ge 0.8$ and amplification $k_i \cong h_{\max}/h_{\min}$. Coefficient k_h quickly decreases at $2a \le \lambda/3$, while at $2a \cong \lambda/2$ two nodal points of u_y distribution appear on edge S_1. However, the side recesses, shown by dashed lines in Figure 2, b, allow increasing the degree of uniformity up to $k_h \cong 0.95$ for $\lambda/3 \le 2a \le \lambda/2$ at insignificant (less than 3 – 4 %) change of the resonance frequency. The possibilities of the above method are quickly exhausted with further increase of width. In elements of greater length ($2a > \lambda/2$) the planar modes of oscillation with quasi-reciprocal distribution of u_y on S_1 surface are formed by means of a number of narrow slots (Figure 2, d) normal to the emitting edge [4, 6]. This provides decomposition of the longitudinal and transverse planar motions, and the sought mode is formed of co-phase longitudinal (usually, half-wave) modes of a set of interslot segments of width $W \le \lambda/3$, i.e. is essentially multilongitudinal. Such shapes have a rather high level of uniformity u_y of distribution of displacements over surface S_1 for engineering applications. The influence of parameters W, S, T and δ on modal characteristics is rather complicated. The results of numerical and experimental studies revealed that for each plate configuration there are optimal values of the above parameters that maximize k_h coefficient. These values vary in the following ranges:

$$W \cong \lambda/5 - \lambda/4, \quad H \cong \lambda/24, \quad T \cong \lambda/12 - \lambda/9.$$

For plates of length $\lambda/2 < 2a < 3\lambda/2$ the uniformity of displacement distribution can be enhanced by using side recesses ($\delta > 0$) or protrusions ($\delta < 0$). The above methods are insufficient at $2a > 3\lambda/2$. Value k_h can be increased by the use of the method of additional small oscillatory systems (ASOS) [6]. The method, essentially, consists in connecting to the upper (non-working) edge of the sonotrode, small oscillatory systems, for instance, rods that increase the uniformity of distribution u_y on working edge S_1. Rod length usually varies in the range of $\lambda/4 < h_1 < \lambda/2$. Parameters and location of the rods are the subject of the problem of optimisation by k_h maximum criterion [7].

On the other hand, the capabilities of slot waveguides are limited. First, at $2a > 2\lambda$ the ASOS technique becomes too complicated, both in its methodological and computational aspects. Secondly, the slots lower the flexural rigidity of the element that essentially densifies the spectrum of parasitic planar modes close to the frequency of the multilongitudinal (working) mode. Thirdly, the presence of slots creates a stress concentration and is the main cause for fatigue fracture of such elements.

A fundamentally new class of extended sonotrodes is proposed in [8]. In these elements the resonance movement with the quasi-reciprocal motion on their long sides, is based on a symmetric mode of thickness resonance of an infinite layer. Similar to the case of slot elements, the possibility is established of a significant increase of the uniformity of displacements

Types of plate waveguides

Type of oscillations	*Type of sonotrode*	*Configuration*
L	L_k	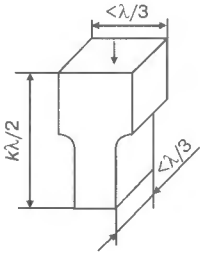
	$pmK_k^{(\alpha)}$	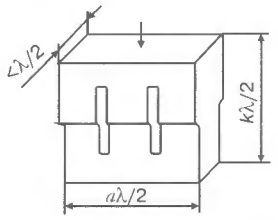
	$pmK_k^{(\alpha)}$ (β)	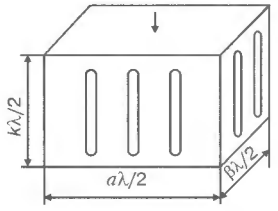
T	$T_k^{(\alpha)}$	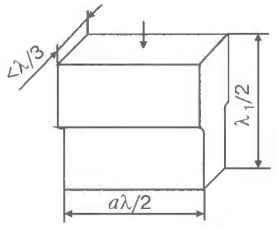
B	pB_k	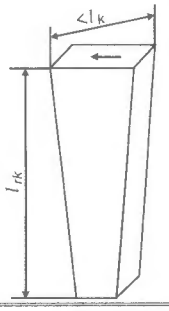

on long edges by ASOS method. More specific determination of the sonotrode geometry can be regarded as the problem of optimal multicriterial design. Studies [9, 10] are devoted to development of this area.

Oscillation types in the considered sonotrodes can be correlated with the modes of oscillations, corresponding to certain sections of the branches of the resonance spectrum of symmetric oscillations of a rectangle with sides $|x| \le a$, $|y| \le b$ under the conditions of a plane stressed state. Such a spectrum for Poisson's ratio $\nu = 0.34$ is given in Figure 3. In this case Ω is the dimensionless frequency, equal to $2\omega b/(\pi C_2)$; ω is the circular frequency of oscillations; C_2 is the shear wave velocity, equal to $\sqrt{G/\rho}$; G is the shear modulus and $c = a/b$.

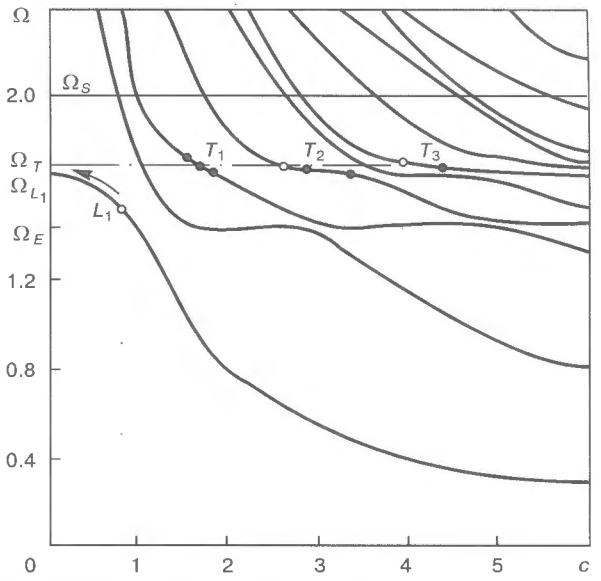

Figure 3. Characteristic sections of the frequency spectrum of symmetric modes

Four characteristic frequencies can be singled out in the considered frequency range (Figure 3). For section L_1 frequency $\Omega_{L_1} = \sqrt{2(1+\nu)} \cong 1.63$, this corresponding to the half-wave resonance of the rod. Analysis shows that distributions of resonance displacements and stresses in half-wave and wave plate sonotrodes (see Figure 2, *b*, *c*) are identical to the modes in sections L_1 and L_2 of the first two branches of the rectangle spectrum. The same sections of the curves are the basis for forming the multilongitudinal modes in plate and cubic slot sonotrodes. Frequency $\Omega_E \cong 1.43$ of a series of lower plateau corresponds to the edge mode, characterised by localisation of the kinematic and dynamic parameters in the nodular point vicinity [5]. Edge modes in plate sonotrodes have so far found no application. Fourth frequency $\Omega_T = \sqrt{2(1-\nu)(1-2\nu)} \cong 1.73$ is the frequency of the second series of plateau T_1, T_2, ... , along which the quasi-thickness oscillation mode is implemented. Characteristic features of this mode allow development of extended sonotrodes with nodeless distribution of normal displacements over the working surface. So, the center of plateau T_1 corresponds to value $c = 1.5$, T_2 — 2.9, and T_3 — 4.0. In this case, for instance, expression $2a \ge 2\lambda$ corresponds to plateau T_3. With the increase of the plateau number, however, the spectrum becomes denser, thus making it more difficult to tune out the adjacent thickness-shear and flexural modes. Second plateau T_2 looks the most attractive from this point of view.

The elements on flexural modes are used for tangential application of oscillations to the load in the case of ineffectiveness of normal application, for instance, in USW of metals or thin films [11, 12].

Based on the modal criterion and taking into account the above considerations, a classification and marking of the sonotrodes, shown in the Table, can be proposed. Element type is determined by motion mode, namely longitudinal (multilongtitudinal), thickness or flexural and is designated by letters *L*,

T and B. The lower index corresponds to the number of the branch or plateau of the frequency spectrum. For longitudinal modes it shows the number of half-waves, that fit in by the element height. Slot sonotrodes based on multilongitudinal mode, are identified as pmL_k. Letter p indicates that these elements are limited by plane surfaces. Numerical information about their length, determining the weld size, is given by the upper indices.

Plate elements of $2h_{max} \le \lambda/2$ thickness, have one row of slots, and used for them is one index α that determines the number of half-waves contained in element length $\alpha = 2a/(\lambda/2)$. Cubic bodies with $2h_{max} \ge \lambda/2$ have two series of crossing slots. The second upper index is used to more precisely determine their size by thickness $\beta = 2h_{max}/(\lambda/2)$. The element is oriented so that inequality $\alpha \ge \beta$ were satisfied.

For completeness of classification, let us define sonotrodes of S type with characteristics of thickness-shear resonance layer. Such motions are implemented in the central parts of the third series of the plateau that is formed in the vicinity of frequency $\Omega_S = 2.0$ at $c \ge 10$. Prevalence of tangential component of motion on the long sides of the rectangle is characteristic of S-mode. This quality comes useful in long-contour welding of rigid or sheet items. It should be noted that this part of the spectrum is insufficiently studied.

The above classification has the aim of simplifying the first stage of the sonotrode design, namely determination of its type and basic configuration. The essence of the second stage consists in its modification to satisfy a set of frequency-modal limitations. It contains values of resonance frequency f_r, intervals of its tuning out Δf^+ and Δf^-, coefficients k_i, k_h, etc. Finally, the third stage includes evaluation of fatigue strength and temperature of dissipation heating of the sonotrode. Performance of the last two stages envisages the use of numerical simulation methods.

Sonotrodes function in intensive oscillations mode. Therefore, the general mathematical model of the process should take into account the physical nonlinearity of the material, vibration heating and temperature dependence of material properties. Problem definition for plate (in $x0y$ plane) bodies of a variable thickness $h = h(x, y)$ is given in [13, 14]. It includes the equations of mechanics and thermodynamics

$$\tilde{\sigma}^*_{ij,j} + \omega^2 \rho^* \tilde{u}_i = 0, \quad \tilde{\varepsilon}_{ij} = \frac{1}{2}(\tilde{u}_{i,j} + \tilde{u}_{j,i}),$$

$$\tilde{\sigma}^*_{ij} = 2\tilde{G}^* \left(\tilde{\varepsilon}_{ij} + \frac{\tilde{\nu}_1}{1 - 2\tilde{\nu}_1} \tilde{\varepsilon}_{kk} \delta_{ij} \right), \quad i, j, k = x, y, \tag{2}$$

$$c^*_\nu \dot{\theta} = (k^* \theta_{,i})_{,i} - 2\hat{\alpha}_1(\theta - \theta_a) + D^*, \; D^* = \frac{\omega}{2}(\sigma^{*''}_{ij} \varepsilon'_{ij} - \sigma^{*'}_{ij} \varepsilon''_{ij}),$$

boundary conditions

$$\tilde{\sigma}^*_{ij} n_j = \tilde{f}^*_i \text{ on } l$$
$$-k^* \theta_{,i} n_i = \alpha^*_2(\theta - \theta_a) \tag{3}$$

and initial condition

$$\theta = \theta_0 \text{ at } t = 0. \tag{4}$$

The following designations are used here:

$$\tilde{G}^* = h\tilde{G}, \; \rho^* = h\rho, \; k^* = hk,$$
$$c^*_\nu = hc_\nu, \; \tilde{f}^*_i = h\tilde{f}_i, \; \hat{\alpha}_1 = \alpha_1(1 + h^2_{,x} + h^2_{,y})^{1/2}, \tag{5}$$
$$\tilde{\nu}^*_1 = \frac{\tilde{\nu}(1 - \tilde{\Delta})}{1 + \tilde{\nu}(1 - 2\tilde{\Delta})}, \; \tilde{\Delta} = \frac{\rho h^2 \tilde{\nu} \omega^2}{24(1 - \tilde{\nu})\tilde{G}},$$

where $\tilde{G}$ and $\tilde{\nu}$ are the complex shear moduli and Poisson's ratio, equal to $\tilde{G} = G' + iG''$; $\tilde{\nu} = \nu' - \nu''$; $\tilde{u}_i$, $\tilde{\sigma}_{ij}$, $\tilde{\varepsilon}_{ij}$ are the amplitudes of components of displacement vector, tensors of stresses and strains; k and c_ν are the coefficients of heat conductivity and bulk heat capacity per unit volume; α_1, α_2 are the coefficients of convective heat exchange; f_i is the amplitude of components of the vector of stresses in contour l; θ_0 is the initial temperature; θ_a is the ambient temperature; $\theta_{,x} = \partial\theta/dx$, $\dot{\theta} = \partial\theta/\partial t$.

Physical nonlinearity is described by the dependence of the shear modulus on the intensity of the stress amplitudes

$$\tilde{G} = \tilde{G}(\omega, \theta, \sigma_u),$$
$$\sigma_u = \frac{1}{2^{-1/2}} (|\tilde{\sigma}_{xx} - \tilde{\sigma}_{yy}|^2 + |\tilde{\sigma}_{xx}|^2 + |\tilde{\sigma}_{yy}|^2 + 6|\tilde{\sigma}_{xy}|^2)^{1/2}.$$

The problem is solved by iteration method of variable parameters of elasticity in combination with the finite elements method [14, 15]. The equations of oscillations and heat conductivity, discretized using the above approach, are reduced to systems of linear algebraic equations

$$(\tilde{C} - \omega^2 M)\tilde{\mathbf{U}} = \tilde{\mathbf{F}}, \; \chi\dot{\mathbf{Q}} = -\xi\mathbf{Q} + \mathbf{D}, \tag{6}$$

where $\tilde{C}$ and M are the matrices of rigidity and mass; $\mathbf{U}$, $\mathbf{Q}$ are the vectors of nodal displacements and temperature; χ, ξ are the matrices of heat capacity and heat conductivity; $\mathbf{F}$, $\mathbf{D}$ are the vectors of exciting forces and heat input. The equation of heat conductivity is integrated by the finite differences method in time. Energy dissipation is taken into account in heat source D.

Calculations related to frequency-modal characteristics can be limited to linear-elastic isothermal approximation of equations (2) – (4). When studying vibration heating and fatigue strength, the problem should be solved in its general definition.

Trial and error method is used to select a rational configuration. In a number of cases it becomes possible to implement optimisation procedures [9, 10]. The role of optimal design methods becomes greater in design of long-contour, multistep and essentially three-dimensional sonotrodes [16], having a high structural sensitivity. Their practical application, however, is hindered by the need for powerful computers and poor adaptability to fabrication of the produced configurations. The working frequencies of the

above elements are in a dense spectrum, therefore, the main problem solved at the stage of more precise determination of their geometry, consists in tuning out the parasitic frequencies. Its successful solution requires precise understanding of the nature of the influence of a change in the geometry of a body on the frequencies of the working and adjacent parasitic modes.

On the whole, the problem of general design goes beyond the design of the sonotrode as an isolated element of the system. Such an idealisation is only acceptable for calculation of its own characteristics and the idle modes. Amplitudes and phases of displacements, deformations and stresses during the process cycle are dependent on such factors as interaction with the load varying in time, band width and type of the driving generator AFC, etc. These factors are determinant in evaluation of the fatigue strength and vibration heating of elements.

The above approach was used to design and manufacture an ultrasonic generator (Figure 4), piezoelectric converter and a number of sonotrodes for USW of actual items of polymers and polymer-based composites at the E.O. Paton Electric Welding Institute and the Institute of Mechanics of the NAS of Ukraine. In keeping with the proposed schematics, the sonotrodes (from left to right) belong to the following classes: L_1, $pmL_1^{(2.30)}$ and $pmL_1^{(1.35),\,(0.70)}$, respectively.

The range of issues outlined above is insufficiently studied so far. Their investigation will, probably, determine the direction of studies in this area in the near future.

CONCLUSIONS

1. Diverse sonotrodes that are used in process units for USW of polymers and polymer-based composites, can be classified by the modal principle. The types of motions, implemented in them, namely longitudinal, thickness, etc., can be correlated with the characteristic sections of the branches of frequency spectra of a rectangle. Sonotrode types are defined as low- and high-frequency by the location of these sections relative to the edge resonance frequency.

2. Marking of plate sonotrodes is proposed, reflecting the type of motions, wave dimensions, as well as types of converted or distributed modes. The main stages of sonotrode design have been defined, namely determination of the type and basic configuration, its modification in keeping with a set of frequency-modal limitations; evaluation of fatigue strength and vibration heating.

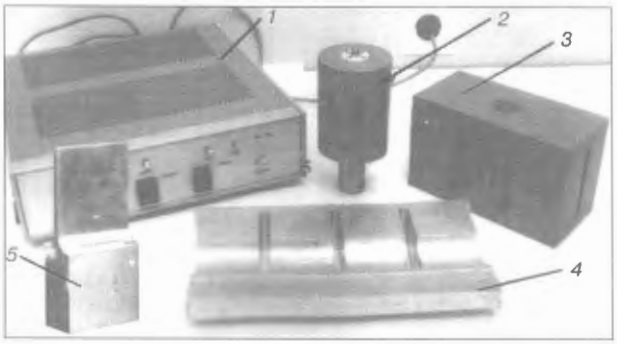

Figure 4. General view of an ultrasonic generator (*1*), piezoelectric converter (*2*), waveguides (*3* – *5*)

REFERENCES

1. Teumin, I.I. (1959) *Ultrasonic oscillatory systems*. Moscow: Mashgiz.
2. (1970) *Physics and technology of powerful ultrasound*. Ed. by L.D. Rozenberg. Moscow: Nauka.
3. Volkov, S.S., Orlov, Yu.N., Chernyak, B.Ya. (1974) *Welding of plastics by ultrasound*. Moscow: Khimiya.
4. Andoh, E., Kagawa, Y. (1985) Finite element simulation of an ultrasonic vibrator for plastic welding. In: *Proc. of IEEE Ultrasonic Symp*. San-Francisco.
5. Grinchenko, V.T., Meleshko, V.V. (1981) *Harmonic oscillations and waves in elastic bodies*. Kyiv: Naukova Dumka.
6. Adachi, R., Ucha, S. (1990) Modal vibration control of large ultrasonic tool with the use of wave-trapped horns. *J. Acoust. Soc. Jap.*, **1**, 208 – 214.
7. Zhuk, Ya.A. (1993) Modal control of planar oscillations of multi-tie plates. In: *Transact. of XVIII Sci. Conf. of Young Scientists of the Institute of Mechanics of the NAS of Ukraine*, May 18 – 21. Kyiv.
8. Zhuk, Ya.A., Kozlov, V.I., Senchenkov, I.K. (1996) A new class of waveguides, applied in ultrasonic welding of plastics. *Akust. Zhurnal*, **4**, 517 – 521.
9. Bogomolov, S.I., Simpson, E.A. (1981) Optimal design of ultrasonic oscillator concentrators. *Ibid.*, **4**, 491 – 499.
10. Simpson, E.A. (1983) Multicriterial problems of optimisation of mechanical components in ultrasonic systems. In: *Strength of materials and structural elements at sonic and ultrasonic loading frequencies*. Kyiv: Naukova Dumka.
11. Silin, L.L., Balandin, G.F., Kogan, M.G. (1962) *Ultrasonic welding*. Moscow: Mashgiz.
12. Merkulov, L.G. (1959) Theory of ultrasonic concentrators. *Akust. Zhurnal*, **3**, 230 – 238.
13. Senchenkov, I.K., Bespalova, E.I., Kozlov, V.I. *et al.* (1991) On the capabilities of a more accurate method of design of planar oscillations in plate bodies. *Prikladnaya Mekhanika*, **11**, 69 – 77.
14. Senchenkov, I.K., Kozlov, V.I., Yakimenko, S.N. *et al.* (1992) On calculation of planar oscillations and vibration heating in plates of a variable thickness. *Ibid.*, **5**, 64 – 69.
15. Motovilovets, I.K., Kozlov, V.I. (1987) *Mechanics of coupled fields in structural elements*. Kyiv: Naukova Dumka.
16. Shuju, L., Fucheng, Z., Xiaonk, G. (1991) Three-dimensional coupled vibrations of block like resonators. *Acta Acoust.*, **2**, 91 – 97.

EFFECT OF SURFACE MICRORELIEF ON ADHESION STRENGTH OF THERMAL SPRAY COATINGS

Yu.A. KHARLAMOV[1] and **Yu.S. BORISOV**[2]
[1]East-Ukrainian National University, Lugansk, Ukraine
[2]The E.O. Paton Electric Welding Institute, NASU, Kyiv, Ukraine

ABSTRACT

Current concepts of the role of parameters of microrelief of the substrate surface in formation of thermal spray coatings are analysed. The analytical model developed on the basis of analysis of experimental data is suggested for selection of optimal parameters of microrelief of the spray coatings

Key words: *thermal spraying, jet-abrasive blasting, surface, abrasive, relief, spray particle, adhesion*

The technology of thermal spraying (TS) of coatings includes three main stages: preparation of the surface of a workpiece, spraying and treatment of the sprayed coatings. One of the most important characteristics of the quality of coatings is strength of adhesion to the base material of a workpiece, the high level of which is achieved not only due to the optimal spraying conditions, but also due to an appropriate surface preparation (removal of contaminants and activation of the substrate surface to climinate barriers that hamper contact of the spray particles with the surface layer of the substrate). Basic techniques used for surface activation involve formation of a rough microrelief on the substrate surface, its deformation to induce a stressed state and preheating. Jet-abrasive blasting (JAB) is most frequently used for this purpose, as it is the simplest and most cost effective method for preparation of surfaces of both simple and complicated shapes. Roughness of the substrate surface influences the adhesion strength through changing the intensity of physical-chemical interaction of the particle and substrate materials in contact. Usually this is associated with a change in the stressed state of the surface layer, better heating through of the micropeaks and concentration of stresses in mouth of the microvalleys. Until now no substantiated recommendations for selection of the surface roughness parameters for thermal spraying are available.

Current state of theory and practice of preparation of surfaces for thermal spraying. Surface preparation is one of the most critical stages of the process of deposition of thermal spray coatings (TSC). Parts of national standards on TS [1 – 3] and numerous publications and studies [4 – 18] are dedicated to substantiation of requirements and appropriate technological recommendations for this operation. However, until now these recommendations and results of the studies are of a contradictory character [19]. First of all, it should be noted that no sufficiently grounded requirements to parameters of a microrelief of the surface prepared for TS are available. So, according to the data of [20, 21], to achieve a maximum adhesion strength of TSC, it is necessary to provide an optimal ratio of the surface roughness parameter to mean size of the spray particles. It is shown in [22] that the maximum adhesion strength is achieved at a certain roughness of the substrate surface produced by JAB using an abrasive material with an optimal specific consumption. According to other data, the necessary condition for achieving the maximum adhesion strength is a certain time of blasting of the surface using an abrasive material [23]. An increase in the specific consumption of the abrasive material in JAB leads to an increase in the adhesion strength of TSC, then follows a trend to its decrease [24].

As shown in [13], in spraying aluminium onto a surface prepared by JAB using different shot and abrasive particles, the maximum adhesion strength is achieved in the majority of cases at an angle of attack of the surface by a gas-abrasive jet equal to 90°. For all types of the abrasive particles of a non-spherical shape a decrease in the angle of inclination of the jet of the particles to the surface treated leads to a decrease in the adhesion strength. The highest adhesion strength was obtained in treatment of the metal surface by aluminium oxide. A decrease in the adhesion strength was fixed in the case of using abrasive materials in the following sequence: copper oxide slag–new acute-angled shot–used acute-angled shot–worn acute-angled shot–round shot. This can be explained by a specific role of the shape of the abrasive particles in determination of the character of interaction with the surface treated. Acute-angled particles are likely to form a more favourable surface microrelief for formation of a strong adhesion of TSC with the substrate. An impact by such a particle is a sort of the elementary acts of microcutting, which lead to removal of microchip and formation of new regions on the surface. Collision with rounded and spherical particles leads to plastic deformation (crushing) of the microregions on the surface of a workpiece. However, the acute-angled particles are rapidly destroyed and their use may lead to introduction of their fragments into the surface being treated, to contamination of the surface,

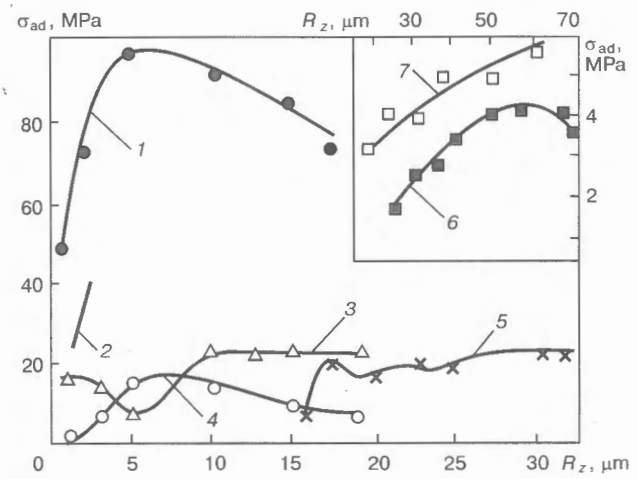

Figure 1. Effect of height of roughness of the substrate surface on adhesion strength σ_{ad} of TSC: *1* — supersonic air-gas plasma spraying of alloy WC-Co with particle size d_p = 10 – 40 μm, substrate hardness *HV* 300 – 800, productivity 19 – 76 g/min, v_0 = 280 – 340 m/s [25]; *2* — plasma spraying of powder Al_2O_3 (d_p = 20 μm), substrate — steel [14]; *3* — plasma spraying of nickel powder PNE-1 (d_p = 50 – 63 μm) on St.45, v_0 = 160 m/s [10 – 12]; *4* — same, v_0 = 70 m/s [27 – 29]; *5* — plasma spraying of iron powder clad with nickel (d_p = 20 – 120 μm), powder consumption 50 g/min, plasmatron travel speed 1.2 m/min, S_m = 50 – 300 μm, JAB using crushed shot 0.3 – 1.5 mm in size [23]; *6, 7* — plasma spraying of powder of chromium-nickel spinel $NiCr_2O_4$ on the substrate of alloy D16AT and steel Kh18N10T, respectively, after JAB using cast iron grit [4]

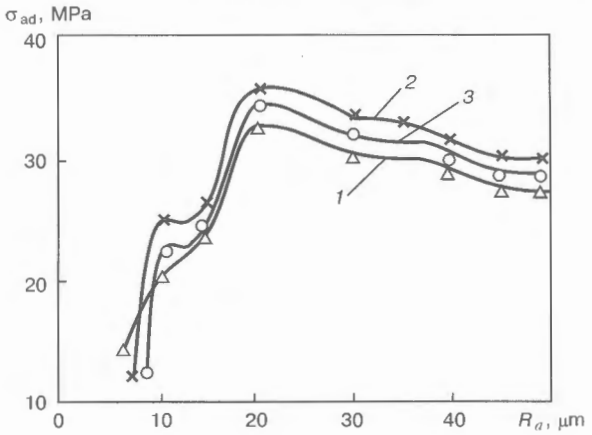

Figure 2. Effect of R_a of the substrate surface of steel St.3 on σ_{ad} (shear) of plasma coatings of powder SNGN 55 at different substrate surface preparation: *1* — turning; *2* — cast iron shot blasting; *3* — steel grit blasting; S_m = 340 – 640 μm [29, 30]

which is unacceptable in many cases, and to a decrease in the adhesion strength.

However, there are cases when the correspondence between a normal angle of blasting of the surface with a gas-abrasive jet and production of the maximum adhesion strength is not kept to. In blasting with a round shot there is smeared maximum within a range of 50 – 60° [13]. It is shown that in spraying with the clad tungsten carbide powder (WC + C–Cr–Fe–B–Si–Ni) the maximum strength of adhesion of TSC to the substrate is achieved at an angle of attack by the gas-abrasive jet during the JAB process equal to 75°.

Experimental data on the effect of height of irregularities R_z on the substrate surface microrelief on the adhesion strength of TSC, which is determined by the pull tests [14, 23, 25 – 28] (Figure 1), are indicative of their ambiguity and probably of the insufficiency of this parameter for estimation of the optimal microrelief of the surface prepared for TS.

More definite relationships between the adhesion strength determined by the shear tests and the arithmetic mean deviation of profile R_a (Figure 2) were derived in studies [29, 30]. With different methods of preliminary treatment of the substrate surface but identical roughness the adhesion strength is almost constant. It is shown in these studies that the basic and significant effect on the adhesion strength is exerted by the following roughness parameters: R_p — height of smoothing (distance from the line of peaks to the mean line); R_{max} — the largest height of irregularities of the profile; R_a — arithmetic mean deviation of the profile and S_m — mean pitch of the irregularities. However, the authors give no experimental dependencies of the adhesion strength upon the values of the R_p and S_m parameters. The requirement for an optimal roughness to achieve the high adhesion strength is explained by the optimal volume of valleys of the microrelief ensuring the required shrinkage of a sprayed layer during cooling. The effect of smoothing height R_p can be explained also by the fact that this parameter characterizes the ratio of volumes of peaks and valleys in a rough layer of the surface coated and is more suitable for estimation of conditions of interaction between the particles and the substrate.

Therefore, the authors of [29, 30] were the first to note the insufficiency of the criteria of roughness R_a and R_z for estimation of the role of the substrate surface microrelief in formation of a strong adhesion of TSC to the substrate. Many authors of other studies also indicated to an important role of topography of the surface prepared for spraying in the mechanism of formation of TSC. As a rule, ensuring the maximum adhesion strength is associated with certain parameters of the microrelief for certain combinations of a spray material, technological parameters of spraying and the substrate material. However, the effect of these factors has not yet been evaluated to a sufficient degree.

Study [31] was conducted to investigate formation of plasma coatings of nickel alloy powders with a particle size of 40 – 50 and 80 – 90 μm deposited on stainless steel 316 with a different controllable preliminary preparation of the surface (electric spark treatment, scratching, grinding and milling). Spraying was done on the surface with a regular two-dimensional topography in the form of periodically spaced peaks and valleys. It turned out that the mechanism of formation of a coating greatly depends upon both topography of the surface and size of the spray particles. Deformation and spreading of the spray particles are substantially affected by the inclination of side surfaces of peaks of the substrate surface microrelief. The coating is formed primarily in the valleys. A layer of a relatively smaller thickness is formed on the peaks.

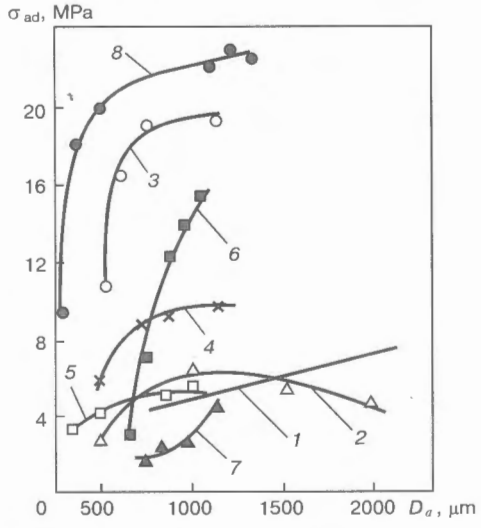

Figure 3. Effect of size of abrasive particles used for JAB on σ_{ad} of TSC: *1* — flame steel coating on steel substrate, D_a = 75 – 100 μm [40]; *2* — plasma coating of powder of alloy NiCrBSi with d_p = 50 – 100 μm on steel substrate [37]; *3* — flame coating of powder of alloy NiCrBSi with d_p = 45 – 126 μm on copper substrate [37]; *4* — plasma coating of zirconia powder on substrate of alloy Br.Kh0.8, coating thickness δ = 0.3 – 0.4 mm at thickness of the BZh98 sublayer equal to 0.10 – 0.15 mm [41]; *5* — wire flame spraying of zinc coating (δ = 0.15 mm) [42]; *6* — aluminium coating deposited by electric metallization (δ = 0.10 mm) [43]; *7* — flame aluminium coating (δ = 0.10 mm) [43]; *8* — plasma coating of iron powder clad with nickel with d_p = 20 – 120 μm on St.45 substrate, δ = 0.7 – 0.8 mm, S_m = 50 – 300 μm [23]

As shown in [32, 33], deformation and spreading of the spray particles on a rough surface depend upon the topography of the surface and, first of all, upon the pitch of the irregularities. A valley between the neighbouring peaks should be sufficiently wide to allow a particle to be deformed to a maximum possible diameter of the disk shape. Otherwise it would flow into a neighbouring valley. If the diameter of a deformed particle is considerably smaller than the pitch of the irregularities, upon striking against the side surfaces of the peaks the small particles will flow in a direction to the bottom of the valley and spatter. Experiments show that, to reduce spattering the deformed particle (disk), diameter D should be within a range of $0.25s < D < s$, where s is the pitch of the irregularities.

It is thought [10] that the main purpose of JAB consists in producing a sufficient roughness to provide mechanical adhesion of spray particles to the substrate. Two probable cases are considered: upon colliding with a micropeak the spray particle deforms it, which leads to formation of an anchor-type adhesion, whereas if the spray particle gets into a valley a mechanical adhesion of the wedge type is formed between the neighbouring peaks.

There is another common opinion that the main purpose of JAB is to clean the surface, which, however, JAB fails to achieve in a proper way. Organic contaminants can be readily removed by organic solvents, whereas inorganic contaminants and thin oxide films can be removed by JAB, chemical and mechanical methods. According to the data of [34], another effect of roughness is that it makes it easier to destruct oxide films at the micropeaks on the surface being struck by the spray particles.

Surface roughness (R_a) increases with a decrease in the elasticity modulus of the substrate material. At an angle of blasting the surface by a gas-abrasive jet equal to 90° the R_a value is a bit higher, but in this case the contamination of the surface with fragments of abrasive grains is higher than at a blasting angle of 45° [10].

It is shown in [35] that traditional parameters of microrelief of the surface cannot be sufficient for estimation of formation of the adhesion between the particles and substrate during TS. In this case a more reliable criterion is a fractal dimension. Its value for surfaces subjected to JAB is ≈ 1.04. Blasting the surfaces by a gas-abrasive jet at an angle of 75° results in a maximum value of fractal dimension equal to 1.07, whereas the mean roughness of the surface remains almost constant (independently of the blasting angle). At a JAB angle of 75° a maximum adhesion strength is achieved. It can be also assumed that this angle of blasting provides a more favourable shape of the recesses.

In JAB one of the decisive roles in formation of the surface microrelief is played by the shape and size of the abrasive particles [19, 36, 37]. The similar effect was fixed also in the case of erosion caused by impact by hard particles. The metal pressed out from the crater flows in a direction of fall of the particles [38]. A particle hitting the metal surface causes plastic deformation which has a directional character [39]. The material is forced out from the recess in a direction of projection of the particle velocity vector. Therefore, in impact by the abrasive particle at an angle the resulting recesses are more elongated and more shallow.

Experimental data on the effect of size D_a of the abrasive particles on the adhesion strength of TSC (Figure 3), determined by the pull method, show a distinct dependence of the latter upon the size of the abrasive particles used for JAB of the substrate surface. However, it should be noted that the microrelief of the substrate surface is not the only factor that determines the absolute value of the adhesion strength. This is more evident from comparison of the adhesion strength of aluminium coatings produced by electric-arc spraying *6* and flame spraying *7*, respectively, other conditions being equal.

Therefore, available recommendations for assigning roughness parameters of the substrate for TS are empirical and concern certain technology conditions. The most common criteria R_a and R_z are insufficient for assignment of the optimal roughness of the surface prepared for TS. That is why it seems necessary to consider in more detail interaction between the particles and rough surface.

Calculation of rational parameters of microrelief of the surface treated. In analysis of physical-chemical interaction of materials in the process of formation of TSC, the consideration is normally given to collision of a spray particle with an ideally smooth surface

[44]. At the same time, availability of indirect experimental data makes it necessary to develop analytical methods for estimation of the role of the microrelief of the substrate surface in thermomechanical interaction with the spray particles.

Studies [45 – 47] consider models of deformation and spreading of the spray particles on a rough surface of the substrate. However, they cover the cases where sizes of the microirregularities are much less than sizes of the spray particles. The micropeaks are modelled by cones, pyramids, hemispheres, cylindrical rods or blind holes. The effect of these factors on the coefficient of friction between the substrate surface and a spreading particle is taken into account in this case. Under actual spraying conditions sizes of microirregularities of the substrate and sizes of the spray particles are comparable.

Consider peculiarities of the microrelief of surfaces produced by different treatment methods. After turning, a cutter leaves a continuous trace, like after threading. At a small feed, when the angle of elevation of a turn is insignificant, the radius of a valley corresponds to the radius of rounding of the cutter tip. Considerable stresses induced by the cutting process result in the formation of tears in the form of transverse cracks. A similar microrelief of the substrate surface is formed in planing, boring and other types of machining using blade-type tools. Grinding results in the formation of intermittent traces in the form of individual marks left by cutting (scratching) using individual abrasive grains. The valley of a tear has a very small radius, which corresponds to the radius of sharpening of an abrasive grain (normally about 2 – 10 μm). Because of formation of high local temperatures, the probability exists of formation of microcracks in a plane transverse to the treatment trace. After JAB, the traces formed by the impact by abrasive particles (grit) are located chaotically and the shape of recesses corresponds approximately to the shape and size of the abrasive particles. Comparison of probable sizes of the spray particles with a shape and size of irregularities of the surface caused by cutting shows the feasibility of modelling of collision of the particles both with a plane and with peaks and valleys of the surface microrelief. However, the most probable collision processes are those where the particles get into valleys on the substrate surface microrelief.

In the liquid particle and plane contact zone one could distinguish three characteristic regions [48] with a different nature of the activation ability: central circular region A — successively affected by the impact and head pressures; middle circular region B — affected by the head pressure of Rayleigh waves and contact friction of the spreading metal of a particle; and peripheral circular region C — affected by the Rayleigh waves and contact friction. The area of region A is no more than 2.5 % and that of region B is 30 % of the total contact area. Therefore, strength and other mechanical properties of coatings are determined to a considerable degree by conditions of

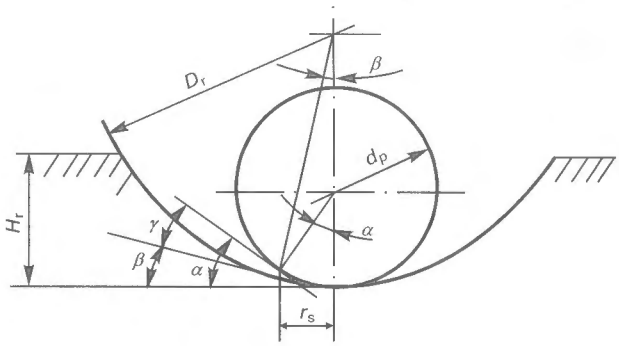

Figure 4. Schematic of collision of the spray particle with a valley on the substrate surface microrelief

activation of the substrate surface in region C, and hence by properties of the formed boundaries between particles in TSC.

Consider the case of an axial collision of a liquid particle with a spherical recess on the substrate with diameter D_r (Figure 4). Radius of the spot, r_s, of the particle–recess contact at the initial moment of spreading [49] is as follows:

$$r_s = d_p v_0 / 2C_p,$$

where d_p and v_0 are the diameter and velocity of the particle and C_p is the sound velocity for the particle material.

Velocity of the cumulative jet formed at collision of the particle with the plane [50] is determined as follows:

$$v_j = v_0 / \sin\gamma + v_0 / \mathrm{tg}\,\gamma, \qquad (1)$$

where γ is the angle between the colliding surfaces at the interface of an expanding contact.

In a case under consideration (Figure 4) it holds

$$\gamma = \alpha - \beta, \quad \sin\alpha = 2r_s/d_p = v_0/C_p,$$
$$\sin\beta = 2r_s/D_r = d_p v_0 / D_r C_p.$$

After transformation we will obtain the following:

$$\sin\gamma = \sin(\alpha - \beta) = (v_0/C_p)\{[1 - (d_p/D_r)^2(v_0/C_p)^2]^{0.5} - (d_p/D_r)[1 - (v_0/C_p)^2]^{0.5}\}. \qquad (2)$$

Reduce expression (2) to the following form:

$$v_j = v_0/\sin\gamma + v_0(1 - \sin^2\gamma)/\sin\gamma. \qquad (3)$$

Calculations using formulae (2) and (3) show that velocity of the cumulative jet in collision of the liquid particle with a spherical valley is several times higher than that in collision of the particle with a plane. Therefore, the most favourable microrelief of the initial substrate surface for formation of strong coatings is that in the form of closely located recesses with a profile radius in excess of the radius of the spray particles. Velocity of spreading of the particles, higher than the initial velocity of collision, corresponds to a more intensive activation of the substrate surface. In addition, this provides flowing of the spreading layer of the particle material to side surfaces of the

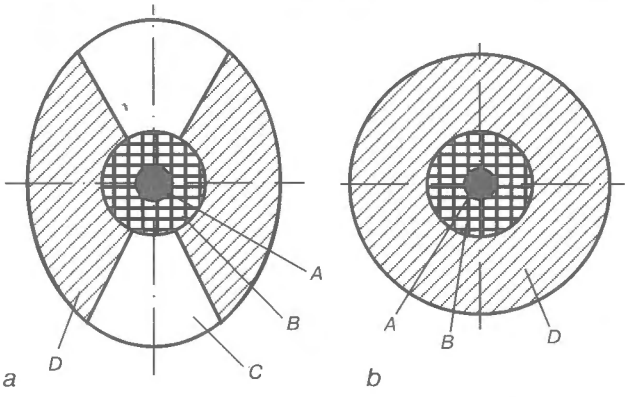

Figure 5. Zones of contact of the spray particle with valleys on the substrate surface microrelief in the form of a tool mark (*a*) and recess (*b*)

valley and expanding of the region affected by the head pressure on the substrate surface. The similar effect is observed in collision of the particle with a side surface of the recess.

For collision of the particle with a recess in the form of a tool mark (groove) the following characteristic regions can be distinguished in the contact zone: region A — activated by the impact pressure, region B — activated by the impact and head pressures, region C — activated by the contact friction and a relatively low head pressure, formed in flowing of the particle material to the inclined side surface of the valley, and region D — activated by the contact pressure and a relatively high head pressure formed in flowing of the material to side surfaces of the valley (Figure 5, *a*). If the valley has the form of a sphere or paraboloid (Figure 5, *b*), there will be no region of type C with a relatively low head pressure. Therefore, transition of a smooth to rough surface increases the relative contact area activated by the head pressure. In the region of type D the head pressure is $P_h = \rho_h v_j^2 \sin\varphi$, where φ is the angle of collision of the jet with a side surface of the recess. Since at high velocities of the particles ($v_0 \le 500$ m/s) the relative velocity of spreading, v_j/v_0, is 3 – 6, in regions of the D type a high head pressure $P_h^D > P_h$ can develop at the high φ values. Therefore, one of the ways of increasing the adhesion strength of TSC is the selection of optimal parameters of the substrate surface microrelief.

Apparently, for formation of a strong adhesion the surface area of the deformed particle–substrate contact should be approximately equal to the area of a spherical segment simulating a valley. Then the geometrical relationships (Figure 4) yield

$$\pi D_r^* H_r = \pi d_j^2/4, \qquad (4)$$

where D_r^* is the optimal diameter of the recess and H_r is the depth of the recess.

Therefore,

$$D_r^* = d_j^2/4H_r.$$

Diameter of a particle deformed to the form of a disk can be determined from the formula given in [50]:

$$d_j/d_p = 1.3\,[\rho\,(v_i/\mu)]^{0.2},$$

where ρ is the density of the particle material, v_i is the collision velocity and μ is the viscosity of the molten particle material.

As it was shown earlier, diameter of the particle deformed on a plane to the shape of a cylindrical disk, the initial diameter of the spherical particle and disk thickness being known, can be determined from the formula given in [48]:

$$d_j = 2d_p/(6\bar{h}_p)^{0.5},$$

where $\bar{h}_p$ is the degree of deformation of the particle equal to h_p/d_p and h_p is the deformed particle thickness.

Then

$$R_r^* = D_r^*/2 = d_p^2/12\bar{h}_p H_r. \qquad (5)$$

Assume that

$$H_r = \bar{H}_r D_r^* = 2\bar{H}_r R_r^*, \qquad (6)$$

where $\bar{H}_r = H_r/D_r^*$ ($\bar{H}_r$ is the optimal relative depth of the recess).

Substitution of expression (6) into expression (5) yields

$$R_r^* = d_p/2(6\bar{h}_p\bar{H}_r)^{0.5}.$$

The calculation data (Figure 6) show that radius of the recess, R_r^*, required for fulfilling relationship (4), decreases with an increase in its relative depth, and does it most intensively at $\bar{H}_r \le 0.3$.

Assuming that the recess radius corresponds to the diameter of an abrasive particle, its diameter can be determined from the following formula:

$$D_a = d_p/(6\bar{h}_p\bar{H}_r)^{0.5}.$$

As the relative depth of recesses increases, the optimal diameter of the abrasive particles decreases (Figure 7). At a preset size of the abrasive particles, where $D_a > d_p$, the optimal depth of the recesses can be determined from the following formula:

$$\bar{H}_r = d_p^2/6\bar{h}_p D_a^2.$$

To determine the relative depth of the recesses, it is convenient to use plots of their dependence of H_r upon the diameter of the spray particles, d_p (Figure 8). The relative depth of the recesses formed by impact by the abrasive particles should not be in excess, as a rule, of 0.5. Therefore, to achieve a high adhesion strength of the coatings with a preset size of the spray particles, it is advisable to choose a minimum possible diameter of the abrasive particles at $H_r \to 0.5$.

The effect of depth of the microvalleys and size of the abrasive particles on the adhesion strength of TSC is proved by the experimental data obtained by N. Katts and E. Linnik [40]. For different combina-

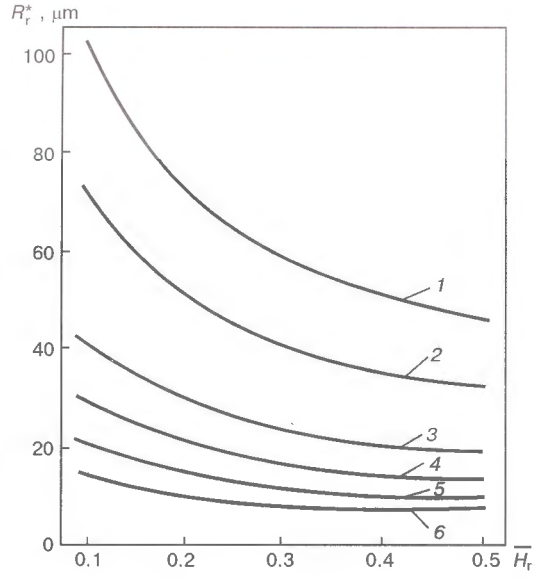

Figure 6. Dependence of the optimal radius of a spherical recess upon its relative depth: *1* — d_p = 50 μm, h = 0.1; *2* — 50 μm, 0.2; *3* — 20 μm, 0.1; *4* — 20 μm, 0.2; *5* — 10 μm, 0.1; *6* — 10 μm, 0.2

tions of the coating and substrate materials there are optimal values of depth of the valleys and diameter of the abrasive particles, at which the maximum adhesion strength is achieved.

In preparation of workpieces for TS, JAB results in formation of a totally new microrelief of the surface. To describe it, it is necessary to take into account the shape and relative arrangement of recesses on this surface. Distribution of the recesses can be assumed to be the Poisson field of points characterizing the deepest points of the recesses. The density of the field is determined by the number of points falling on a unit area of the surface treated [51]. Make the following assumption:

• monodisperse spherical abrasive particles are used for treatment;

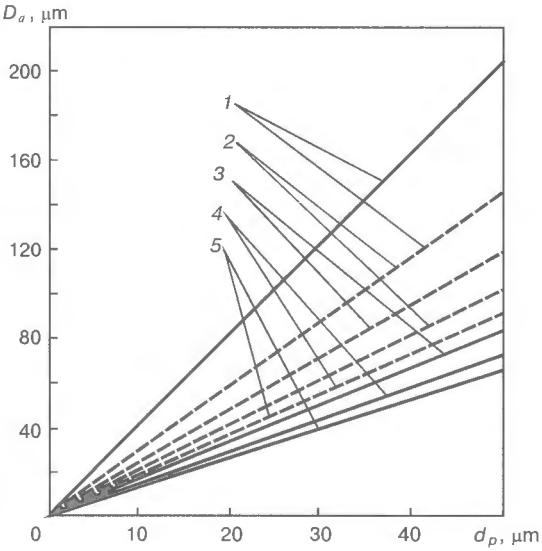

Figure 7. Dependence of the optimal value of D_a upon d_p at $\overline{H}_r$ = = 0.1 (*1*), 0.2 (*2*), 0.3 (*3*), 0.4 (*4*), 0.5 (*5*); here and in Figure 8 solid line is for h_p = 0.1 and dashed line is for h_p = 0.2

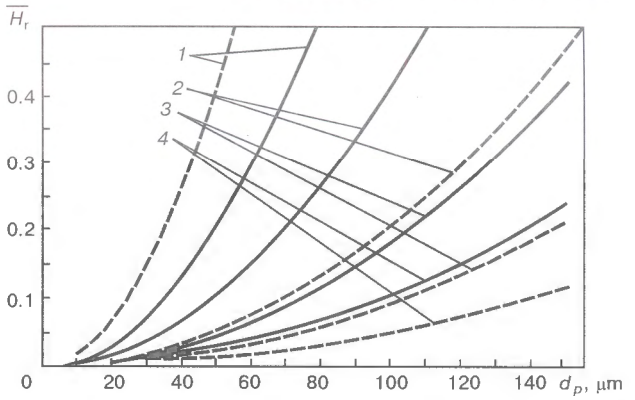

Figure 8. Dependence of the optimal value of $\overline{H}_r$ upon d_p at D_a = = 100 (*1*), 200 (*2*), 300 (*3*) and 400 (*4*) μm

• sizes of the particles being identical, a repeated impact on the recess causes an insignificant change in its shape and size;

• a new recess is formed on the surface if a centre of the impact is projected beyond the already existing print.

Assume also that recesses are densely located on a treated surface (Figure 9). According to geometrical relationships, the radius of a recess in the plan view is as follows:

$$R_{tsp} = [R_r^2 - (R_r - H_r)^2]^{0.5} = (2R_rH_r - H_r^2)^{0.5} =$$
$$= [H_r (D_r - H_r)]^{0.5} = D_r [\overline{H}_r(1 - \overline{H}_r)]^{0.5},$$

where R_{tsp} is the radius of the treated surface point; and the pitch between the recesses in a transverse direction is

$$S_{tr} = (4R_{tsp}^2 - R_{tsp}^2)^{0.5} = (6R_rH_r - 3H_r^2)^{0.5} =$$
$$= [3H_r (D_r - H_r)]^{0.5} = D_r[3\overline{H}_r (1 - \overline{H}_r)]^{0.5}$$

and in the longitudinal direction is

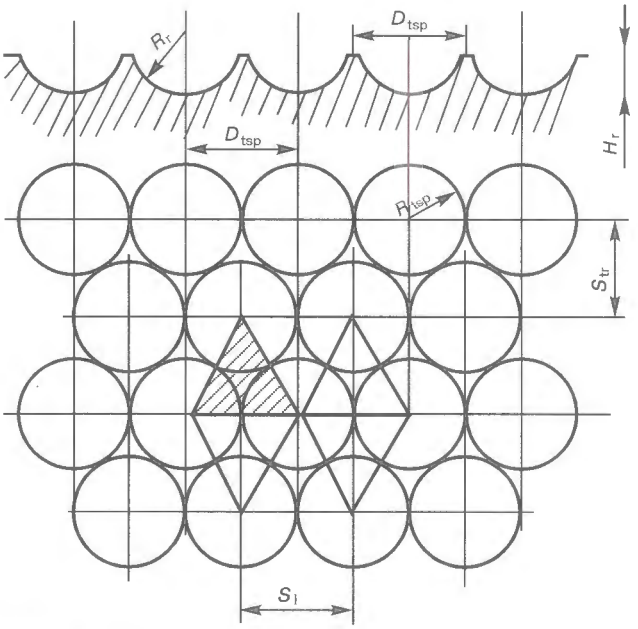

Figure 9. Model of microrelief of the substrate surface

$$S_l = 2R_{tsp} = D_{tsp} = 2[H_r (D_r - H_r)]^{0.5} =$$

$$2D_r[\overline{H}_r (1 - \overline{H}_r)]^{0.5}.$$

Determine the probability of hitting the recess by the spray particles

$$P = \sum F_r / F,$$

where $\sum F_r$ is the total area of projections of the recesses on a surface treated and F is the area of the treated surface. To simplify the method of calculation of this value, delineate on the surface treated an elementary geometrical figure in the form of an equilateral hexagon covering the recess. In turn, delineate in this recess a triangle covering an intermediate region between the neighbouring recesses (Figure 9). The ratio of areas of the untreated region of the surface and parts of the three recesses included into this triangle will determine the desired value P, which can be written in the following form:

$$P = F_1/F_2,$$

where F_1 is the area of the three sections of the recesses included into the triangle and F_2 is the area of the elementary triangle.

As it can be seen from the geometrical relationships (Figure 9), these areas are equal to

$$F_1 = \pi D_{tsp}/8, \quad F_2 = 0.433 D_{tsp}^2.$$

Then the probability of hitting the recesses by the spray particles to be determined is as follows:

$$P = F_1/F_2 = 0.907.$$

Therefore, the probability of hitting the densely located recesses by the spray particles is very high. However, even at hitting the centre of an untreated region by a spray particle, this region is fully covered by this particle and affected by the head pressure.

CONCLUSIONS

1. Parameters of microrelief of the surface prepared for thermal spraying have a dominant effect on the coating to substrate adhesion strength.

2. Peculiarities of geometry and parameters of microrelief of the substrate surface have a considerable effect on the area and intensity of mechanical activation of this surface in the zone of contact with the spray particles.

3. Spherical abrasive particles of an approximately identical diameter, corresponding to that of the spray particles, are indicated for jet-abrasive blasting of the surface.

4. To achieve a high adhesion strength and tight interface in the coating–substrate contact, diameter of the abrasive particles should exceed that of the spray particles by a factor of 1.5 – 3.0. The smaller the relative depth of the recesses, which is recommended to range from 0.1 to 0.5, the larger this excess should be.

5. It is necessary to elaborate methods of surface preparation to ensure formation of the substrate surface microrelief in the form of densely located recesses with optimal values of the depth, matching sizes of the spray particles and an approximately axisymmetrical shape in the plan view. The latter condition corresponds to the hexagonal shape, which provides the possibility of a full surface covering.

6. It is necessary to elaborate approaches of fractal geometry to prediction and evaluation of microrelief of the surface prepared for thermal spraying, which would make it possible to reflect the processes of formation, evolution and dynamic properties of such surfaces, including in formation of a coating, as traditional methods have exhausted their capabilities for a sufficiently comprehensive description of such complex objects.

REFERENCES

1. (1985) *Thermal spraying. Practice, theory and application*. Miami, Florida: AWS.
2. (1983) *Schweißtechnische Richtlinien. Thermisches Spritzen*. Berlin: VEB Verlag Technik.
3. (1987) *PTM-2–87*. Preparation of surfaces of parts for deposition of thermal spray coatings. Typical technological process. Kyiv: PWI.
4. Metalli, M., Grimaud, A., Leger, A.C. *et al.* (1997) Alumina grit blasting parameters for surface preparation in the plasma spraying operation. *J. of Thermal Spray Technology*, **6**, 217 – 227.
5. Zaat, J.M. (1983) Thermal spraying. In: *Ann Rev. Mater. Sci.*, Vol. 13.
6. Kitahara, S., Hasui, A. (1974) A study of the bonding mechanism of sprayed coatings. *J. Vac. Sci. Technol.*, **4**, 747 – 753.
7. Bergmann, C.P. (1993) Preheating of substrate as adherence agent of plasma sprayed coatings. In: *Proc. of Conf. on Thermal Spraying'93*, Dusseldorf, May. Dusseldorf: DVS.
8. Funk, W., Goebe, F., Manz, M. (1988) The influence of substrate temperature on the bond strength of plasma sprayed oxide ceramics. In: *Proc. of 1st Plasma-Technik Symp.*, Lucern, May. Wohlen.
9. Metalli, M., Fauchais, P., Grimaud, A. (1996) Influence of substrate roughness and temperature on alumina coatings adhesion-cohesion. *Surface and Coating Technol.*, **2/3**, 275 – 286.
10. Wigren, J. (1988) Grit blasting preparation before plasma spraying. In: *Proc. of 1st NTSC*, Orlando, Sept.
11. Beauvais, C. (1982) Surface preparation, introduction, surface treatment. *J. Techniques de l'Ingenieur. Metallurgie*, **5**, 1435.
12. Dupras, J.J., Garnier, G. (1982) Chemical degreasing, surface treatment. *Ibid.*, 1450.
13. Apps, R. L. (1974) The significance of surface preparation in the flame spraying of metals. *The Chemical Eng.*, **292**, 769 – 773.
14. Amada, S., Yamada, H., Yomatsu, S. *et al.* (1992) Modeling and measurement of adhesive strength of thermal spray coatings. In: *Proc. of 13th ITSC*, Orlando, May – June.
15. Amada, S., Yamada, Y. (1993) Introduction of fractal dimension to adhesive strength of plasma sprayed coatings. In: *Proc. of 11th Int. Symp. on Plasma Chemistry*. Loughborough.
16. James, D.H. (1984) A review of experimental findings in surface preparation for thermal spraying. *J. of Mech. Work. Technol.*, Vol. 10, 221 – 232.
17. Yankee, S.J., Salsbury, R.L., Pletka, B.J. (1991) Quality control of hydroxylapatite coatings: the surface preparation stage. In: *Proc. of 4th NTSC*, Pittsburgh, May.
18. Metalli, M. (1992) Influence of roughness and temperature of substrates on adhesion. In: *Thesis of University of Technology of Compiegne on Cohesion and Residual Stresses of Plasma Sprayed Alumina Coatings*, Compiegne, Dec. 18.

19. Vityaz, P.A., Ivashko, V.S., Manojlo, E.D. *et al.* (1993) *Theory and practice of flame spraying of coatings*. Minsk: Navuka i Tekhnika.
20. Golego, N.L., Panamarchuk, V.G. (1974) On the effect of roughness of a material with the titanium substrate on adhesion strength of plasma nickel coatings. *Fiz-Khim. Mekhanika Materialov*, **6**, 32 – 35.
21. Yakovlev, G.M., Korolko, A.A., Ivashko, V.S. (1977) Effect of surface roughness on quality of a sprayed layer. *Mashinostroyeniye i Priborostroyeniye*, Issue 9, 15 – 17.
22. Medvedev, Yu.A., Morozov, I.A. (1975) On the effect of roughness and cold working degree on adhesion strength of plasma coatings. *Fizika i Khimiya Obrab. Materialov*, **4**, 27 – 30.
23. Stroganov, A.I., Drobyshevsky, A.S., Gots, A.B. (1982) Effect of roughness of the steel substrate on adhesion strength of the plasma coating. *Poroshkovaya Metallurgia*, **10**, 91 – 95.
24. Ivashko, V.S. (1979) Adhesion strength of coatings of self-fluxing hard alloys. *Mashinostroyeniye*, Issue 2, 103 – 105.
25. Matsubara, Y., Tomiguchi, A. (1992) Surface texture and adhesive strength of high velocity oxy-fuel sprayed coatings for rolls of steel mills. In: *Proc. of 13th ITSC*, Orlando, May – June.
26. Kupriyanov, I.L., Geller, M.A. (1990) *Thermal spray coatings with an increased adhesion strength*. Minsk: Navuka i Tekhnika.
27. Verstak, A.A., Kupriyanov, I.L., Iliushchenko, A.F. (1987) Peculiarities of interaction of spray particles with a rough substrate surface. *Svarochnoye Proizvodstvo*, **2**, 5 – 6.
28. Verstak, A.A., Kupriyanov, I.L., Iliushchenko, A.F. (1987) Effect of conditions of jet-abrasive blasting of part surfaces on adhesion of thermal spray coatings. *Avtomaticheskaya Svarka*, **8**, 69 – 70.
29. Ryzhov, E.V., Suslov, A.G., Fedorov, V.P. (1979) *Technological support to performance of machine parts*. Moscow: Mashinostroyeniye.
30. Ryzhov, E.V., Chistopian, A.F., Kharchenkov, V.S. (1973) Strength of adhesion of spray coating with steel substrate. *Vestnik Mashinostroyeniya*, **12**, 32 – 35.
31. Guipont, V., Cochelin, E., Borit, F. *et al.* (1998) Application of lattice gas models to plasma spraying. *Surface Eng.*, **5**, 400 – 404.
32. Sobolev, V.V. (1998) Morphology of splats of thermally sprayed coatings. In: *Proc. of the 15th Int. Thermal Spray Conf.*, Nice, May 25 – 29.
33. Gawne, D.T., Griffiths, B.J., Dong, G. (1995) Splat morphology and adhesion of thermally sprayed coatings. In: *Proc. of 14th ITSC*, Kobe, May.
34. James, D.H. (1984) Overview of experimental findings in surface preparation for thermal spraying. *J. of Mech. Work. Technol.*, **10**, 221 – 232.
35. Amada, S., Hirose, T. (1998) Influence of grit blasting pretreatment on the adhesion strength of plasma sprayed coatings: fractal analysis of roughness. *Surface and Coatings Technol.*, **102**, 132 – 137.
36. Provolotsky, A.E. (1989) *Jet-abrasive treatment of machine parts*. Kyiv: Teknhika.
37. Borisov, Yu.S., Kharlamov, Yu.A., Sidorenko, S.L. *et al.* (1987) *Thermal spray coatings of powdered materials*. Kyiv: Naukova Dumka.
38. Raff, A.U., Viderkhon, S.M. (1982) Erosion at collision of solid particles. In: *Erosion*. Moscow: Mir.
39. Kleis, I. (1959) Wear of metals in abrasive jet. In: *Transact. of Tallinn Polytechn. Institute*, Series A.
40. Katts, N.V., Linnik, E.M. (1953) *Electrometallizing*. Moscow: Selkhozgiz.
41. Nikiforov, G.D., Kitaev, F.I., Tsidulko, A.G. (1970) Adhesion strength of coatings sprayed by a plasma jet. In: *Problems of Technology of Fabrication of Flying Vehicles*, Issue 41. Kuibyshev.
42. Endeh, M., Shinmen, S. (1976) Influences of principal factors of pretreatment on surface roughness of mild steel substrate and adhesive strength of Zn sprayed coating. In: *Proc. of prepr. of papers for 8th Int. Thermal Spray Conf.*, Florida, May.
43. Havrda, M., Pitter, J., Lastovkova, O. (1976) Possibilities of lowering the costs for preliminary surface treatment by grit blasting under electrometallized coatings. *Ibid*.
44. Kudinov, V.V. (1977) *Plasma coatings*. Moscow: Nauka.
45. Sobolev, V.V., Guilemany, J.M., Martin, A.J. (1996) Influence of surface roughness on the flattening of powder particles during thermal spraying. *J. of Thermal Spray Technology*, Vol. 5(2), 207 – 214.
46. Fukanuma, H. (1996) Mathematical modeling of flattening process on rough surfaces in thermal spray. In: *Proc. of the 9th ITSC of Thermal Spray: Practical Solutions for Engineering Problems*, Cincinnati, Ohio, Oct. 7 – 11.
47. Feng, Z.G., Montavon, G., Feng, Z.Q. *et al.* (1998) Finite elements modeling of liquid particle impacting into flat substrates. In: *Proc. of the 15th Int. Thermal Spray Conf.*, Nice, May 25 – 29.
48. Kharlamov, Yu.A. (1990) On modeling of the process of collision of particles with surface in thermal spraying of coatings. *Fizika i Khimiya Obrab. Materialov*, **4**, 84 – 89.
49. Kharlamov, Yu.A. (1983) Cleaning of substrates from surface films in the process of spraying of powders. *Poroshkovaya Metallurgia*, **11**, 41 – 47.
50. Madejski, J. (1976) Solidification of droplets on a cold surface. *Int. J. Heat Mass Transfer*, Vol. 19, 1009 – 1013.
51. Arakelyan, A.A. (1985) Surface roughness in jet-abrasive treatment. *Tekhnologiya, Organizatsiya i Ekonomika Mashinostroit. Proizvodstva*, **7**, 5 – 8.

IMPROVEMENT OF METHODS AND MEANS OF PROTECTION FROM WELDING AEROSOLS

O.G. LEVCHENKO
The E.O. Paton Electric Welding Institute, NASU, Kyiv, Ukraine

ABSTRACT

The paper presents a review of works conducted at the E.O. Paton Electric Welding Institute concerning welders's protection from the harmful effect of welding aerosols. The need in an integrated approach, i.e. the combination of technological and sanitary-technical measures with a use of effective means of individual protection of respiratory organs of the welders, is substantiated.

Key words: *welding aerosols, technological recommendations, filter-ventilation units, means of individual protection of respiratory organs of welders, computer information-retrieval system, hygienic characteristics of welding aerosols*

The labour of welders is characterized by a presence of a number of hazardous and harmful production factors which are inevitable consequence of the welding process. Among them, a welding aerosol (WA) is most hazardous for the welders's health, as until now the welder is poorly protected from it. This is proved by the results of medical examinations which show that, among the occupational diseases of welders of Ukraine and other states of CIS about 80 % belongs to the bronchopulmonary diseases caused by the WA action [1]. There are also data about the fact that the action of WA on the respiratory organs can increase the risk of developing the oncological diseases [2]. The progress in welding fabrication requires the improvement of labour conditions of the workers-welders. The work in this direction is carried out in all the industrialized countries. In Ukraine the appropriate law was adopted on labour protection which prohibits the conductance of different types of works, including welding jobs, under the conditions which do not correspond to the existing standard requirements.

The measures directed to the improvement of the welders's labour conditions, did not give the positive results. The problem of creation of healthy and safe labour conditions of welders is still urgent. First of all, it is necessary to solve the problem of protection of the respiratory organs from the WA action. For this purpose, a radical approach is required.

As the world and domestic experience shows, the combination of technological and sanitary-technical measures on the elimination of the harmful effect of WA, and also the use of means of an individual protection of the respiratory organs (MIPRO) of welders make a basis for the system of measures on the protection of welders and environment from the WA action.

The first direction of this system (technological) consists in reducing of the WA evolution level into the air by the improvement of the process, selection of the technology and method of welding, type and grade of welding consumables, shielding gas and welding conditions. The second direction (sanitary) consists in localizing and neutralizing of WA by using the advanced effective local ventilation facility. The third direction consists in using the MIPRO of the new generation which makes it possible to protect the respiratory organs of the welders under different industrial conditions.

Depending on the labour conditions and also on the requirements to the welded joint quality it is necessary to use either the complex of these measures or some of them. Due to realizing of all the mentioned complex of measures the similar problems of welding fabrication in the foreign industrialized countries are almost solved. In many European countries special catalogues and computer databases are compiled on the basis of a detailed examination of chemical composition and levels of WA evolution, thus providing opportunity to select the most favourable welding consumables and welding conditions as to the hygienic aspect.

To provide protection from WA, the effective facility of a local ventilation is used of such known companies as «Plimo Vent», «Nederman», ESAB, «Kemper» and others, MIPRO (welder's masks with a system of pure air supply to the respiratory zone) of companies «Racal». «Nederman», «Hornell Speedglas, Inc.», etc. In Russia, a mass production of advanced facility of a local ventilation (for the working stations of welders) by the companies «SovPlim», «Ekoyurus-Vento», etc. has been mastered.

In Ukraine, the welders's labour conditions were also improved over the recent decade according to the above-mentioned directions.

The realization of the first direction, i.e. development of technological methods of reducing the WA evolution, is feasible on the basis of a thorough study

of process of their formation. As to two other directions, these data are also initial in developing the appropriate methods and equipment of the WA neutralizing.

At the E.O. Paton Electric Welding Institute of NAS of Ukraine the investigations of the processes of WA formation were made and the recommendations were issued for the reducing and neutralizing of their evolution in arc welding. For this purpose, it was necessary to study the regularities of WA formation in arc welding [3], to make a review of technological recommendations for the decrease in the WA evolution [4], to develop the classification of WA, formed in different methods of welding [5], to create the computer information-retrieval system of hygienic characteristics of WA and methods of welding, during which they are formed [6], and, on this basis, to suggest the methods and equipment of WA neutralizing.

When developing the technological recommendations on the improvement of hygienic characteristics of the arc welding processes, the experience of earlier investigations made at the PWI, was taken into account [7]. Therefore, taking into consideration the positive results, obtained in manual welding with coated electrodes, our investigations were aimed mainly at the mechanized methods of welding, which occupy the second place as to the volume of application after the welding with coated electrodes. The results of the mentioned investigations, as the experience showed, can also be used for the improvement of labour conditions in case of using other methods of the arc welding.

Methods of investigations. The investigations of amount of evolutions and chemical composition of hard constituents of WA (HCWA) were carried out using the generally-accepted procedures approved by the Ministry of Health [8 – 10] in special benches adapted for definite methods of welding.

The study of filtering characteristics of grained materials used for the air purification from WA was made using procedure, developed at the Physical-chemical Institute of Protection of Environment and Mankind of Ministry of Education and NAS of Ukraine (PhChIPE&M) in collaboration with the PWI, in a special bench. Aerosol, forming during welding in a special chamber, was passed through a column with a filtering material and a wind tunnel for the WA sampling. The filter effectiveness was determined by measuring the concentration of HCWA and gases, sampled before and after filtering.

To evaluate the amount of WA evolutions, two new characteristics, except usual characteristics (intensity of WA formation, g/min, and specific evolution, g/kg) [8], were also used, such as coefficient of intensity of WA evolution, g/(kW·h), and coefficient of specific evolution of WA, g/(kW·kg) [11]. These characteristics take into account the main parameters of the welding conditions, influencing the WA evolution and providing more objective hygienic evaluation of welding consumables and methods of welding.

At the same time, to evaluate the WA toxicity or degree of effect on the organism at a definite method of welding, the characteristics of air exchange of the general ventilation by dilution, i.e. volume of air which is necessary to supply to the production room to dilute the WA harmful elements up to limiting admissible concentrations (LAC) were used. The air exchange of ventilation was expressed in cubic meters per kilo of welding consumable in accordance with locally accepted procedures, and also in cubic meters per hour (time unit) in accordance with the IIW methodology.

An initial characteristic, determined experimentally, is only intensity of WA formation, while the other characteristics are to be calculated. Therefore, to process a large amount of data obtained at different methods of welding, a computer information-retrieval system of databases of WA hygienic characteristic, named «ECO-WELD», was developed in collaboration with programmers of the PWI [6]. It consists of three databases: for coated electrodes; welding materials designed for the mechanized welding (solid and flux-cored and activated wires for shielded-gas welding, and also self-shielding and surfacing strips) and for welding fluxes. Each of them takes into account its peculiarities and factors influencing the level, chemical composition and toxicity of WA. The initial data, put into this system, are the level of evolutions and chemical composition of WA. The rest data required for a comprehensive hygienic evaluation are displayed on the monitor screen and printed. In addition, depending on the welding material grade, the information system issues recommendations about the necessary means of protection of welders and environment. These recommendations are based on the hygienic and chemical classification of WA, developed by us, and methods of welding at which they are formed. The main advantages of the offered computer system in a scientific aspect are, first of all, the feasibility to perform a comparative hygienic evaluation of welding materials and to issue the recommendations of protection from WA, and, secondly, the feasibility of a comprehensive analysis of effect of all the factors of the welding process on hygienic characteristics, including also the required volume of the ventilation air exchange.

Selection of welding method (welding material). Using our information-retrieval system, the effect of method of welding, type of welding material and class of alloying of the parent metal on the volume of the ventilation air exchange was evaluated. The results of comparative hygienic evaluation of methods by minimum and maximum values of volume of the air exchange for different grades of welding materials (Table) prove that the required volume of the ventilation air exchange for all the methods of welding is increased, first of all, with increase in a degree of

Required volume of ventilation air exchange depending on the method of welding and used welding consumables

Class of steel	*Method of welding and welding consumables*	*Required volume of ventilation air exchange, m^3/kg*
High-alloyed	MAW, using electrodes with coatings:	
	basic	11800 – 89000
	rutile-basic	13900 – 76000
	rutile	4200 – 35000
	Flux-cored wire	5200 – 70200
	Solid wire in shielding gases	1300 – 28300
	AAW with fluxes:	
	fused	80 – 1350
	ceramic	70 – 530
Alloyed heat-resistant	MAW, using electrodes with coatings:	
	basic	7400 – 39000
	rutile-basic	3700 – 3900
	Flux-cored wire	3100 – 6100
	Solid wire in shielding gases	1100 – 5850
	AAW with fluxes:	
	fused	90 – 570
	ceramic	400 – 550
Carbon and low-alloyed	MAW, using electrodes with coatings:	
	basic	2200 – 24000
	rutile-basic	2400 – 11700
	acid	6200 – 11500
	ilmenite (acid-rutile)	4000 – 9800
	rutile	2400 – 9500
	cellulose	3000 – 3600
	acid-cellulose	4100 – 4200
	Flux-cored wire	2300 – 21500
	Activated wire	2100 – 6500
	Solid wire in shielding gases	1100 – 5900
	AAW with fluxes:	
	fused	30 – 570
	ceramic	30 – 550

steel alloying, that is explained by the presence of toxic elements in WA of the first and second classes of hazard (GOST 12.1.005–88), i.e. compounds of cancerogenic hexavalent chromium and nickel, compounds of manganese, soluble and insoluble of fluorides, hydrogen fluoride and silicon tetrafluoride. At the same time, the volume of ventilation air exchange depends also on the method of welding: maximum volume in welding with coated electrodes, lower volume using the flux-cored, then activated wires, much lower volume at welding with solid wires in shielding gases and minimum volume in automatic SAW (Table). More precise comparison depends on the definite grade of the welding material. The cause of increased toxicity of WA forming in welding with the flux-cored wires, as compared with solid wires, is the presence of fluorides (fluorite and sodium fluosilicate) in it, except of manganese. It is their presence that increases the required volume of the ventilation air exchange. As to the coated electrodes, then the WA toxicity is determined by the kind of the electrode coating: maximum toxicity was observed in aerosols evolving in use of the electrodes with a basic coating, due to presence of fluorides in them. This toxicity is reduced by introducing the rutile into the coating (Figure 1). Cellulose coating is a source of a large amount of aerosol due to burning of cellulose with an evolution of carbon monoxide and CO_2, hydrogen and vapours of water, which, however, contains a negligible amount of elements which define its toxicity.

In mechanized welding of any types of steels a larger amount of WA is formed in a flux-cored wire welding. The highest WA toxicity is observed in welding of high-alloyed steels (Figure 2). This is explained by the presence of a hexavalent chromium in them in the form of potassium and sodium chromates forming in interaction of chromium with potassium and sodium compounds available usually in the wire core. Natu-

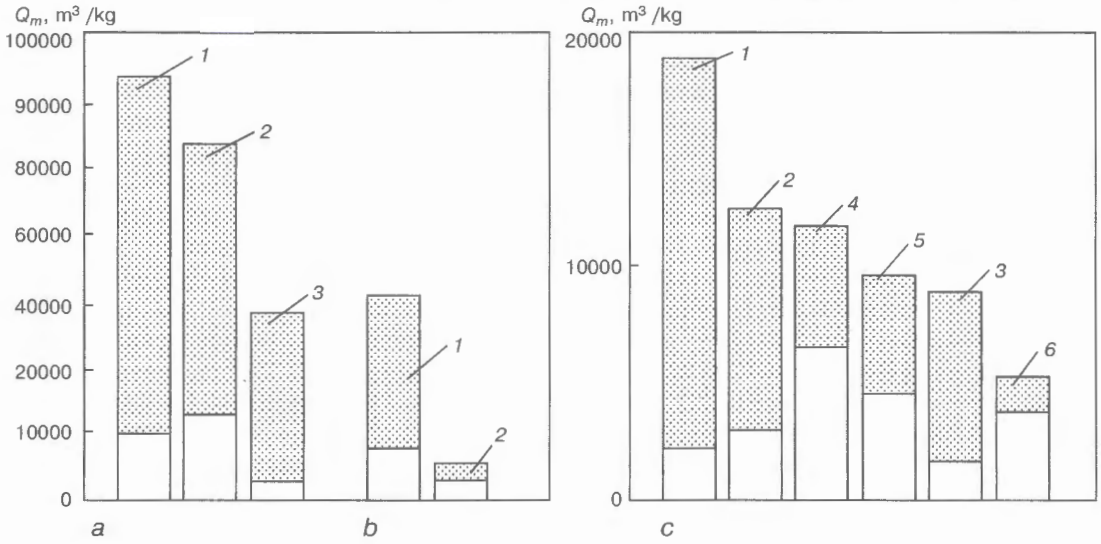

Figure 1. Effect of type of electrode coating on the volume of air exchange, Q_m, of ventilation in welding with coated electrodes: *a* — high-alloyed; *b* — alloyed; *c* — carbon steels; *1* — basic; *2* — rutile-basic; *3* — rutile; *4* — acid; *5* — ilmenite; *6* — cellulose coatings; here and in Figures 2 and 3 the hatched parts of diagrams are the limits changing the volumes of air exchange for different grades of welding materials

rally, there are no potassium and sodium chromates in WA during solid wire welding. Therefore, the solid wires have great advantages as compared with flux-cored wires.

In SAW the volume of the air exchange ventilation is negligible (Table) in spite of presence of a large amount of manganese and fluorides in WA. This is explained by the effect of a flux protective layer on the WA evolution, which, except its direct purpose, fulfils also the role of grained filter on which the aerosol from the weld pool is precipitated. When the ceramic (agglomerated) flux is used, the level of WA evolution is lower (Figure 3) as the grain sizes of the ceramic flux are finer, being the more effective filter than the fused flux.

Comparative hygienic evaluation of definite grades of welding materials to select the most favourable from the hygienic aspect is made by comparison of the characteristics of the required volume of air exchange, when they are used. Here, the offered computer system is a tool for the conductance of these comparisons.

Control of WA composition. Examination of HCWA chemical composition showed its great difference from the estimated composition of saturated vapour over the melt (in accordance with Konovalov's law) [12]. This is due to the fact that in electric arc process the HCWA is formed as a result of not only equilibrium but also explosive evaporation as a result of failure of the metallic bridge between the electrode and weld pool, and also because of a fast erosion of upper layers of surface in constricted regions of the arc, thus leading to an abrupt decrease in content of a volatile manganese in HCWA.

The allowance for the above-mentioned phenomenon made it possible to decrease the content of manganese in HCWA and also to reduce more than twice the intensity of its evolution in welding at a pulsed modulated current instead of a continuous current [13]. This is explained by the decrease in the total arc power at the expense of pauses in current supply which reduce the total arc energy typical of welding at a continuous current and leading in some cases to

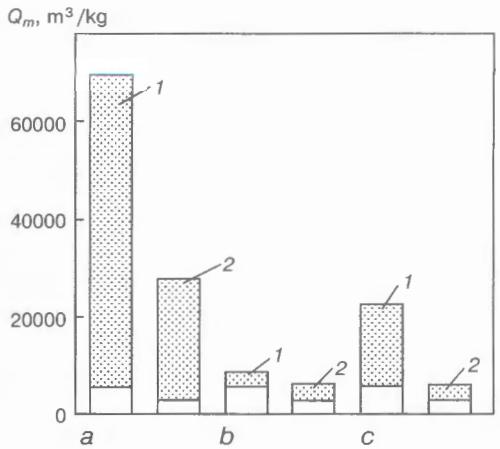

Figure 2. Effect of type of welding wire on the volume of ventilation air exchange: *a* — high-alloyed; *b* — alloyed; *c* — carbon and low-alloyed steels; *1* — flux-cored wire; *2* — solid wire

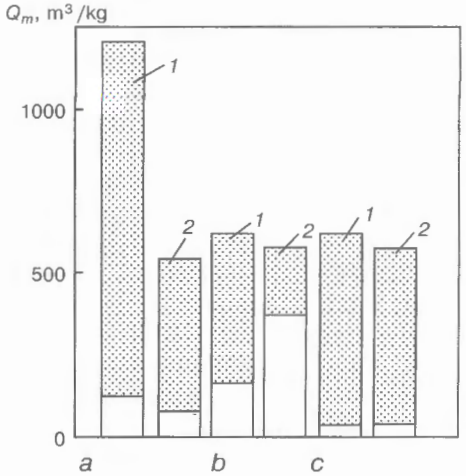

Figure 3. Effect of flux type on volume of ventilation air exchange: *a* — high-alloyed; *b* — alloyed; *c* — carbon and low-alloyed steels; *1* — fused; *2* — ceramic flux

overheating and evaporation of metal. The intensity of WA formation and content of manganese in it are decreased also with a decrease in current and voltage of pulses and also with an increase in their duration. Therefore, the selection of optimum condition of current modulation allows the HCWA evolution to be decreased without reducing the welding efficiency [11].

Selection of welding conditions. It was observed during study of the effect of welding conditions on the HCWA evolution that dependencies of the levels of their evolution on welding current have a complex form with maximum and minimum [4, 14]. The examination of the penetration shape of the parent metal using macrosections could establish that minimum evolution of HCWA corresponds to a maximum depth of the weld pool, i.e. maximum arc immersion to the parent metal [15].

Results of investigations of dependencies of levels of WA evolutions on the welding conditions and welding wire diameter showed that the HCWA evolution is reduced with the decrease in the welding wire diameter. There are definite values of welding currents for each wire diameter, at which the intensity of aerosol evolution is maximum, and also a region of currents providing a minimum evolution of the aerosol. It was revealed during investigations of the relations between the intensity of formation of components of a gaseous constituent (GCWA), i.e. carbon monoxide and nitrogen oxides, and welding conditions, that their evolution is minimum at maximum immersion of the arc into the parent metal and decrease in area of contact of the welding arc with the air, surrounding the arc, and shielding gas.

Results of these investigations have led to the conclusion that the level of the WA evolution is defined by the system of factors, indicating that the intensity of the WA formation is defined, first of all, by the arc capacity, i.e. welding conditions, compositions of welding material and shielding atmosphere, which in their turn define the type of the electrode material transfer and level of its spattering, which also influence the level of the WA evolution. Therefore, the electrode metal transfer control by the selection of optimum compositions of welding materials, shielding gas, application of modulated current welding and adjustment of its conditions made it possible to decrease the WA evolution.

When selecting the optimum compositions of welding materials and welding conditions it is necessary to follow the system: composition–welding conditions, as there are definite welding conditions for each grade of welding materials at which a minimum amount of the aerosol is evolved [16]. We have developed the system of prediction of the levels of WA evolution, which is necessary in the development and improvement of welding consumables and technologies [11, 12].

Sanitary-technical measures. Technological recommendations allowed the level of WA evolutions to be decreased only within the certain ranges and the volume of air exchange of ventilation, and, consequently, the expenses for the ventilation to be decreased by the same times. However, when following only technological recommendation it is not always possible to reach the decrease in the content of harmful elements up to LAC at the existing systems of ventilation. It is necessary to use also other sanitary-technical means, among which the self-contained filtering-ventilation units (FVU) are most effective. They are designed for trapping the aerosol evolving during welding from the place of its formation, purification of air from it and return to the same room. As compared with a general ventilation by dilution these units are more effective and reduce the expenses for ventilation and heating of industrial rooms.

If it is impossible to use FVU and the existing systems of ventilation are not effective, the MIPRO should be used in the form of welder's masks with a system of a forced supply of the purified air into the respiratory zone (under the shield), which are most effective and convenient in use.

To develop these means of ventilation and individual protection of the respiratory organs and also their proper purpose depending on the method of welding it is necessary to have data about the chemical composition of aerosols forming at different methods of welding. In addition, the application of FVU with versatile filters trapping of both HCWA and GCWA is not always rational. Therefore, to create the highly-efficient FVU of the new generation and selection of suitable filtering materials we have examined the compositions of WA forming at different methods of welding. Here, it was assumed that FVU and MIPRO should purify air not only from HCWA but also from toxic gaseous WA components (hydrogen fluoride, silicon tetrafluoride, carbon monoxide, nitrogen oxides and ozone) whose presence is typical in some combinations of either methods of welding. We have suggested the WA classification by chemical composition and methods of welding at which they are formed [5]. Methods of WA neutralizing and purification of air from them are defined for each class. As for the purification from HCWA the mechanical filtering is mainly used on cloth filters, which is feasible only at some methods of welding, for example, with electrodes having fluoride-free coating, then it was necessary to search for the new filtering materials for the neutralizing of gases. For this purpose the filtering characteristics of different grained materials were examined. As a result, the new filtering material was suggested on the base of a natural mineral of alumosilicate, the Transcarpathian zeolite-clinoptilolite [17]. The new filtering material purifies the air from the carbon monoxide by its catalyst oxidation to dioxide, i.e. transforms the harmful carbon monoxide gas to a harmless CO_2.

Means of protection of respiratory organs of welders and environment of the new generation for different methods of welding and conditions almost from

all the classes of WA have been developed: mobile FVU «Temp-2000» [18], «Mriya-1M» [19], stationary filtering system on the FVU «Temp-2000» base [19], grained filter [20], portable ventilation unit «Shmel-2500» [21, 22].

FVU «Temp-2000» and stationary filtering system on its base developed at the PWI in collaboration with MNTTs «Temp» provide a high efficiency in WA trapping, due to a ventilation unit of a special design, higher life of the filtering element and convenient cleaning of the filter. The increase in the filter service life is provided by using a rotary precipitation of large particles of aerosol by a special device, and finer particles – by a cloth hose filter. The filter cleaning from HCWA is automatic at the moment of switching on and off of the unit due to a abrupt drop of pressures [18].

The known FVU «Mriya-1» developed in PhChIPE&M in collaboration with the PWI was modified. Filtering element from the modified clinoptilolite was used in it as the second stage of the filter for trapping gases (carbon monoxide and nitrogen oxides) [17].

In collaboration with PhChIPE&M a single-stage grained filter was developed using the clinoptilolite for the air purification from HCWA and GCWA. Regeneration of filter is performed by an abrupt mechanical shaking of filtering elements by a wedge-type lifting-dropping mechanism [20].

To remove WA from hard-to-reach working places and closed volumes (ship holds, etc.), a small-sized portable ventilation unit «Shmel-2500» [21] was developed in collaboration with Design Office of A.V. Bogatsky Physical-chemical Institute of NAS of Ukraine. This unit is peculiar by the presence of a special electrical unit-rectifier, decreasing the voltage from 220 to 12 V, that makes it possible to use this unit in extrahazardous conditions.

Means of individual protection of respiratory organs. For the conditions where the use of ventilation systems is difficult, the following MIPRO have been developed: hose mask of the welder with a system of the air purification and supply [19], self-contained welder's mask with a portable system «Shmel-50» of the purified air supply [23] and self-contained device «Shmel-40» for the air purification and supply to the respiratory zone [19, 22].

The hose mask of the welder with a system of the air purification and supply is designed for the protection of respiratory organs during work at the stationary welding stations. It is effective due to a high efficiency of air supply to the respiratory zone (150 – 200 l/min) and using a two-stage filter with clinoptilolite in it which purifies the air from HCWA and GCWA [19].

When the work is done at non-stationary sites a protective mask is offered with a portable system of air purification and supply (joint development of the PWI and Design Office of A.V. Bogatsky PhChI), named «belt-filter» [23]. This device which is fastened at the welder's belt consists of a filter, ventilation unit, bank of batteries for electrical supply and charging.

Device of a new design «Shmel-40» [19, 22] for the air purification and supply to the respiratory zone combines the advantages of the system of a forced feeding of the purified air and a filtering respirator. The air, purified in the belt-filter is supplied via the air duct connected not to the welder's shield, but to a respiratory half-mask that guarantees the complete isolation of respiratory organs from the air contaminated with aerosol at minimum its supply (30 – 40 l/min) providing the required breathing cycle of the man. This system is used in a set with a shield of any type, not adapted for connection to the belt-filter.

The above-mentioned means of a local ventilation and MIPRO have passed the industrial tests and implemented at the enterprises of Ukraine and Russia including the Works of elevators and «Energiya» Works (Kiev), joint stock ship company «Ukrrechflot», Monastyrishchi machine-building plant, enterprises of ports of Odessa and Yuzny cities, at Votkinsk Hydroelectric Station (Russia) and many other enterprises. The serial production of local ventilation units is mastered at MNTTs «Temp».

Thus, the investigations carried out at the PWI made it possible to offer the new technological recommendations which consist in use of well-grounded methods of welding and welding consumables taking into consideration the developed hygienic classification of WA, thus providing the minimum toxicity of the process. When developing the new welding technologies it is necessary to try to use the welding materials with a low content of main toxic components, to decrease the oxidizing ability of the shielding gas, to select the welding conditions that provide the minimum WA evolution, to use the current sources with a welding current modulation. The selection of adequate means of protection of welders and environment from WA by a user (but not a specialist on hygiene, ecology and labour protection) can be made by a computer system «ECO-WELD» based on classification of WA. It issues the information about the hygienic characteristics of WA (intensity and specific evolution, coefficients of intensity and specific evolution of WA components, volume ventilation air exchange), and also (depending on the grade of the welding material used) about the required means of ventilation and individual protection of respiratory organs with an indication of the enterprises-manufacturers. The developed means of protection have passed the tests under the industrial conditions and are now implementing in industry.

REFERENCES

1. Gorban, L.N., Lubyanova, I.P. (1991) Intensification of arc welding processes and problems of preservation of welder's health. *Svarochnoye Proizvodstvo*, **3**, 33 – 34.
2. (2000) IIW VIII-1888–00. Incidence of cancer among welder and other shipyard workers with information on previous work history (JEOM) by T.E. Danielsen et al., provided by K. Brown (USA). *JEOM*, **1**, 101 – 109.
3. Levchenko, O.G. (1996) Processes of welding aerosol formation (Review). *Avtomaticheskaya Svarka*, **4**, 17 – 22.

4. Levchenko, O.G. (1998) Technological methods of reducing the level of welding aerosol formation (Review). *Svarochnoye Proizvodstvo*, **3**, 32 – 38.
5. Levchenko, O.G. (1999) Classification of welding aerosols and selection of methods of their neutralizing. *Avtomaticheskaya Svarka*, **6**, 38 – 41.
6. Demchenko, V.F., Levchenko, O.G., Metlitsky, V.A. *et el.* (2000) Databank of welding aerosols. *Svarshchik*, **4**, 29.
7. Pokhodnya, I.K., Gorpenyuk, V.N., Milichenko, S.S. *et al.* (1990) *Metallurgy of arc welding: processes in arc and electrode melting*. Kyiv: Naukova Dumka.
8. (1980) *MU No.1924–78*. Hygienic assessment of welding consumables and methods of welding, surfacing and cutting of materials. Moscow: Minzdrav USSR.
9. (1989) *MU No.4945–88*. Methodical recommendations on determination of harmful elements in welding aerosol (hard phase and gases). Moscow: Minzdrav USSR.
10. Pokhodnya, I.K., Shlepakov, V.N., Suprun, S.A. *et al.* (1983) *Methodology of primary sanitary-hygienic evaluation of flux-cored wires*. Kyiv: PWI.
11. Golovatyuk, A.P., Levchenko, O.G. (1985) Characteristics of gross evolutions of welding aerosols and their use in practice. *Svarochnoye Proizvodstvo*, **10**, 40 – 41.
12. Podgayetsky, V.V., Golovatyuk, A.P., Levchenko, O.G. (1989) About the mechanism of formation of welding aerosol and prediction of its composition. *Avtomaticheskaya Svarka*, **8**, 9 – 12.
13. Levchenko, O.G. (2000) Formation of aerosols in CO_2 modulated-current welding. *The Paton Welding J.*, **8**, 47 – 49.
14. Levchenko, O.G., Metlitsky, V.A. (1997) Express evaluation of welding aerosol evolutions. *Avtomaticheskaya Svarka*, **4**, 40 – 45.
15. Levchenko, O.G. (1992) Effect of technological conditions of CO_2 welding of structural steels on the aerosol evolution. *Ibid.*, **9/10**, 31 – 33.
16. Golovatyuk, A.P., Levchenko, O.G. (1990) *Hygiene of labour in shielded-gas welding*. Kyiv: PWI.
17. Shevchenko, L.A., Pashchenko, A.A., Andrianov, Yu.I. *et al. Method of sorbent producing for purification of gases from carbon monoxide*. USSR author's certificate **1549583**, Int. Cl. B 01 D 53/02. Publ. 15.03.90.
18. Levchenko, O.G., Metlitsky, V.A., Rudoj, V.D. *et al.* (1999) Filter-ventilation unit «Temp-2000». *Avtomaticheskaya Svarka*, **5**, 64 – 65.
19. Levchenko, O.G., Metlitsky, V.A. (1999) *New means of protection from welding aerosols*. Kyiv: Ekotekhnologiya.
20. Ennan, A.A., Butvin, A.N., Kvasenko, A.F. *et al. Grained filter*. USSR author's certificate **1393455**, Int. Cl. B 01 D 23/10. Publ. 07.05.88.
21. Iliinsky, N.I., Andrianov, Yu.I., Levchenko, O.G. *et al.* (1995) Portable ventilation unit for removing welding aerosol from closed volumes. *Svarochnoye Proizvodstvo*, **9**, 35 – 36.
22. Levchenko, O.G. (1999) Complex of new means of protection of welders' respiratory organs. *Ibid.*, **10**, 42 – 45.
23. Levchenko, O.G., Metlitsky, V.A., Iliinsky, N.I. *et al.* (1996) Protective welder's mask with a portable system of air purification and supply to the respiratory zone. *Ibid.*, **7**, 32 – 33.

OBJECT-ORIENTED PROGRAMMING OF SYSTEMS OF WELDING TECHNOLOGICAL PROCESS CONTROL

F.N. KISILEVSKY and **V.V. DOLINENKO**
The E.O. Paton Electric Welding Institute, NASU, Kyiv, Ukraine

ABSTRACT

The use of object-oriented programming in the development of systems of welding technological process control is considered. A fragment of the electron beam welding installation is selected as an example of a complex object of control. The object-oriented analysis is made, the diagram of relations and synchronizing is plotted and a conceptual solution for the network control system of the automated system of welding technological process control is suggested.

Key words: *automated control system, object-oriented programmimg, decomposition, abstraction, hierarchy, model of control, diagram of relations and synchronizing, network architecture, real time, Markovian processes, graphs of state, software reliability.*

The advanced automated systems of welding technological process control represent complex information management systems with a comprehensive software, in which the interaction with an operator-welder or operator-technologist is provided. During welding the various units and mechanisms, having complex algorithms of functioning, are often used. In this connection it is very important to create the software for automated system of the welding technological process control. The developers of these upgraded systems for complex welding objects should take into consideration the strict requirements which are specified to the software, namely:

- increased reliability of software functioning in combination with hardware of automated control systems under the conditions of high electromagnetic and others noises;
- sufficient «friendliness» of interface of the software operator by using the graphical interactive objects and means;
- minimum time of development.

At present the developers of the automated systems of technological process control pay attention more often to the object-oriented design (OOD). The experience in use of this technology in the engineering projects shows its high effectiveness [1].

The OOD includes the following methods:

1. Decomposition. Unlike the algorithmic decomposition, the object-oriented decomposition is used with abstractions of objects in a subject field of welding;

2. Abstracting and formation of classes of objects having similar functions;

3. Hierarchy. In this case the organizing of the hierarchic system of classes of objects, organizing of the model itself of the object of control and architecture of the automated system of the technological process control is meant. Such approach can provide more steady processing of data flows using the software in very complicated systems of control.

OOD includes several methodologies. First, object-oriented analysis (OOA) which represents a methodology of decomposition and creation of models both as an object of control and also systems of control as a whole. In the given case the requirements to the models are formed on the basis of concepts of classes and objects from the field of welding.

Secondly, the object-oriented programming (OOP) which represents the methodology of programming or realizing of abstract models of programming using the object-oriented languages. Thus, the working program represents a system of objects, where each of them is a realization of a definite class and characterized by an own algorithm of behaviour and interaction with other objects.

As is known, the main methods of OOD is inheritance, polymorphism and encapsulation. Therefore, the objects can inherit their properties from the objects of other classes, change their behaviour depending on external conditions and contain the necessary data, procedures or other objects.

Let us dwell on the following practical aspects of application of OOD approach when developing software for the automated system of welding technological process control:

- use of OOA;
- plotting of diagrams of relations and synchronizing of objects;
- use of object-oriented languages, such as C++ or Java;
- use of graphs of state, describing the behaviour of objects in a real time;
- use of results of theory of graphs for the software automated testing and running.

To illustrate the feasibility of use of the OOD approach in the problems of automation of welding processes, we shall consider a definite case of automation of a complex object of control in EBW. Not pretending on the completeness of discussion of the problem of automation in EBW, we shall consider only a fragment of a complex object of control (Figure 1), namely a vacuum welding chamber and

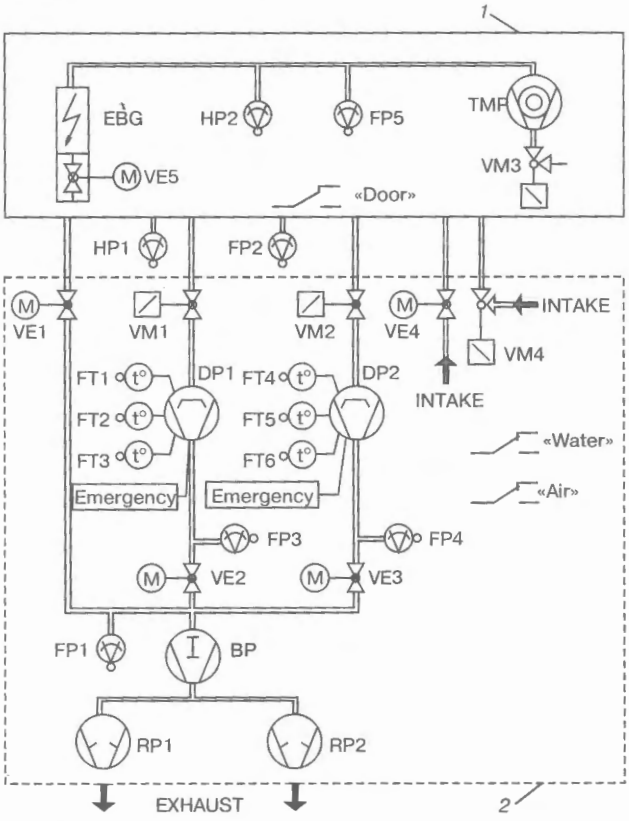

Figure 1. Example of a complex object of control of the automated system of welding technological process control: *1* — vacuum welding chamber; *2* — evacuation system; EBG — electron gun; VE5 — gun gate; HP1, HP2 — high vacuum sensors of pressure; FP1 – FP5 —, low-vacuum sensors of pressure; VM1 – VM4 — vacuum valves; VE1 – VE4 — electromechanical gates; FT1 – FT6 — low-temperature sensors of temperature; BP — pump of Roots; DP1, DP2 — diffusion; RP1, RP2 — forevacuum; TMP — turbomolecular pumps

pumping system [2]. Surely, in this case we have to take into account also that these two key subsystems cannot be regarded separately from other subsystems of the electron beam installation. Therefore, in discussing the problem of synchronizing the objects, the subsystems of drives of displacement of electron gun and workpiece manipulator, and also the electron beam equipment (EBE) will also be mentioned. Unfortunately, due to a limited volume of this article, there is no opportunity to consider these subsystems in detail, as well as others, which can be included into the composition of the electron beam installation: TV follow-up system [3], subsystem of monitoring of the welding process, etc.

In spite of this, the fragment of the objects of the EBW control, selected as a demonstration model, gives a picture about the level of complexity and variety of abstractions which are used by the software developers.

In the present article an attempt is made to show that OOD approach makes it possible to fulfil the more complete and detailed statement of the problem of development of the software of the welding control system. Here, a subjective aspect is greatly limited, typical of heuristic, intuitive solutions during selection of architecture and decomposition of control system, the base of formal rules is widened, thus resulting in guarantee of producing stable non-contradictory results at each stage of the project realization.

Let us illustrate the result of a preliminary analysis in the form of the diagram of classes of the control object model (Figure 2), thus omitting the stages of analysis of EBW automation, and also the description of the process of grouping and distinguishing of classes of objects (units, executive mechanisms and subsystems). Here, the following designations of classes are used: TGraf — graphs of states which describe the behaviour of objects in time; TAparatus — parental for all the devices and mechanisms, presets an emergency flag, time characteristics of the unit «on-off», stores the operation conditions (manual, automatic or idle), and also flag of running the command of control of the state switching; TDigIn — signals of discrete input; TDigOut — signals of discrete output; TFilter — filters which are used for filtering of input signals (median filter, low-frequency filters, etc.); TAnaIn — signals of analog input; TDigSensor — sensors of discrete mode of «on-off» type; TAnaSensor — sensors of analog mode (pressure, etc.); TFurnace — heating elements which are used in some types of pumps; TValve — vacuum valves including pneumatic and electromagnetic; TBolt — gates, which, unlike the valves, have two sensors of position («open» and «closed»); TPump — pumps; TDiffusPump — diffusion pumps, inheriting the properties of TPump and TFurnace; TVacChamber — vacuum welding chamber which uses three classes of objects in its composition (TValve, TBolt, TPump); TBeamGun — electron gun, using three analog signals of control (current of beam, focusing and filament) and one discrete signal of control; TPumpSystem — evacuation system; TWeldSystem — welding system (as well as TVacChamber and TPumpSystem, encapsulates TGraf for realization of necessary conditions of operation of the automated system of welding technological process control). It should be noted that the classes of TVacChamber and TPumpSystem make references to each other use in their realizations. This is necessary for the combined work of objects of these classes in a single welding system.

As it is impossible to dwell on each object in detail, some statements will be presented only in the form of results.

The diagram of classes of the object of control makes it possible to synthesize the model of the object of control in the object concepts of a definite type of welding.

At the next stage of OOD-design a model of the automated system of welding technological process is created, which contains a model of object of control and has usually a network hierarchic structure. The typical scheme of networking the hierarchy of control levels is as follows:

system → subsystems → units and mechanisms → → sensors (analog, discrete, etc.) → signals (analog, discrete, etc.).

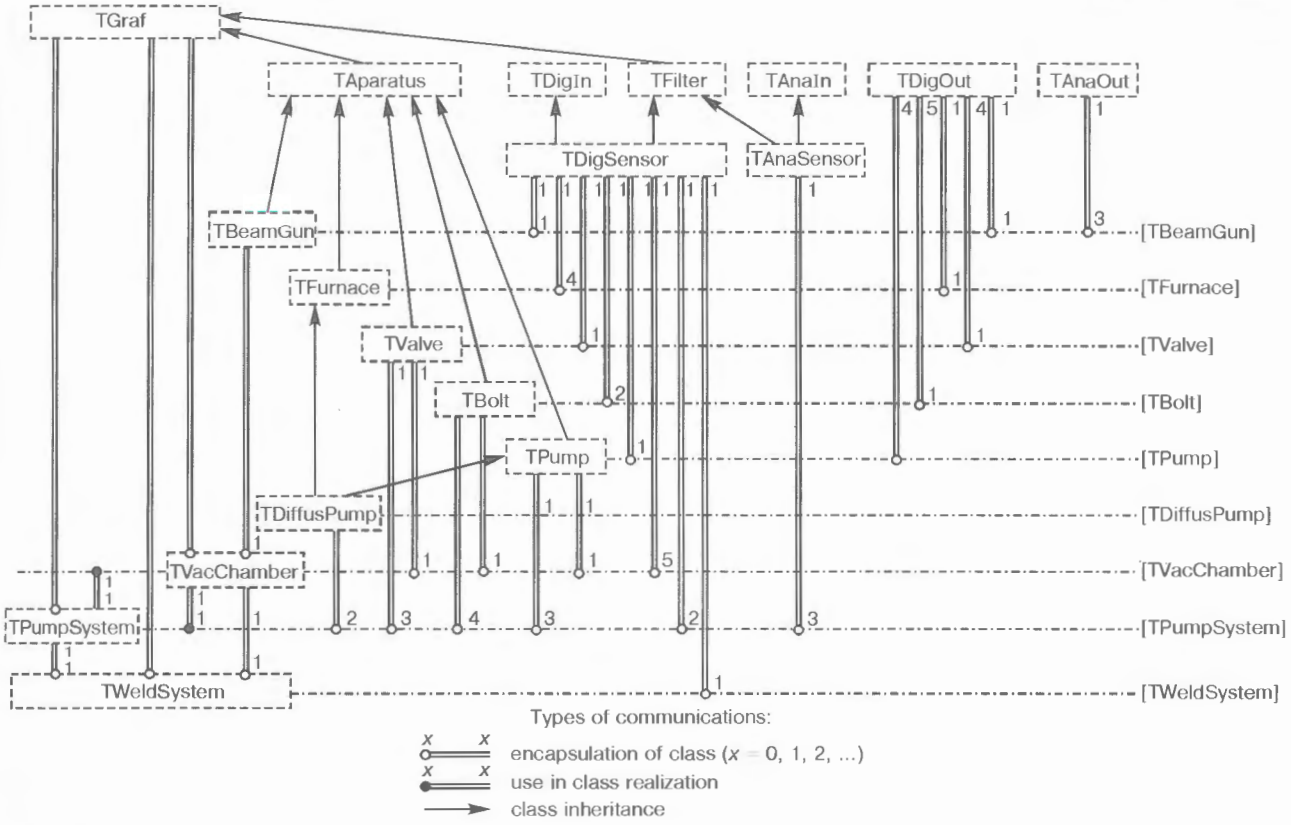

Figure 2. Diagram of classes of control object in the automated system of the welding technological process control

In construction of the object model a principle of distribution of «intellect» is used, which consists in the fact that each object in the model is functioning by its own algorithm which is typical of objects of its class. Such behaviour algorithm is convenient to be presented in the form of a directed graph of states or Petri network with necessary time delays, which preset the behaviour of the object in a real time.

Figure 3 presents a diagram of relations and synchronizing, which realizes the model of the control object where special designations show the nature of relations between objects that determine the functioning of the automated system of welding technological process control in a real time. The following types of synchronizing are most often used:

- synchronous (rigid, simple) — the action is fulfilled not depending on the readiness of a receiving signal;
- asynchronous — the expectation of mutual readiness of transmitting and receiving objects is realized;
- delayed — asynchronous type with a specified time of response expectation;
- postpone — asynchronous type, but in case of non-readiness of the receiving object the transmitting object does not fulfil operation.

Diagram of communications and synchronizing of the objects is used for decomposition of the automated system of the welding technological process control into the subsystems. Depending on its complexity and type of the welding technological process the distributed, centralized, network or other architecture can be selected. The network structure of the automated system of the welding technological process means such an organization at which the information channels of communication and protocols of information exchange have a system-organizing meaning.

The present tendency in construction of the automated system of welding technological process control is an application of network architectures in which several kinds of information network channels of communication can be used. At the upper levels of the automated systems of technological process control the networks of Ethernet (Industrial) and modem communication with protocols of exchange TCP/IP are more often used. At the level of controllers and sensors the FieldBUS-networks, for example, PROFIBUS, CANBUS or BITBUS are used.

Traditionally, when the types of network interfaces and parameters of network protocols are selected it is necessary to provide the necessary minimum time step of synchronizing and level of reliability of data movement between the objects of the automated system of welding technological process.

In that case when the network protocols are used with a random nature of conflict resolution (for example, Ethernet) or with a synchronous movement of data (for example, PROFIBUS-DP) the running of jobs in the automated system of the welding technological process control can have a probability nature and depend greatly on the selected time step of synchronizing. For example, the examination of TCP/IP of protocol in network Ethernet 10 Base-T shows that for the synchronizing time step of less than 10 ms the running of jobs of subsystems can have a probability nature, while for the protocols DP of network PROFIBUS it is determinated.

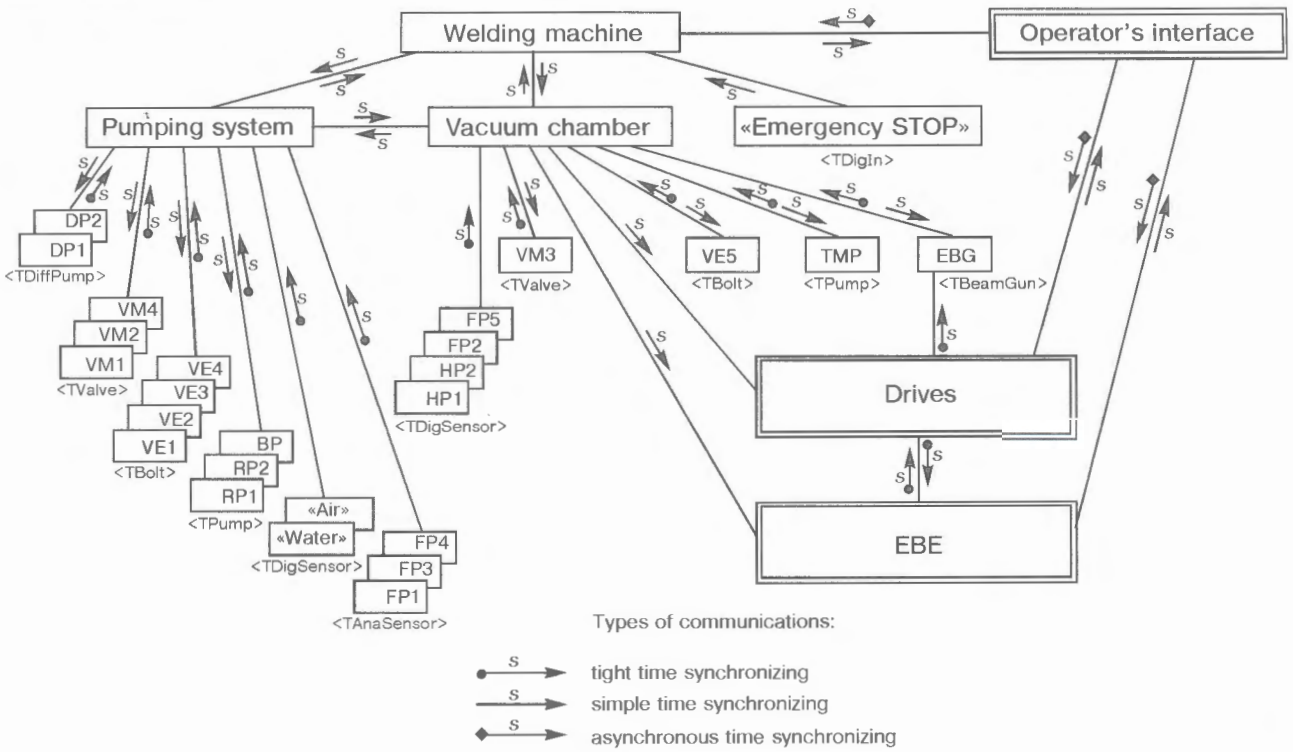

Figure 3. Diagram of relations and synchronizing of objects of software of the automated system of welding technological process control

In our case it is necessary to provide both a simple synchronizing between the objects (subsystems) and also a tight synchronizing with a step time of not less than 10 ms. The presence of the latter is stipulated by the necessity of a combined operation of the subsystems of displacement of the electron-beam gun (vacuum chamber), manipulator of the workpiece and power source (ELE) that, in principle, defines the quality of welding.

Based on the above-mentioned, it is possible to assume a conceptual scheme of the network system of control of the object-oriented automated system of the welding technological process control (Figure 4). The structure of this control system has several levels of interaction of subsystems. At the upper level the following objects of subsystems are arranged: «Operator's interface», «Welding machine», «Evacuation system», «Vacuum chamber», «ELE», «Drives», etc. All the subsystems of the upper level have the information channels of communication with the network Industrial Ethernet 10/100 Base-T which has a lock into the network of a higher level (for example, factory) or into Internet. The scheme shows that it is desirable to realize the objects of subsystems in a common controller (computer) to provide a tight time synchronizing. At the lower level the controllers with models of objects of units, mechanisms, sensors and signals are arranged. The objects «Vacuum chamber» and «Vacuum evacuation» have a direct information communications with objects of the lower level via the protocols of exchange by interface FieldBUS. The offered system of the objects interrelation is invariant in a general case to a number and types of the controllers, therefore, the development of the hardware and software can be made in parallel.

Such architecture as a whole does not contradict the typical two-level architecture of automated system of EBW technological process control which is used at present in industrial models of the technological systems [4].

It should be noted that at present the tendency of creation of the object-oriented «open» systems of control is increased [5 – 8]. Special language means of designing, for example, a system of designing UML (Universal Modeling Language) were created for the development and modeling of these system [9].

Let us consider the problem, arising in realization of abstract models, by using the methods and means of OOP. The OOD methodology provides programmers with a mathematical hardware which can be used as a basis of networking of control programs and realization of abstracts of the control objects, being dynamic in its nature. This mathematical hardware is based on using a Markovian scheme of modeling and analytical research of complex systems of a type of systems of a mass service. Here, a key concept is a Markovian process representing a model with a finite set of states, describing the system functioning. In this connection, the model of the Markovian process can be used as a generalized model for the dynamic system [10]. To realize the Markovian processes the directed graphs of states can be used. The development of models of the control object and automated system of the welding technological process control is performed as a whole from the abstract models of Markovian process of the higher order to the lower order. Therefore, OOD gives, as a result, a hierarchic system

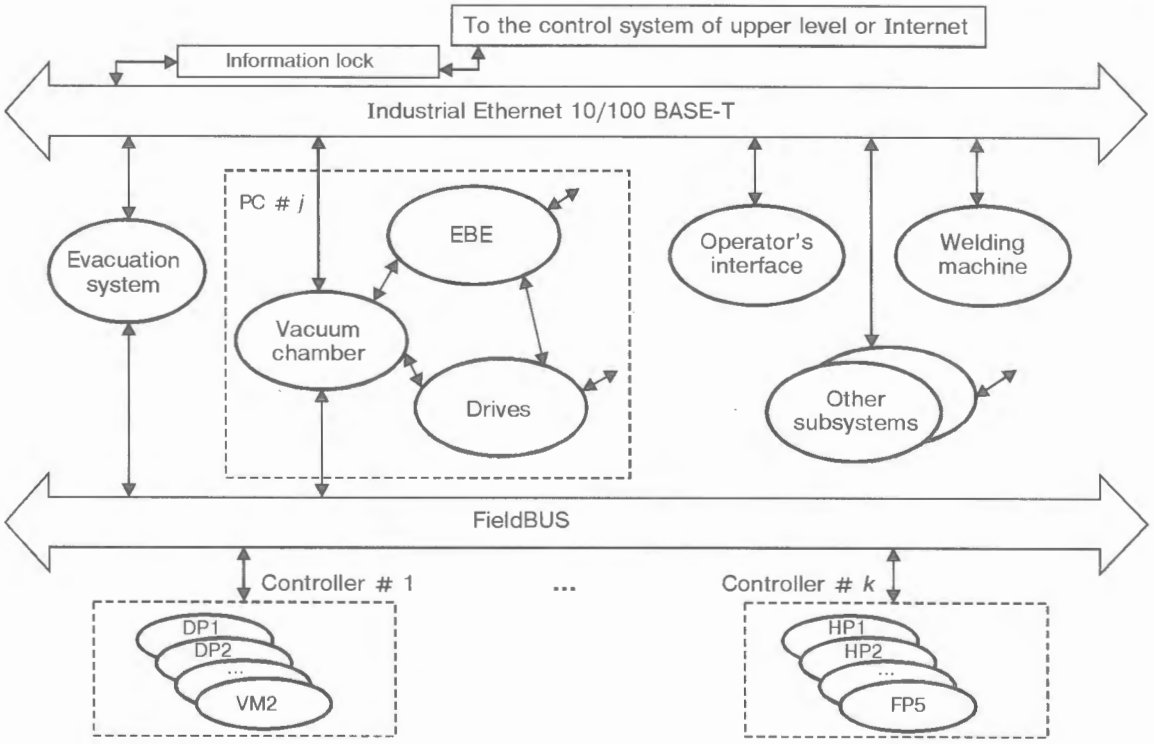

Figure 4. Conceptual scheme of network object-oriented system of automated system of welding technological process control (for designations in Figure 1)

of the Markovian schemes realized in the form of the directed graphs of states.

In the hierarchic scheme of basic classes (see Figure 2) each object encapsulates the object of type TGraf, which presets the object behaviour in a real time. The realization of the object of type TGraf in the language of the machine programming can be formalized, for example, with the help of the standard block «switch — case of». To organize the work of such model in a real time it is necessary to synchronize the graph tightly with a period of a real time interval. This should be provided by an appropriate selection of both an operational system of the controller and also the programming language compiler. For example, to work in a real time of graphs of states with 0.1 s time step it is possible to use an operational system MS Windows NT and the programming system Borland C++ Builder, while for work with 1 ms time step an operational system OS-9 and language compiler Microware Ultra C++ is required.

Conformity of programming problems and theory of graphs

Programming problem	*Tasks of theory of graphs*
Optimizing of programs, including distinguish of fragments (structuring) and decomposition	Finding of dominators
	Listing of biocomponents, circuits, intervals, hammocks, linear components
	Finding of inserted zones of graphs
	Finding of inserted circuits
	Interval presentation of graph
Checking of program correctness	Finding of transitive and reverse transitive short circuiting
	Finding of short circuiting relative to vertex set
	Listing of routes, circuits
Definition of sequence of processing of operators at flow analysis	Numbering of vertexes
	Networking of long successive vertexes
Testing of programs	Finding of coverage for:
	vertexes by routes
	arcs by routes
	required routes by routes
	Finding of shortest route in presence of additional limitations
	Finding of set of fundamental cycles
	Determination of cyclomatic number

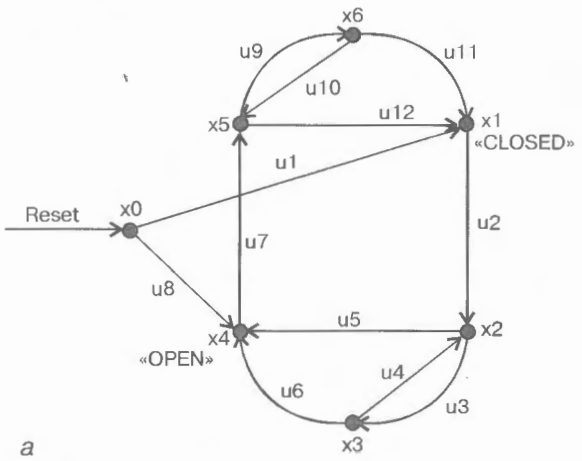

a

```
#define TRUE 1
class TVacuumValve : public TValve, public TGraf {
//... body of class definition
public:
   enum TStates {x0, x1, x2, x3, x4, x5, x6};
   int State ;
   virtual   void  Graf();
}
void TVacuumValve : : Graf( ) {
      if ( Reset  = = TRUE)   State = x0;
      switch (State) {
            case x0:
                  if(u1 = = TRUE) State = x1;
                  if(u8 = = TRUE) State = x4;
                  break;
            case x1:                  // Valve is CLOSED
                  if(u2 = = TRUE) State = x2;
                  break;
            case x2:
                  if(u3 = = TRUE) State = x3;
                  if(u5 = = TRUE) State = x4;
                  break;
            case x3:
                  if(u4 = = TRUE) State = x2;
                  if(u6 = = TRUE) State = x4;
                  break;
            case x4:                  // Valve is OPEN
                  if(u7 = = TRUE) State = x5;
                  break;
            case x5:
                  if(u9 = = TRUE) State = x6;
                  if(u12 = = TRUE) State = x1;
                  break;
            case x6:
                  if(u11 = = TRUE) State = x1;
                  break;
            default :  State = x0;
                  break;
      }
}
```

b

Figure 5. Example of realization of the Markovian model of object «VACUUM VALVE»: *a* — graph of states; *b* — text of program in language C++

As an example, let us consider the Markovian model of the object «VACUUM VALVE», whose graph of states is given in Figure 5, *a*. After reset, the model is transferred into state x0. There are two steady states: x1 — «CLOSED» and x4 — «OPEN», During operation the graph can be in states x2, x3, x5 and x6, which can be characterized as intermediate. To realize the given model we shall use language C++

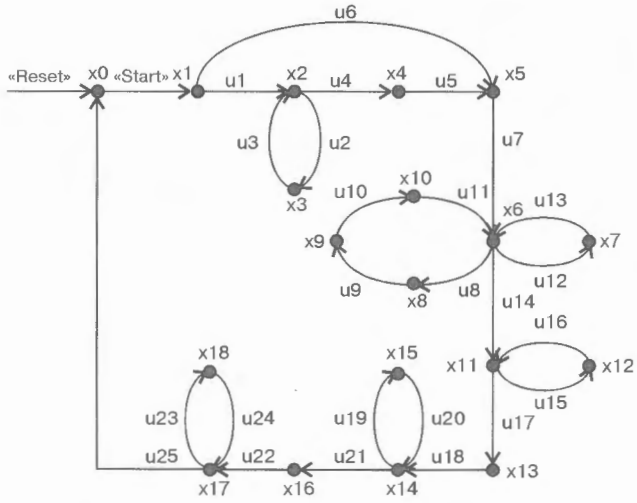

Figure 6. Example of a complex managing graph

as a program. Figure 5, *b* shows a fragment of the program code which corresponds to the graph in Figure 5, *a*.

It is possible to outline the advantage of programming objects by this formal procedure which consists of a visuality and interindentity of the object model and the programming code. This makes it possible to reduce greatly the time of development and to increase the reliability of software operation of automated system of welding technological process control.

The aphorism, known among the programmers, which states that «each last revealed error in the program is last but one», reflects the important problem of search and elimination of errors in software of the automated system of the welding technological process control. A significant advantage of OOD approach is the fact that the arising tasks in design and running of the program can be reduced to the problems of theory of graphs or used as bases for solution. They include the problems of testing and checking the program accuracy, assessment of complexity and time of fulfilment, etc. Table shows interrelation between such problems and problems of the theory of graphs from [11].

As an example, let us consider the control graph of the technological condition «EVACUATION OF VACUUM CHAMBER» (Figure 6). Vertex x1 is input, and x0 is output of the graph. Assume, that it is necessary to design a program of testing the given graph. For this, we shall find a minimum coverage of vertexes by

$$\mu 1 = [\text{«Reset»}, \text{«Start»}, u1, u2, u3, u4, u5, u6, u7, u8, u9, u10, u11, u12, u13, u14, u15, u16, u17, u18, u19, u20, u21, u22, u23, u24, u25] \quad (1)$$

and arcs by

$$\varphi 1 = \mu 1, \quad (2)$$

$$\varphi 2 = [\text{«Reset»}, \text{«Start»}, u6, u7, u14, u17, u18, u21, u22, u25]. \quad (3)$$

Thus, we have two minimum coverages $\mu 1$ and $\varphi 2$ which can be put into a basis of the test program for a managing graph being considered.

An additional advantage of this approach is also the fact that programmers have to document their managing graphs and to plan precisely the process of the program running and testing. This makes it possible to provide a comprehensive accompanying and service of the software of the automated system of the welding technological process control.

CONCLUSIONS

1. The advanced automated systems of the welding technological process control represent complex information managing systems with a comprehensive software. In development of software of these systems the main problem is a selection of suitable formal procedure of designing which could transform the «external complexity» of the architecture and program code of the software of the automated system of welding technological process control. The OOD approach using the methods of decomposition, abstraction and hierarchy allows realization of the principle of the «inner simplicity» both for the software itself and also for the automated system of the welding technological process control as a whole. As a result the time of development and implementation is decreased and the increased reliability of the software functioning of the developed system of automated control of the welding technological process is also attained.

2. The use of the results of the theory of graphs makes it possible to formalize the procedures of running and testing of the software for the automated system of the welding technological process control, thus giving an opportunity to develop programs with a complex logic of the operation which are practically free of errors.

REFERENCES

1. Buch, G. (2000) *Object-oriented analysis and designing (with examples using C++)*. Moscow: Binom.
2. Chvertko, A.I., Nazarenko, O.K., Kajdalov, A.A. (1999) Tendencies of development. In: *Machine-building*. Encyclopedia. Moscow: Mashinostroyeniye.
3. Nazarenko, O.K. (1998) Secondary-electron follow-up system with electromechanical drive. *Avtomaticheskaya Svarka*, **12**, 47 – 50.
4. Nazarenko, O.K., Kajdalov, A.A. (1999) Microprocessor systems of a local control of parameters of electron beam welding process and electromechanical complex. In: *Machine-building*. Encyclopedia. Moscow: Mashinostroyeniye.
5. Ryzhenko, A.I., Svirid, U. (2000) Object-structuring ASC TP of flour mill. *Sovremen. Tekhn. Avtomatizatsii*, **3**, 46.
6. Quinn, T.P., Gilsinn, J.D., Ripply, W. (2000) A welding cell with its own Website. *Welding J.*, **1**, 46 – 48.
7. Ripply, W., Gilsinn, J., Flitter, L. (2000) Networking of welding applications. *Ibid.*, **1**, 49 – 53.
8. (1999) No other PC-bases shape-cutting control touches it. BURN 10 shape-cutting motion control. *Ibid.*, **6**, 41.
9. Buch, G., Rambo, D., Jackobson, A. (2000) *Language UML. Manual for user*. Moscow: DMK.
10. (1974) *Encyclopedia of cybernetics*. Kyiv: Ukr. Sov. Enc.
11. Evstigneev, V.A. (1985) *Application of graphs in programming*. Ed. by A.P. Ershov. Moscow: Nauka.

DESIGN AND ELECTRON BEAM WELDING OF VACUUM CHAMBERS

O.K. NAZARENKO, V.M. NESTERENKOV and **Yu.V. NEPOROZHNY**
The E.O. Paton Electric Welding Institute, NASU, Kyiv, Ukraine

ABSTRACT

New principles of vacuum chamber design and technology of their assembly for EBW were developed and implemented in fabrication of five vacuum chambers of 15 to 34 m^3 and two of 0.2 m^3 volume.

Key words: *electron beam welding, vacuum chamber, shell, load-carrying capacity, reduction of metal content, welding deformations, machining, vacuum tightness*

Modern engineering is integrally connected with vacuum technologies of drying, welding, brazing, melting, metallizing, etc., requiring the application of various vacuum chambers — critical and labour-consuming structures that should combine the required rigidity under the impact of atmospheric pressure with minimal metal content. This particularly applies to large-sized chambers with the working volume of 20 to 40 m^3, consisting of several hundred parts.

Large-sized vacuum chambers of a rectangular shape, widely used in EBW units, contain one vacuum-tight shell, fitted with longitudinal, transverse or longitudinal-transverse load-carrying chords [1]. These chords give the shell the overall stability and rigidity under the impact of atmospheric pressure during the chamber pumping down. However, the maximal deformation of the wall of such a chamber can be up to 3 mm, this precluding the mounting of precision manipulators of displacement of the gun and the item being welded without using additional structures allowing these mechanisms to be disconnected from the chamber walls. Application of the above structures reduces the coefficient of utilisation of the chamber volume (ratio of the volume of the item being welded to the total volume of the chamber), i.e. increases the pumped down volume, vacuum system cost and the resultant cost of the entire unit.

Application of arc welding processes in fabrication of vacuum chambers often generates a need for subsequent heat treatment and machining to stabilize the dimensions and condition of surfaces, in particular in the zones of location of vacuum seals, and at large overall dimensions of the vacuum chambers — in making use of the services of specialised mechanical engineering factories and vehicles.

Use of EBW, creating minimal welding deformations, allows the design and technology of fabrication of vacuum chambers to be fundamentally changed. The E.O. Paton Electric Welding Institute of the NAS of Ukraine, was able to implement a new technology, due to availability of EBW unit UL193 with the vacuum chamber of 320 m^3 volume (4.25 × 6.3 × × 11.9 m) located in a shop with 30 t gantry crane. The technology has the following features:

- use of vacuum-tight and high-strength shells, connected to each other by stiffeners — fins. The chamber doors are made by the same principle;
- elimination of any finish machining of the vacuum chamber surfaces after welding, as panels are supplied for welding and assembly, after their finish treatment.

Principles of design of vacuum chambers of a new generation. Proceeding from the requirements of service personnel protection from X-ray radiation, the total thickness of the inner and outer shells for EBW units with the accelerating voltage of 60 kV and beam power of 60 kW was selected to be 25 mm [2]. The inner shell can be made both of structural, and of stainless steel 8 to 14 mm thick.

Application of a box-like structure for the vacuum chamber wall and doors, instead of the regular tec-structure, allows achieving, at the same geometrical parameters H, B and δ of the structure, a 2 times greater moment of inertia [3], and, hence, a smaller deflection of the wall during pumping down (Table). The need for application of a longitudinal load-carrying chord has practically been eliminated. It is used only in the areas of the walls weakening by the holes for viewing windows and vacuum system branchpipes. This will considerably (by 25 %) reduce the specific metal content of the structure, i.e. the weight recalculated to the vacuum chamber volume.

Design values of wall deflection were compared with the actual values for the pumped down chambers, in particular for 2.5 × 2.5 × 5.0 m chamber (Figure 1). Negligible values of these deflections allowed mounting the manipulator of the gun displacement directly on the chamber side wall (Figure 2, see insert). This light-weight and compact gun manipulator, based on precision linear modules with ball-screw pairs and linear tilting roller supports provides a high accuracy of displacement and positioning (± 0.08 mm at 2500 mm travel), low resistance to displacement and high dynamic properties of gun displacement.

Technology of vacuum chamber fabrication. All the panels are supplied for assembly and welding after their finish treatment, namely the panel surface facing

Comparative characteristics of vacuum chambers configurations with walls of П-shaped and box-like cross-section

Cross section type	*Design element of vacuum chamber wall*	*Design moment of inertia, cm^4*	*Maximal design deflection, mm*	*Spesific metal content, t/m^3*
П-shaped	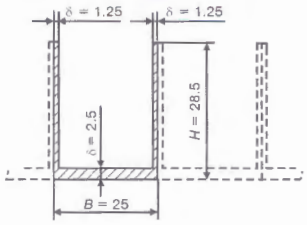	7560	0.84	1.12
Box-like	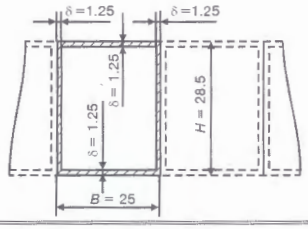	17515	0.36	0.85

inside the chamber is ground or milled to surface roughness not less than R_a = 0.8 – 3.2, panel edges are treated in a boring machine, till they are parallel to within not more than 0.1 mm. Pins, argon-arc welded to the reverse side of the plates, are used to fasten the plates in the assembly-welding jig. The structural steel panels are checked for residual magnetisation level and in the case, if $2 \cdot 10^{-4}$ T values are exceeded, they are de-magnetised in a large-sized solenoid [2].

The main type of welded joint of the shell wall and the shell proper, is a full penetration butt joint that provides minimal angular deformations. Prior to welding, the panels are cleaned to remove emulsion and oil, and the edges to be welded are thoroughly washed with industrial alcohol.

In the assembly jig (Figure 3, see insert), the plate edges to be welded are assembled with misalignment of not more than 0.2 mm. Run-on and run-off tabs are mechanically fastened at the ends of the butt joint. Tack welding of the tabs to the plates and the EBW proper, are conducted in UL193 welding unit at the vacuum of $1.1 \cdot 10^{-1}$ Pa. Electron beam guiding to the butt and butt following during welding are performed with Rastr-5 system [2], and a computer system controls all the power parameters of the welding process.

The welding process is divided into several stages. After the electron beam has been superposed on the butt that is clearly visible in the computer monitor, the operator cleans the butt surface with the electron beam. With this purpose, beam scanning around a circle of 12 mm diameter is switched on, beam current is increased up to 10 mA and cleaning of the surface to be welded is performed at the speed of 8 mm/s. The second stage consists in making tack welds from the center to the edges at beam power equal to 30 % of the rated value of welding current. The length of tack welds is 100 mm, the distance between them being 300 mm. Tack welding program is entered into the computer and switched on in the required point of the joint. Welding of panels, for instance, of 14 mm structural steel, is performed using ELA-60/60 power

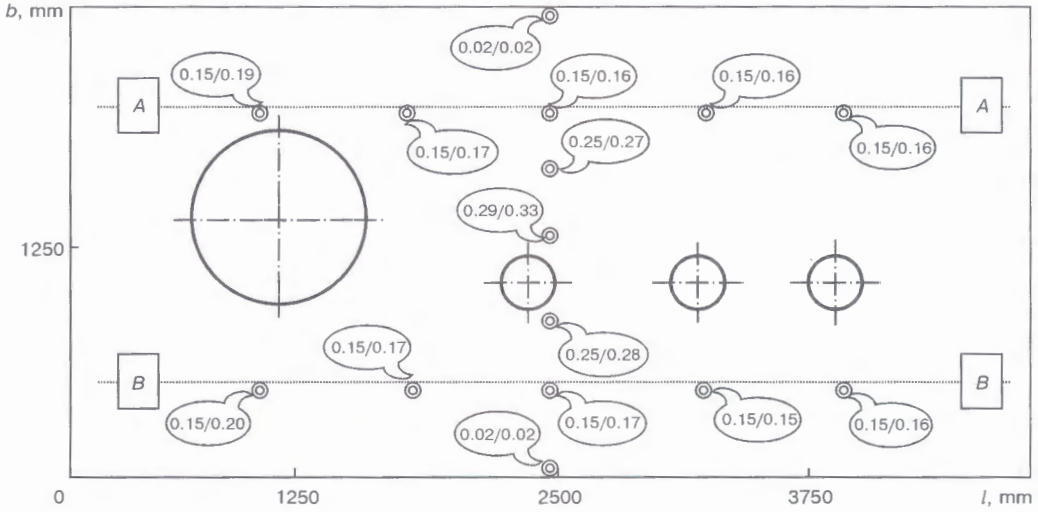

Figure 1. Design (numerator) and measured (denominator) values of wall deflections in 2.5 × 2.5 × 5.0 m chamber under vacuum: *A–A* and *B–B* — the axes of fastening the upper and lower guides of the manipulator of the gun displacement along the chamber; *l*, *b* — are the length and height of chamber walls, respectively

supply at beam current of 160 mA, welding speed of 8 mm/s and focal spot located on the item surface. As was noted above, such a welding mode provides full penetration of an optimal shape.

The final stage of welding is a cosmetic pass made with a defocused beam at the current equal to about 25 % of the rated welding current, to produce an even smooth surface of the weld that is necessary to meet the hygienic requirements on vacuum chamber operation.

Preparation for assembly of the welded chamber walls (Figures 4, 5, see insert) is performed as follows. First, the run-on and run-off tabs are removed, then the edges to be welded are scraped and degreased. Chamber fins are fastened in a separate even shop area. All the four walls of the inner shell are sequentially brought into the thus formed frame (Figure 6, see insert). Preliminary attachment of the walls to the fins is performed with pins, earlier used in welding of the panels. Special bolts of the assembly fixture are used to adjust the gap in the assembled butts that should not exceed 0.15 mm. Run-on and run-off tabs are mounted and mechanically attached in the eight corners of the inner shell, with their subsequent tack welding by the electron beam to the walls. The assembled shell in the fin framing is placed into the vacuum chamber for EBW. A feature of this stage is making welds between the fins, starting from the center to the wall edges. The welding program envisages a smooth increase of current to the working value at the start and its smooth decrease at the end of welding. This ensures the absence of defects in the zones of weld overlapping.

After welding the four corner butt joints by intermittent welds, the shell is taken out of the welding chamber, the fins are moved along the walls so that the unwelded portions of the butts were accessible. A feature of subsequent welding of these sections is guaranteed overlapping of the zones of the beam current increase and decrease on the earlier made intermittent welds and making new intermittent welds with new sections of the beam current increase and decrease.

At the final stage the inner shell is tack welded to the fins around the entire perimeter by CO_2 welding. The above technology is used to assemble and weld the chamber outer shell. In this case the outer shell plates are joined to the fins by plug welding. Chamber painting is preceded by vacuum testing first of the interwall space and then of the assembled chamber with the doors, thus providing convenient access to all the welds. In vacuum testing air in-leakage into the inner chamber during welding operations performance is practically eliminated.

As an illustration, let us give the results of measurement of the tolerances of the actually provided dimensions in 2.5 × 2.5 × 2.5 m vacuum chamber that are equal to ± 0.5 mm for the diagonals of the chamber cross-section, with 0.4 mm deviations from the plane of the chamber end face surfaces. No clamping mechanisms are used to achieve a good sealing of the chamber doors, it is sufficient to just start the pumping down process. The general view of the finished chamber is given in Figure 7 (see insert).

REFERENCES

1. Chvertko, A.I., Nazarenko, O.K., Svyatsky, A.M. (1973) *Equipment for electron beam welding*. Kyiv: Naukova Dumka.
2. Nazarenko, O.K., Kajdalov, A.A., Kovbasenko, S.N. *et al.* (1987) *Electron beam welding*. Kyiv: Naukova Dumka.
3. Pisarenko, G.S., Yakovlev, A.P., Matveev, V.V. (1975) *Reference book on resistance of materials*. Kyiv: Naukova Dumka.

IMPROVEMENT OF TECHNOLOGICAL CHARACTERISTICS OF PLASMA-MIG SURFACING USING FLUX-CORED WIRE

N.A. MAKARENKO, A.V. GRANOVSKY and **K.A. KONDRASHOV**
Priazovsky State Technical University, Mariupol, Ukraine

ABSTRACT

Peculiarities of proceeding reactions between some components of the flux-cored wire during plasma-MIG surfacing process were considered. It is shown that the presence of halogenide compounds in arc column favours stabilization of the process of the consumable electrode arc self-adjustment. The formation of boron trifluoride in the flux-cored wire core at the stickout during heating improves the weld bead formation.

Key words: *plasma-MIG surfacing, flux-cored wire, arc burning stabilization, bead formation, press-moulds*

The plasma-MIG surfacing with a flux-cored wire is used in repair of the cast iron press-moulds and manufacture of moulds from steel 45 for forming pieces from chemically-aggressive as-hot materials, in particular glassy insulators [1]. The plasma-MIG surfacing provides a small depth of the parent metal penetration, improves the efficiency of the melting process, and also possesses several technological advantages as compared with other methods of surfacing [2 – 5].

During plasma-MIG welding (surfacing) one arc *4* is burning between the edge of the inner consumable electrode *2* of a half-cylindrical shape and a workpiece *6* (Figure 1). This arc is formed in the channel of a plasma-forming nozzle *3*. The electrode *1* is fed along the plasmatron axis. There is no electrical contact between the non-consumable and consumable electrodes. The non-consumable electrode arc is supplied from a power source with a falling external volt-ampere characteristic, while the consumable electrode arc *5* is supplied from the power source with a rigid characteristic.

The plasmatron is designed so that the current conductor is located at 100 – 130 mm distance from the nozzle cut, the length of the plasma arc, embracing the consumable electrode, exceeds by 5 – 8 mm the length of the arc burning from this electrode. Thus, the wire at this stickout region is heated additionally by the plasma arc heat, except the heating by a passing current.

It was observed that the process of plasma-MIG welding (surfacing) is less stable than the majority of other arc methods of surfacing. The violation of its stability is due to a low intensity of the electrical field E in the arc column of the consumable electrode. This arc has a lower temperature than the plasma arc and receives an additional energy and charge carriers from the side of the latter [4]. This explains the low-efficiency of the process of the consumable electrode arc self-adjustment.

The present investigations were aimed at the increasing of the stability of the surfacing process and improvement of the deposited metal quality.

The investigations were made using the plasma-MIG surfacing of 2Kh13N12GS2P2 (C – 0.2; Cr – 13.0; Ni – 12.0; Mn – 1.0; Si – 2.0; W – 2.0 wt.%; Fe – balance) type metal with 2 mm diameter flux-cored wire consisting of a steel sheath and a charge of different compositions in a plasma-forming and shielding argon. To increase the wear-resistance a negligible mass share of aluminium and copper was introduced to the deposited metal.

The surfacing conditions of separate beads are as follows: in case of plasma arc – I_w = 100 – 200 A, U_a = 40 – 45 V; in case of consumable electrode arc – I_w = 100 – 120 A, U_a = 26 – 30 V; plasma-forming argon consumption is 5 – 7 l/min; shielding – 10 l/min; movement speed – 30 m/h.

Stability of proceeding of the plasma arc burning and electrode wire melting was judged from changing of electrical parameters, recorded on the oscillograph S2-16 screen, and also from the nature of formation of the deposited bead (visual inspection). The investigations were performed at constant conditions with

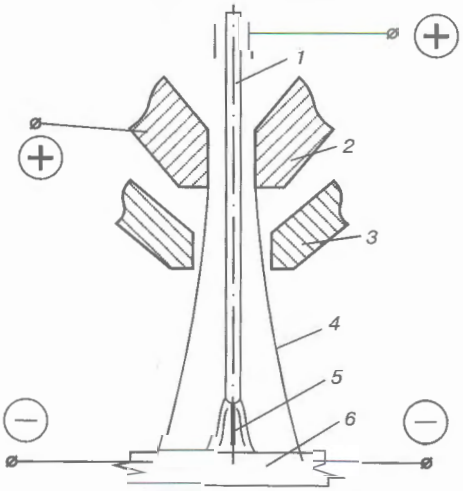

Figure 1. Diagram of plasma-MIG welding (surfacing) process (see designations in text)

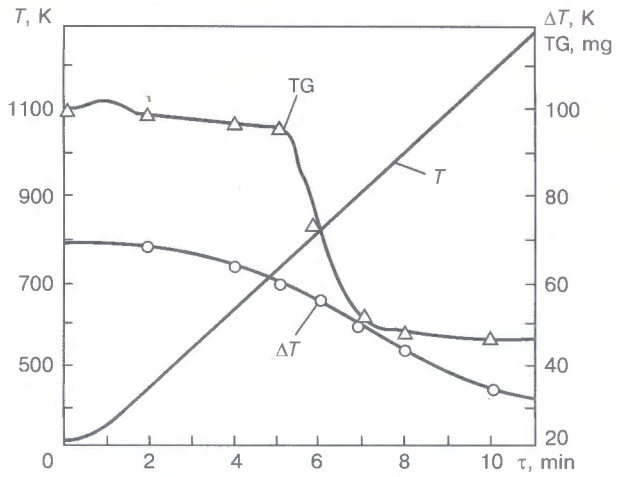

Figure 2. Thermogram of formation of BF_3 from AlF_3 and B_2O_3: T — heating temperature of charge components; TG — mass losses; ΔT — difference of temperatures inside the crucible and heating medium; τ — test duration

pre-adjusted condition parameters. Only the composition of the flux-cored wire was changed, i.e. without halogenides of metals and with halogenides of silicon, aluminium, potassium and copper.

The investigation results showed that the introduction of such components as fluorides and chlorides into the flux-cored wire composition improves the stability of the surfacing process. Thus, fluorine, evolving from SiF_4 has a high (16.9 V) potential of ionizing and deteriorates the electric conductivity of the arc column, thus leading to the increase in the electrical field intensity in the arc column and improves the process of the consumable electrode arc self-adjustment. However, in this case the poor bead formation was observed. During investigations, the experiments on replacement of silicon tetrafluoride by boron trifluoride BF_3 which is used in brazing and provides a reliable wetting of the parent metal with a brazing alloy even without melting of the latter, were performed [5].

The reactions of interaction can proceed by the following schemes:

$$B_2O_3 + 2AlF_3 \rightarrow BF_3\uparrow + Al_2O_3, \quad (1)$$

$$B_2O_3 + 3MgF_2 \rightarrow BF_3\uparrow + 3MgO. \quad (2)$$

Values of isobar-isothermal potential of the reactions of formation BF_3 at different temperature were calculated according to [6, 7].

Figure 2 presents the thermogram of reaction (1), which shows that it is proceeding at the melting temperature of B_2O_3. In addition, BF_3 and BF_2, BF in negligible amounts are evolved.

In practice, not pure components, but their compounds, molten borax and cryolite, are introduced into the flux-cored wire composition. At simultaneous introducing of borax and cryolite, the number of oxide inclusions in the deposited metal is reduced that is explained by dissolution of the latter in the forming slag.

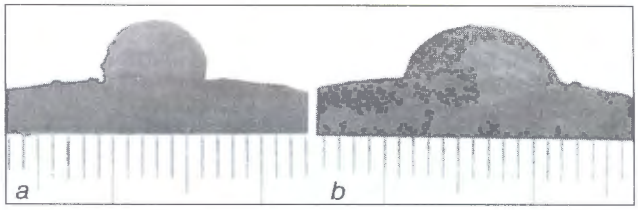

Figure 3. Zone of parent and deposited metal fusion when flux-cored wires, evolving SiF_4 (*a*) and BF_3 (*b*), are used

Stability of the plasma-MIG surfacing process is increased with introducing the fluorides into the charge. Moreover, the lack of fusion of the deposited metal with the parent metal is not observed. Due to the excessive temperature of the filler metal and high activity of BF_3 and SiF_4 the process is proceeding almost without melting of the parent metal. At the same time the satisfactory yielding of the bead metal over the surface being deposited is observed (Figure 3).

To refine the deposited metal, and consequently, to increase the wear resistance of the piece, the chlorides, mixture of $CuCl_2$ and KCl, were introduced to the flux-cored wire. Chlorine, the same as fluorine, increases the intensity of the electrical field in the arc column (potential of ionizing is 13 V). Chlorides also contribute to the removal of oxide impurities from the surface of particles of the wire core metallic components after its calcination.

During calcination of the flux-cored wire the $CuCl_2$ is decomposed:

$$CuCl_2 \rightarrow CuCl + Cl. \quad (3)$$

Atomic chlorine, evolved as a result of reaction (3), is very active. In combination with oxides on the surface of the powder particles, it forms fusible oxychlorides.

The presence of KCl leads to the formation of eutectic CuClKCl, having 120 °C melting temperature, and dissolving easily the oxychlorides. As a result of reaction according to scheme

$$Me + 2CuCl \rightarrow MeCl_2 + Cu\downarrow$$

the copper is precipitated on the powder particles and prevents them from their further interaction with the melt CuClKCl. High probability of proceeding of similar reactions was confirmed experimentally by the method of immersion of the metal samples into CuClKCl melt. Here, the oxide film on the surface of the particles is dissolved. The results of metallographic examinations showed that in metal, deposited with the flux-cored wire, containing $CuCl_2KCl$, has no almost inclusions of not only of oxide, but also of nitride nature (Figure 4). This phenomenon can be explained by the fact that the nitrides exist together with oxides on the powder particle surfaces, thus leading to the removal of precipitations of both types.

The presence of $CuCl_2KCl$ in the composition of the flux-cored wire charge leads to the fact that reaction, due to dissolution of AlF_3 and B_2O_3 in the charge, is proceeding at the moment of the wire cal-

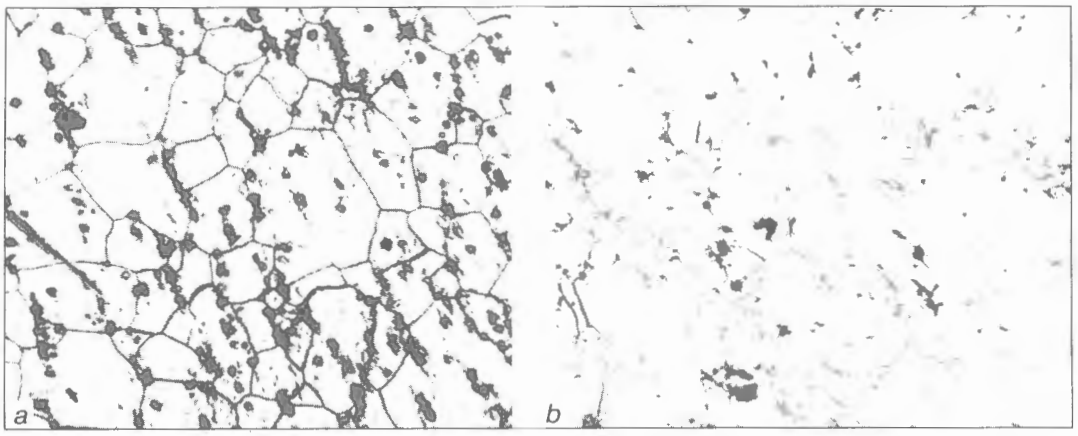

Figure 4. Microstructure of deposited metal obtained when the flux-cored wires, evolving SiF_4 (*a*) and BF_3 (*b*), are used (×200)

cination, because the change in a thermodynamic potential ΔG of this reaction has a negative value at room temperature [8]. In this case it is more rational to introduce MgF_2 and B_2O_3 into the flux-cored wire charge, as the value ΔG becomes negative only at temperature of the surfacing process proper.

The peculiarities of proceeding of chemical reactions of the charge components of the charge under the conditions of plasma-MIG surfacing is taken into account in the development of the flux-cored wire compositions.

CONCLUSIONS

1. To improve the stability of arc burning and flux-cored wire melting in plasma-MIG surfacing it was suggested to introduce the fluorine- and chlorine-containing compounds into the wire composition which improve the potential of ionizing.

2. Formation of the boron trifluoride in the flux-cored wire core during its heating at the stickout promotes the improvement of wettability of surface of the steel or cast iron pieces being surfaced and yielding of the bead metal.

REFERENCES

1. Makarenko, N.A. (1998) Plasma surfacing with an axial feeding of flux-cored wire. *Avtomaticheskaya Svarka*, **1**, 40 – 43.
2. Mucsy, G., Vas, A., Bica, I. (1983) Wirtschaftlichkeit und Technologie beim Plasma-MIG-Schweißen. *Lis-Mitt.*, **1**, 60 – 67.
3. Moestue, H. (1981) Plasma-MIG rolls over SA for steel plant repairs. *Weld. and Metal Fabric.*, **8**, 465 – 467.
4. Ton, H. (1975) Physical properties of the plasma-MIG welding arc. *J. Physics D: Applied Physics*, **8**, 922 – 938.
5. Esunberlin, R.E. (1972) *Brazing and heat treatment of parts in gas medium and vacuum*. Leningrad: Mashinostroyeniye.
6. Petrov, G.A., Tumarev, A.S. (1967) *Theory of welding processes*. Moscow: Vysshaya Shkola.
7. (1965) *Thermodynamic properties of inorganic substances*. Handbook. Ed. by A.I. Zefirov. Moscow: Atomizdat.
8. Yavojsky, V.I., Rubenich, Yu.I., Onenko, A.G. (1980) *Non-metallic inclusions and properties of steel*. Moscow: Metallurgia.

MACHINE EQUIPPED WITH AN ELECTRIC-CONTACT HEATING SYSTEM FOR DRAWING OF WELDING TUNGSTEN WIRE

A.N. SHAPOVAL
State Engineering Centre for Hard Alloys «Svetkermet», Svetlovodsk, Russia

ABSTRACT

Technological parameters of the new wire drawing machine are presented in comparison with characteristics of mass-produced domestic and foreign machines equipped with the electric-contact heating system. Advantages of the new machine are presented.

Key words: *drawing, tungsten wire, machine, electric-contact heating, technological parameters*

Tungsten electrodes for argon-arc welding are made from rods and wire by the powder metallurgy methods [1]. The critical technological operation, which is responsible for the quality of welding electrodes, is drawing of rods and wire billets using chain and block drawing benches. New drawing processes characterized by an increased reduction per pass, vibration drawing in particular [2], have been applied in the last years. Based on the analysis of the existing methods for heating the metal prior to deformation [3], we assumed the electric-contact heating (ECH) to be the basic process for intensification of processes of pressure treatment [4].

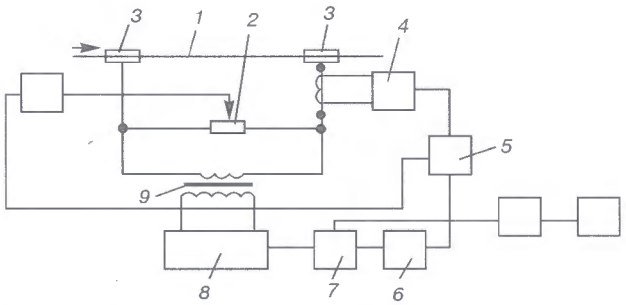

Figure 1. Block diagram of the system for automatic regulation and maintaining of power in heating a wire (see designations in the text)

Making of contact devices to allow the required power to be supplied to a workpiece is one of the challenges arising in development of machines for continuous ECH. Power can be stabilized by using a block diagram shown in Figure 1.

Signal of voltage at a heated region of billet *1* between contacts *3* is fed from voltage sensor *2* to quadratic detector *4*. The signal of current flowing through the billet is also fed from the measurement transformer of the current to the quadratic detector. Then both signals are fed to power meter *5* and power

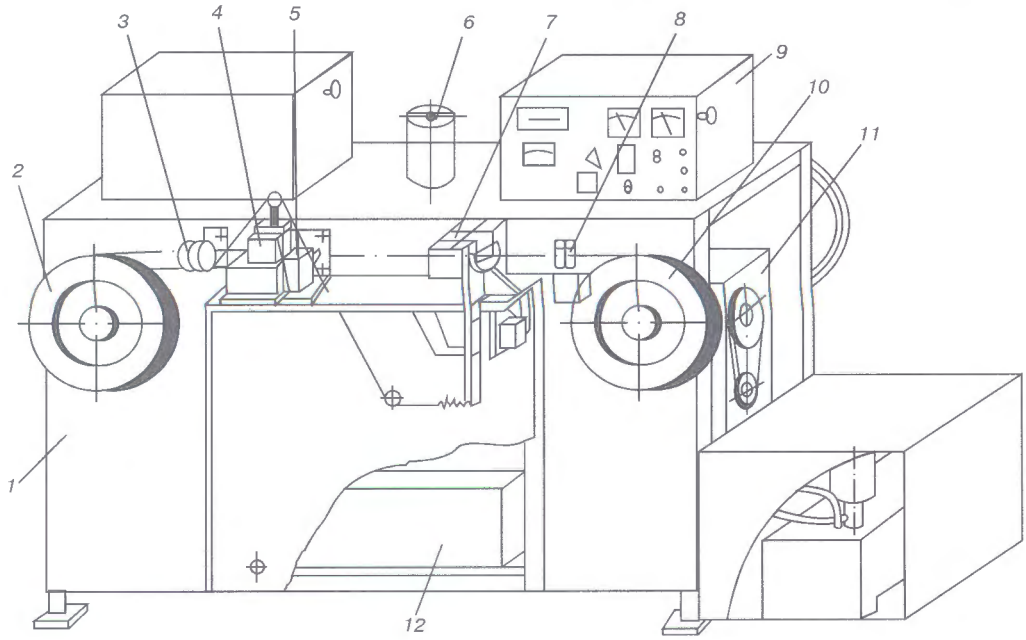

Figure 2. Layout of the UVE-1000 machine (see designations in the text)

Specifications of the UVE-1000, MV-1000V and L2 machines

Characteristic	Type of machine		
	UVE 1000	MV 1000V	L2
Drawing speed, m/min	10.5 – 24.0	10.5 – 13.5	5.0 – 20.0
Accuracy of maintaining wire heating temperature, deg.	± 20	± 50	± 30
Degree of deformation per pass, max, %	28	22	16
Intensity of cooling of wire at outlet from the deformation zone, deg./s	4000 – 5000	500 – 800	200 – 250
Productivity, kg/h	1.10	0.59	0.68
Yield of the process, %	96.07	94.98	96.80
Irrevocable loss, %	0.5	1.5	1.1
Specific consumption of power supplies:			
gas, m^3/kg	–	8.47	1.84
air, m^3/kg	–	84.7	18.4
electric energy, kW/(h·kg)	3.40	3.55	2.20

selector *6*. The error signal amplified by amplifier *7* is fed to thyristor regulator *8* that maintains, through matching transformer *9*, the selected power at the billet heated, which provides a more accurate stabilization of the heating temperature.

We developed a new design of the tungsten wire drawing machine with ECH. To ensure rational utilization of the available equipment, the development was made on the basis of a mass-produced drawing machine of the MV-1000V model which is widely applied at factories manufacturing wire from refractory metals. Overall dimensions of the MV-1000V drawing machine, providing that the air-gas piping system and gas heating furnace are dismantled, allow accommodation of all electrical equipment of the drawing machine with ECH (UVE-1000). This does not increase dimensions of the basic MV-1000V drawing machine. Table gives specifications of the UVE-1000 machine in comparison with the mass-produced MV-1000B machine and the «Toho Kinzoku» (Japan) machine L2 with gas heating of the metal. Almost all of the characteristics of the UVE-1000 machine are much in excess of those of the other machines.

The UVE-1000 machine is mounted (Figure 2) on frame *1* of a welded structure and comprises reel drum *2*, «cold» contact assembly *4* with lubrication bath *5*, «hot» contact assembly *7* and winding drum *10*, located on the two sides in line of drawing. Operation of the machine is controlled from unit *9*. To load the wire billet into a drawing die, its end is subjected to thermochemical sharpening in assembly *6* using a sodium nitrate melt. Strict linearity of the wire treated and its guiding consistently along the drawing axis are provided using a braking device of reel drum *2* and guide *3*.

The drawing process is carried out until the entire wire billet leaves the deformation zone. Trapping mechanism *8* serves to trap the wire end, prevent its crushing and ensure linearity after leaving the deformation zone. Power unit *12*, which supplies power to the machine, is located inside frame *1*. Drives *11*, separate for each of the sides, provide a two-stage regulation of the drawing speed by re-adjustment of the wedge belt.

The new contact system of the UVE-1000 drawing machine provides a spark-free transfer of the electric energy with a density of up to 150 A/mm^2 at a minimum time needed to load the wire to be treated.

The new ECH system is used now to advantage with the technology for manufacture of welding tungsten wire and tungsten strip and cathodes for electron beam processes [5, 6]. As shown by practical operation of the UVE-1000 machine, the rational number of drawing passes within a diameter range from 0.88 to 0.51 mm is 4. In this case the degree of deformation per pass ranges from 20 to 28 %, and the rated number of passes serviced by one worker is five.

REFERENCES

1. Shapoval, A.N., Izotov, V.M., Poznansky, V.I. *et al.* (1986) Advanced technological processes of pressure treatment of refractory metals. In: *Inform. Review of TsNIItsvetmet, Economy and Information on Treatment of Non-Ferrous Metals*, Issue 2. Moscow.
2. Shapoval, A.N., Izotov, V.M. (1985) Vibration treatment of metals. *Ibid*.
3. Butko, E.V., Troitsky, O.A., Shapoval, A.N. (1983) Electric contact heating in treatment of metals. *Ibid*., Issue 4.
4. Kovrev, G.S. (1975) *Electric contact heating in treatment of non-ferrous metals*. Moscow: Metallurgia.
5. Shapoval, A.N., Gorbatyuk, S.M., Shapoval, A.A. (1999) Technology for manufacture and properties of tungsten strip for electron beam technologies. *Tsvetnye Metally*, **2**, 78 – 80.
6. Shapoval, A.N., Tretiakov, O.V., Shapoval, A.A. (2000) Development of new technological processes for manufacture of refractory metal strip. In: *Proc. of the 3rd Int. Conf. «BRM-2000» on Noble and Rare Metals*. Donetsk: Don. GTU.

REAL-TIME AUTOMATIC SEAM TRACKING AND OBSERVATION SYSTEM «RASTR» FOR EBW

- The principle of obtaining information on the state of the workpiece surface by scanning with a probe — a sharp-focus electron beam.
- At the similar cost the main advantages of RASTR in comparison with the optical and television systems are:
  - no optical illuminators and optical elements, which are contaminated by metal vapors;
  - the operator works under comfortable conditions.

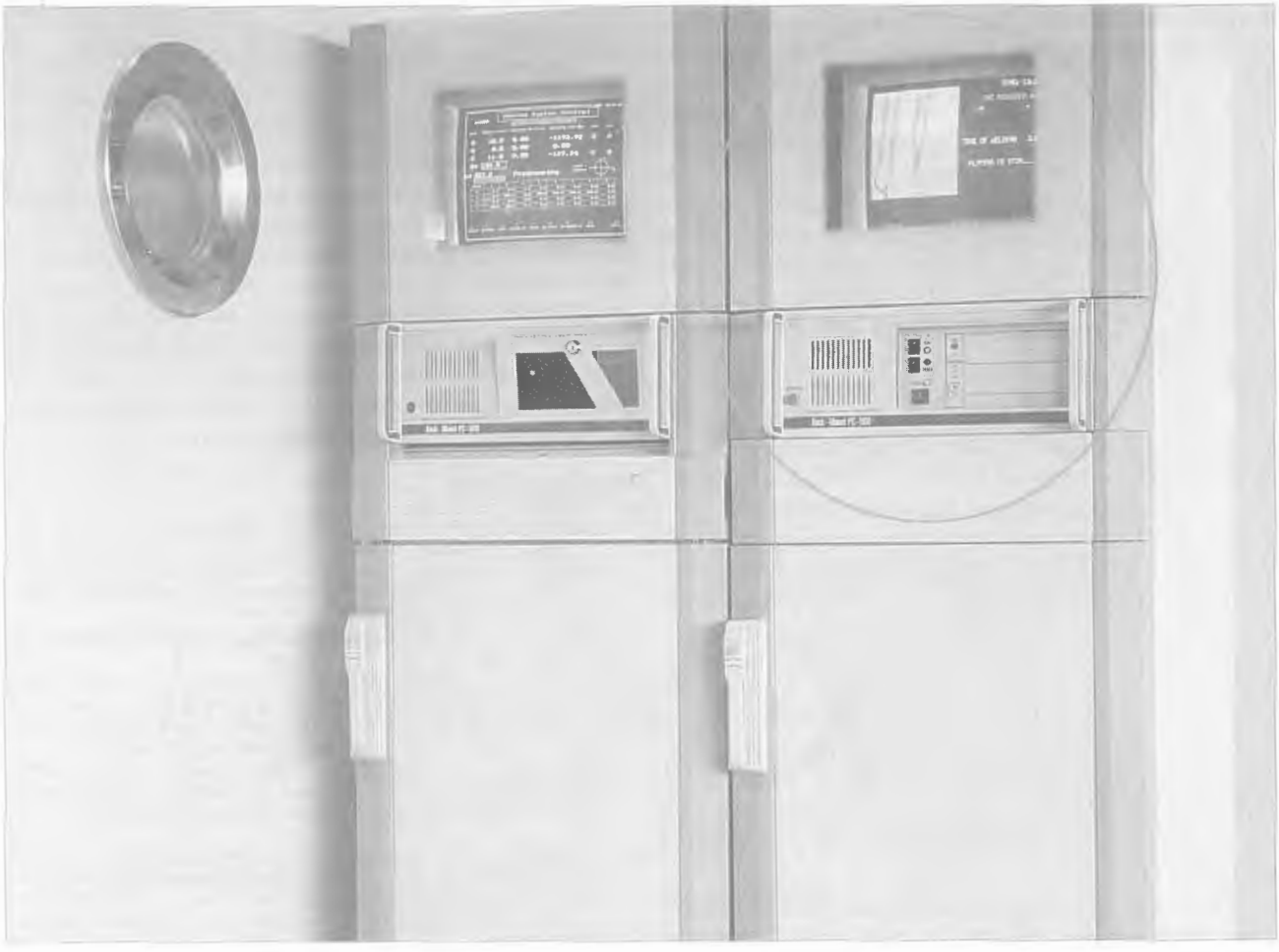

PRINCIPLE AND APPLICATION

✦ The image of a 60 × 60 mm section containing the weld, the weld pool and the joint forms three times per second when the beam scans over the surface of the component whithin a short period. The process of EBW does not exclude the possibility of its interruption for this short period of time $\tau_{int} = 0.1\, d_e/v_w$, where d_e is the affected diameter of the beam; v_w is the welding speed. For d_e = 1 mm (the size of the beam typical of powerful guns) at v_w = 6 m/h (1.7 mm/s) the interruption of the welding process for τ_{int} < 60 ms does not cause any disturbance in weld formation. At v_w = = 60 m/h (17 mm/s) this time period decreases to 6 ms. During these periods the welding beam may be switched to the probing mode, and the weld pool and the weld in the immediate vicinity of the pool may be visualised, and the joint line can also be aligned with the centre of the weld. At the same time, the system automatically computes the value of mismatch between the position of the joint and the weld during welding, and a deflection system aligns the beam with the butt line.

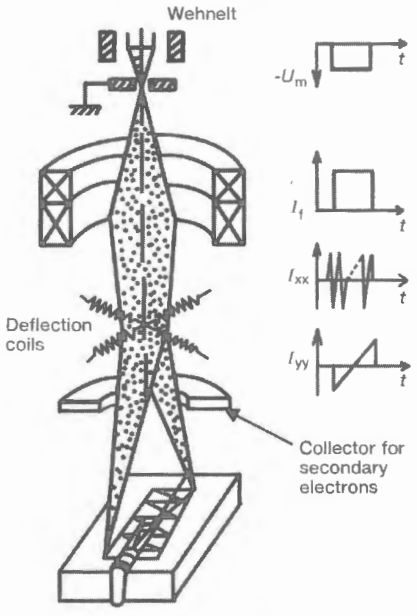

Principle of the secondary emission image formation while EBW procedure

TECHNICAL DATA

Number of the sampling, pixels ..... 256 × 256

Dynamic error of the joint tracking, mm ..... ± 0,1

System works with power units of the ELA type with a power of 15, 60 and 120 kW

ELECTRON BEAM WELDING GUNS AND POWER SUPPLIES

Electron beam equipment is a result of an effective team work of the E.O. Paton Electric Welding Institute (Kyiv, Ukraine) and JSC Selmi (Sumy, Ukraine)

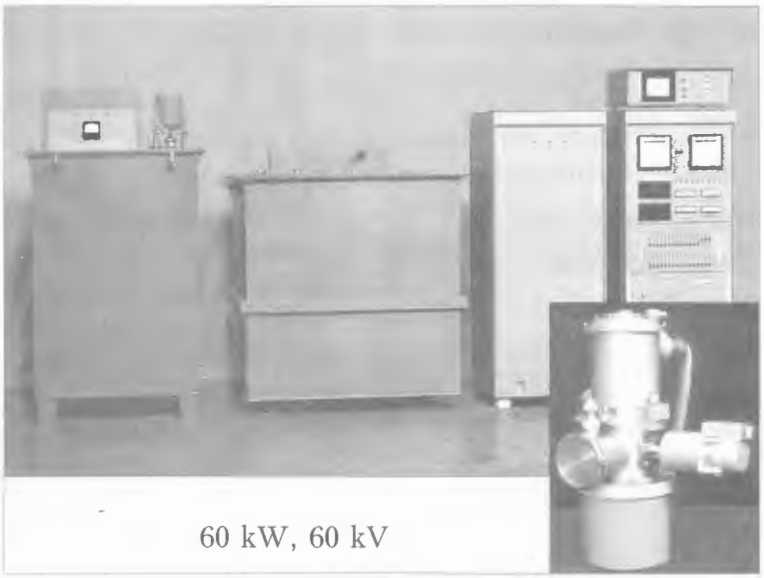

60 kW, 60 kV

120 kW, 120 kV

- The electron gun permits welding in continuous and pulse modes; it may be used inside a vacuum chamber at any altitude. As the gun has a small mass, it may be installed on a robot-type manipulator.
- The triode electron-optical system provides smooth adjustment of the beam power; it employs a highly efficient indirectly heated cathode made of lanthanum hexaboride.

  Cathode replacement takes only 10 min. The cathode timelife is more then 40 h.
- Continuous operation time is not limited. Guarantee time of control electron tubes — 1000 – 2000 h.

HIGH QUALITY WELDS AND RELIABLE PERFORMANCE ARE PROVIDED BY THE HIGH VOLTAGE UNIT. SPECIAL ELECTRON TUBE IN THE HIGH VOLTAGE CIRCUIT MAKES IT POSSIBLE:

- ✦ to prevent spark discharges from transition into arc discharges;
- ✦ to eliminate weld defects caused by gun discharges;
- ✦ to decrease average beam current down to several tens of mA in the load shortcircuit mode;
- ✦ to ensure quick response of the stabilizer, high stability, small pulsation and possibility of impulse modulation.

High voltage unit electric circuit diagram:

1 — high voltage source; *2* — welding current stabilizer; *3* — bombardment current stabilizer; *4* — focus current stabilizer; *5* — beam deflection current source; *6* — accelerating voltage stabilizer; *7* — control tube unit; *8* — current limiter

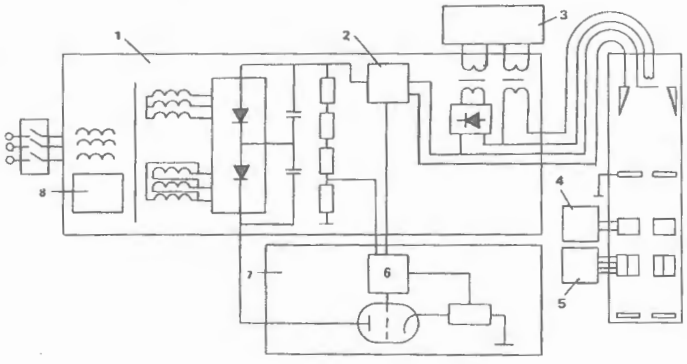

The main parameters

Parameters	ELA-3	ELA-15	ELA-30B	ELA-30/45	ELA-60	ELA-120/6	ELA-120B
Maximum power of beam, kW	3	15	30	45	60	6	120
Accelerating voltage, kV	60	60	60	30	60	120	120
Range of welding current adjusting, mA	0.1 – 50.0	0.1 – 250.0	0.1 – 500.0	0.1 – 1500.0	0.1 – 1000.0	0.1 – 50.0	1.0 – 1000.0
Stability of accelerating voltage and welding current, %	± 0.5	± 0.5	± 0.5	± 0.5	± 0.5	± 0.5	± 0.5
Angle of beam deflection, deg.	± 7	± 7	± 7	± 7	± 7	± 7	± 7
Distance from gun section to the workpiece, mm	100 – 300	100 – 300	100 – 300	100 – 300	100 – 300	100 – 300	100 – 300
Power supply: voltage, *V*, at frequency 50 60 Hz	380 220	380/220	380/220	380/220	380/220	380/220	380/220
Consumed power, kVA	5	25	57	70	90	8	220
Cooling water:							
pressure, MPa	0.3 – 0.4	0.3 – 0.4	0.3 – 0.4	0.3 – 0.4	0.3 – 0.4	0.3 – 0.4	0.3 – 0.4
consumption, l min	5	10	15	20	25	5	35
Equipment weight, kg	1500	2500	3000	3000	3000	3500	6000
Computer-aided	Yes	Yes	Yes	Yes	Yes	Yes	Yes
Maximal depth of weld materials, mm:				Application:			
steels	10	50	75	EB melting	100	15	250
titanium and its alloys	15	80	110	and	150	20	400
aluminium-based alloys	20	120	150	evaporation	200	35	450

WELDING ELECTRON BEAM ANALYZER

- The space current density distribution has the significant effect on the weld penetration, weld width, and quality of electron beam welds.
- In our electron beam analyzer the high-power electron beams are analyzed by very fast (~1 km/s) deflection of the beam over the edge of the flat sensor — tungsten plate. Beam current is measured in a circuit of this insulated sensor.
- Main area of our analyzer application is simple-to-use analysis of powerful electron beams, which are formed by the disk cathodes.

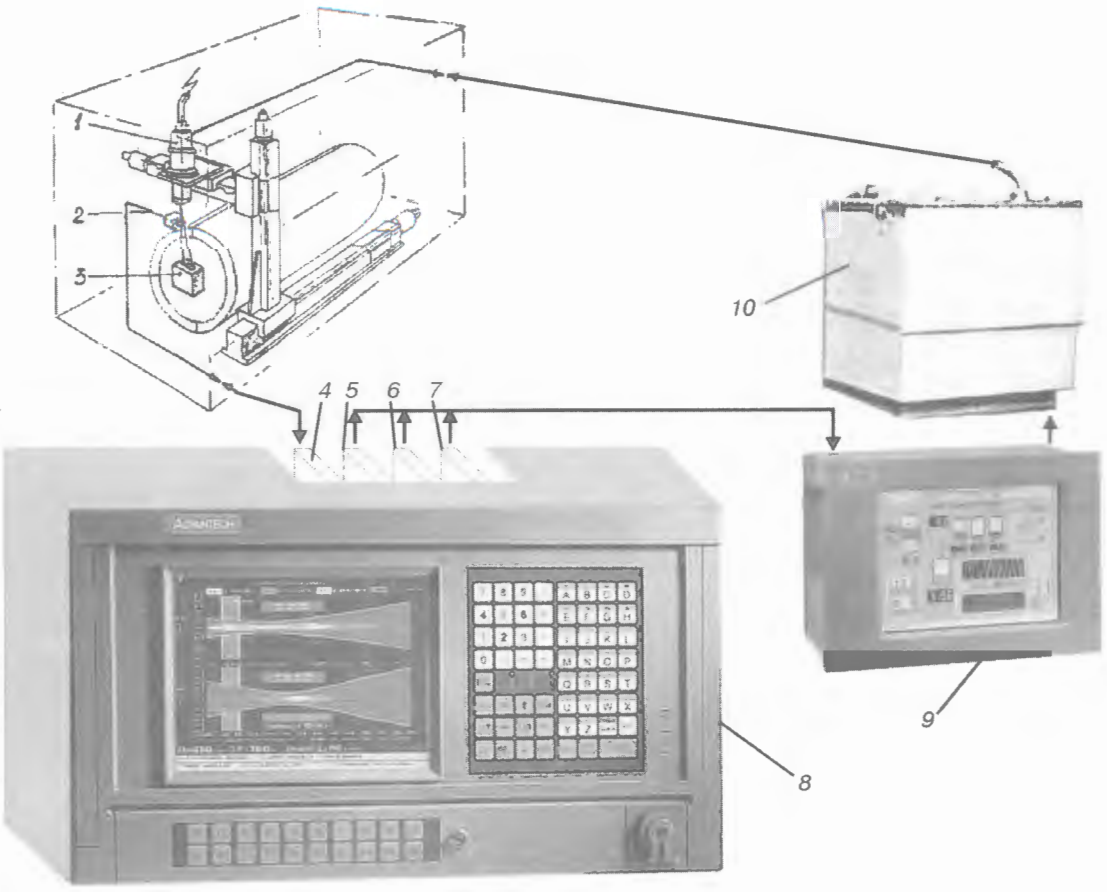

Block diagram of the machine with the electron beam analyzer: *1* — electron beam gun; *2* — insulated flat sensor; *3* — massive copper body; *4* — 40 MHz, 8-bit A/D converter; *5* — generator of deflecting pulses; *6, 7* — D/A converters; *8* — electron beam analyzer; *9* — main computer; *10* — gun power supply

✦ The current density distribution is a function of the speed of increase in the current. As a result of the calculations a computer gives a distribution of the beam current density. Therefore, by changing the focus it is possible to get a lengthwise section of the beam along its axis, to define the position of the beam focus, the distribution and values of the beam current density.

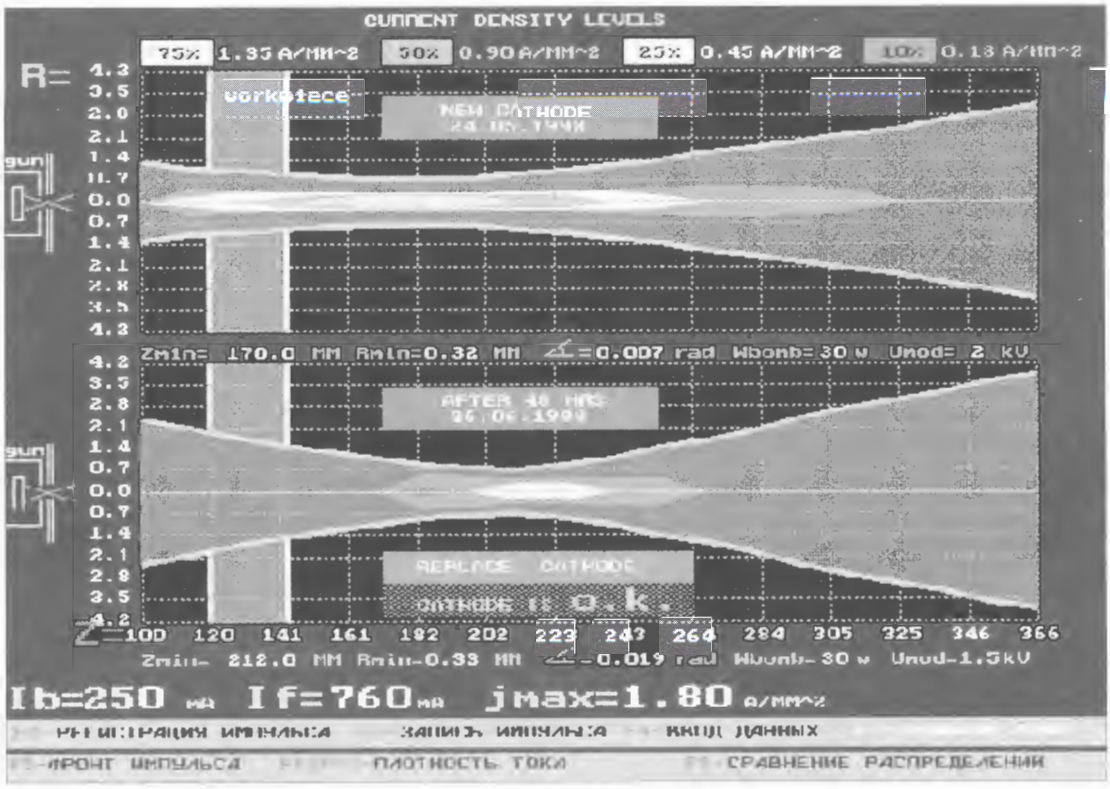

Longitudinal sections of the welding electron beams, formed by new (above) and used (48 h) cathode (below) with the «Replace cathode» requirement, because the focus position and current density are changed essentially

DESIGN

✦ The sensor and copper body are located in a special position of the vacuum chamber. Prior to welding, an operator gives the command to move the gun to the position of the beam diagnostics. Electron beam analyzer is assembled inside industrial 19" rack/panelmount workstation with added A/D and D/A converters and deflecting pulses generator.

TECHNICAL DATA

Maximum electron beam power, kW, up to	120
Accuracy of beam focus distance control, %	1
Effective frequency of beam deflection system, kHz	20
Duration of deflection pulse, μs	30...50

PERIODICAL 2002

PATON PUBLISHING HOUSE

IN ENGLISH

THE PATON WELDING JOURNAL
Monthly scientific-technical and production journal
ISSN:0957-798X. Since 1993
Subscription price: (USD 460, postage included, effective 2002)

English translation of the monthly «Avtomaticheskaya Svarka» journal published in Russian since 1948. Journal presents the results of extensive theoretical and experimental research carried out at the PWI in the field of welding. The Institute is a world leader in this field. The journal includes a wide range of scientific-technical and promotion information in the field of technologies, equipment and materials for welding, surfacing, brazing and deposition of protective coatings, and also abstracts of books coming out of the press, information on exhibitions, conferences and defended thesis.

ADVANCES IN SPECIAL ELECTROMETALLURGY
Quarterly scientific-technical and production journal
ISSN:0267-4009. Since 1993
Subscription price: (USD 184, postage included, effective 2002)

Translation into English of «Problemy Spetsialnoj Elektrometallurgii» journal. Main topics: electroslag remelting; casting; plasma-arc melting and remelting; vacuum-arc remelting; induction melting; electron beam remelting; electron beam evaporation; technologies of producing titanium alloy ingots; energy- and resources-saving technologies; physical and chemical fundamentals of steel production; theories of metallurgical processes; investigations into gas-slag-metal systems; mathematical modelling of processes.

IN RUSSIAN

AVTOMATICHESKAYA SVARKA (Automatic Welding)
Monthly scientific-technical and production journal
ISSN: 0005-111X. Since 1948
Subscription price: (USD 156, postage included, effective 2002)
Russian version of «The Paton Welding Journal»

Text in Russian, contents and summaries in English. The journal presents a wide range of scientific-technical and promotion information in the field of technologies, equipment and materials for welding, surfacing, brazing and deposition of protective coatings. It publishes abstracts of books coming out of the press, information on exhibitions, conferences and defended thesis and also the databank on «Who is Who in welding industry of the CIS countries».

TEKHNICHESKAYA DIAGNOSTIKA I NERAZRUSHAYUSHCHIJ KONTROL
(Technical Diagnostics and Nondestructive Testing)
Quarterly scientific-technical and production journal
ISSN: 0235-3474. Since1989
Subscription price: (USD 52, postage included, effective 2002)

Text in Russian, contents and summaries in English. The journal presents the latest achievements in the field of technical diagnostics and NDT (acoustic emission, magnetic, eddy current, radiowave, thermal, optical, radiation and dye penetrant methods). Procedures used to evaluate and predict the strength of welded structures are dealt with extensively.

PROBLEMY SPETSIALNOJ ELEKTROMETALLURGII
(Advances in Special Electrometallurgy)
Quarterly scientific-technical and production journal
ISSN: 0233-7681. Since 1985
Subscription price: (USD 52, postage included, effective 2002)
Russian version of «Advances In Special Electrometallurgy»

Text in Russian, contents and summaries in English. The journal presents the results of theoretical and experimental research carried out at the PWI in the field of electrometallurgy. Special attention is given to electroslag technology (electroslag melting, refining and casting). The journal is divided into the following main sections: electroslag technology; electron beam processes; plasma arc technology; vacuum arc remelting and vacuum induction melting; general problems of special electrometallurgy.

Advertising Rates:
Format: 210 mm wide x 297 mm high
Type area: 200 mm wide x 290 mm high
Front cover (4 colour): USD 300
2nd cover (4 colour): USD 250
3rd cover (4 colour): USD 250
4th cover (4 colour): USD 300
Inserts (4 colour): USD 200

Black and white pages:
Type area: 170 mm wide x 250 mm high
USD 80 per page

Discounts:
For 3 repeats or 2 pages - 10 %
For 6 repeats or 4 pages - 25 %
For 12 repeats or 6 pages - 33 %

Subscription to the journals can be made from the catalogs of «Presa» agency Ukraine (www.ukrpressa.kiev.ua), «Rospechat» agency Russia (www.rosp.ru), as well as in the editorial office. Back issues available.

For further information contact please:
PATON WELDING INSTITUTE
International Association «Welding»
11, Bozhenko Str.,
03680, Kiev-150, Ukraine
Tel.: (38044) 227 67 57
Fax: (38044) 227 46 77
E-mail: journal@paton.kiev.ua